1-1-1977

Capacitance probe measurements on the surface of a horizontal tube in a fluidized bed.

Donna Moore Edwards

CAPACITANCE PROBE MEASUREMENTS ON THE SURFACE OF A HORIZONTAL TUBE IN A FLUIDIZED BED

by

Donna Moore Edwards

A Thesis
Presented to the Graduate Committee
of Lehigh University
in Candicacy for the Degree of
Master of Science
in
Mechanical Engineering

Lehigh University
1977

This thesis is accepted and approved in partial fulfillment of the requirements for the degree of Master of Science.

May 9, 1977
(date)

Professor in Charge

Chairman of Department

ACKNOWLEDGMENTS

I gratefully acknowledge the advice and support of my thesis advisor, Professor J. C. Chen. His pertinent suggestions contributed invaluably to the successful completion of this investigation.

I am also thankful to Mr. R. Chandran and M. R. A. Baker for the use of their data.

I extend my appreciation to the technicians of the Department who built the capacitance probe and offered many helpful comments.

Financial support for this program, provided by Corporate Research and Development, General Electric Company, is gratefully acknowledged.

TABLE OF CONTENTS

TABLE OF CONTENTS (continued)

TABLE OF CONTENTS (continued)

LIST OF FIGURES

LIST OF TABLES

NOMENCLATURE

A	area
C	capacitance
D_p	particle diameter
G	mass flow rate of gas
T	temperature
T_b	bulk temperature of the bed
T_w	wall temperature of the immersed surface
u	gas velocity
u_{mf}	gas velocity corresponding to minimum fluidization
v_b	bubble volume
c_p	packet heat capacity
d	separation distance between probe plates
f_o	fraction of the total time that the immersed surface is covered by bubbles
$\bar{h}$	time mean local heat transfer coefficient for conduction only
h_i	instantaneous conduction heat transfer coefficient
$\bar{h}_L$	total time mean local heat transfer coefficient
h_o	heat transfer coefficient to a bubble
h_r	heat transfer coefficient for radiation only
h_{θ_p}	mean heat transfer coefficient for conduction over one packet residence time only
k_e	effective thermal conductivity of a packed bed in the absence of gas flow
$\bar{k}_e$	effective thermal conductivity of a packed bed due to gas flow

NOMENCLATURE (continued)

k_g	thermal conductivity of gas
k_p	thermal conductivity of a packet
k_s	thermal conductivity of solid particles
ℓ_n	natural Logarithm
n	number of bubbles
q_w	wall heat flux from immersed surface
t	time
x	distance from the immersed surface
$\bar{x}$	penetration depth

<u>greek</u>

α	mass velocity of gas flowing in the direction of heat or mass transfer/mass velocity of gas based on sectional area of empty tube in the direction of gas flowing
α_p	thermal diffusivity of a packet
β	ratio of the average length between the centers of two neighboring particles in the direction of heat flow to the average diameter of the solids
γ	ratio of the effective length of a solid particle for heat transfer to the average diameter of the solid particles
ϵ	void fraction
ϵ_p	packet void fraction
ϵ_q	void fraction for a quiescent bed
η	dielectric constant
θ	time
θ_o	angle corresponding to boundary of heat flow area for one contact point

NOMENCLATURE (continued)

θ_p	packet residence time
θ_p'	root-square average packet residence time
π	3.1415926
ρ_p	packet density
ρ_s	solid density
ϕ	a measure of the effective thickness of gas film adjacent to the contact surface of two solid particles

ABSTRACT

Fluidized bed technology continues to be of growing interest in many different industrial applications. The need for dependable engineering design capability has increased as the applications broaden. Improved understanding and description of funadamental mechanisms are required for various aspects of fluidized bed behavior. This work investigates the particular concepts of bed dynamics at the surface of heat transfer tubes submerged in fluidized beds.

A capacitance sensing technique was used to obtain experimental measurements of time varying bed behavior at the surface of an immersed tube in an air fluidized bed of glass spheres. From these measurements the following information was derived: residence periods of packets and voids, time averaged void fractions, fractional bubble contact times, frequency of packet/bubble exchanges, and transient emulsion densities. Data were obtained at various air flow rates for circumferential local positions around the tube. To the author's knowledge such

information has not previously been available.

It is found that three distinct regimes of fluidization exist around the tube. These are a solids-dense zone of closely packed particles at the top of the tube, a heterogeneous packet/bubble zone at the sides, and a lean, gaseous emulsion zone at the bottom of the tube. The occurrence of these different regimes depend upon fluidization flow rate. The quantitative fluid dynamic information and mean residence time information are used for two purposes. First, observations are made of the quality of fluidization around the tube. Secondly, local heat transfer coefficients are predicted by a "packet exchange" model and compared to previous experimental data.

Based upon the time varying density of a packet during its time of residence at the tube surface, it is proposed that packets "squirm" as they contact the wall. The use of time averaged packet property values in heat transfer calculations is therefore suggested.

These observations restrict the usefulness of the packet renewal model for heat transfer, which is based upon a heterogeneous packet/bubble regime. The packet renewal model, for certain velocities, applies only to the sides of the tube where it satisfactorily predicts heat transfer coefficients. For this same velocity range, the packet renewal model does not accurately describe the solids-dense and dilute conditions at the top and

bottom of the tube, respectively. It is found that the packet renewal model underpredicts heat transfer at the top of the tube, and generally overpredicts heat transfer coefficients at the bottom of the tube.

1. INTRODUCTION

1.1 Applications of Fluidized Beds

Fluidized bed technology is rapidly introducing pronounced changes into many industrial processes. The good gas/solids contact, vigorous mixing and agitation, and excellent heat transfer characteristics of fluidized beds make them uniquely adaptable for many industrial uses. A brief survey of fluidized bed application follows.

1.1.1 Nuclear Industry

In the nuclear industry the feasability of incorporating fluidized beds into the fuel processing cycle is being investigated [1]. The thermal properties of fluidized beds allow for economical operation of process reactions which include: reduction, hydrofluorination, fluorination, denitration, and calcination. These reactions are essential for preparing feed material, reprocessing spend fuel, and disposing of radioactive waste material.

1.1.2 Coal Combustion

Among the most active areas of coal research is the study of fluidized bed coal combustors [2]. In a fluidized bed combustor, finely divided limestone and coal particles are fluidized with hot air which oxidizes the coal, liberating heat and gaseous products. Sulfur is removed from the combustion gases due to reaction with the limestone. The heat of combustion is transferred to immersed

coils or tubes within the bed. This heat is efficiently recovered due to the high heat transfer coefficients for immersed surfaces in fluidized beds.

1.1.3 Coal Hydrogasification

Coal hydrogasification has been achieved by fluidizing coal particles with hydrogen to obtain methane [3,4]. The advantages of fluidizing this process are several, including: 1) the increase in methane production, 2) less hydrogen per pound of coal consumed, and 3) reduced capitol costs.

1.1.4 Environmental Control

Fluidized beds have proven to efficiently remove sulfur dioxide from flue gas [5]. This application makes fluidized beds potentially useful as a pollution control device.

1.1.5 Waste Treatment

Fluidized beds are a logical choice of oxidation or pyrolysis unit for solid wastes [6]. There is no residual sludge as in usual waste treatment processes. The heat transfer characteristics for fluidized beds allow for greater thermal recovery from this type of burner as compared to a conventional unit.

1.1.6 Metallurgical Industry

The metallurgical industry uses fluidized beds to perform

drying and separative processes, and for heat treatment of metal parts [7], [8], [9], [10].

1.2 Heat Transfer in Fluidized Beds

1.2.1 Past Works

As earlier noted, a consequence of the thermal behavior of fluidized beds is their application to processes involving heat exchange. To accommodate fluidized beds as a unit operation for heat exchange, the thermal design of both the fluidized bed and immersed heat transfer surface is required. This thermal design demands a knowledge of the characteristics of bed to surface heat transfer.

The earliest investigations of heat transfer between a fluidized bed and an immersed surface were attempts to fit experimental heat transfer coefficients to a power law relationship, $Nu = A(Re)^n$ [11]. In order to fit heat transfer data to an equation of this type required the manipulation of dimensionless parameters. The result was that the power law equations expanded to unwieldy proportions and became increasingly specific to individual experimental conditions [12]. Moreover, relationships of this kind for Nu were nonphysical, being the result of dimensional analysis.

The next generation of bed/surface heat transfer studies were attempts to describe the mechanism of heat transfer. These studies produced numerous semi-empirical relations for heat transfer coefficient. The more prominent of these models fall into two

categories, film model and unsteady penetration model.

1.2.1.1 Film Model

In the film model, Leva et al. [13], Dow and Jakob [14], and Levenspiel and Walton [15] considered that heat is conducted through a gas boundary layer adjacent to the heat transfer surface. The heat transfer coefficient $h = k/\delta$, is influenced by the solid particles only to the extent to which they scour the boundary layer thickness δ. The particle scouring action is a function of fluidizing velocity, u. The shortcoming of this model is the fact that it takes no account of the thermal/physical properties of the solid particles.

1.2.1.2 Penetration Model

Historically, the penetration or surface renewal model for heat transfer was proposed by Mickley and Fairbanks [16], [17]. This model postulates that there is transient conduction of heat from the immersed surface to "packets". These packets are loosely locked aggregates of particles and interstitial gas which are carried to and from the surface by gas bubbles. The heat transfer coefficient is strongly dependent on the dwell time and renewal frequency rate of packets at the wall. In addition, the thermal/physical properties of the packets influence heat transfer.

There are numerous variations to the original model of Mickley and Fairbanks in the literature. One variation is to evaluate the packet thermal conductivity based on a heterogeneous two phase

gas/sound medium [18]. This differs from the effective thermal conductivity of the original model, which is based on mean packet properties. Other corrections [19] provide for wall thermal contact resistance included in the evaluation of heat transfer coefficient. A third modification is to consider that the penetration heat transfer mechanism is due to surface renewal by individual particles instead of packets [20], [21].

1.2.2 Recent Research at Lehigh

The transient nature of the packet renewal type model requires a knowledge of residence time behavior for packets before heat transfer coefficients can be calculated. Residence times have traditionally either been 1) arbitrarily assumed [22], 2) artificially imposed by stirrers [23], or 3) the mean residence time taken to be proportional to the reciprocal of the packet renewal frequency at the surface [16], [24]. An accomplishment of the heat transfer study at Lehigh University has been to develop a technique to experimentally measure local residence times [25].

By using the above technique [25] to obtain packet residence time information, Ozkaynak [26] predicted heat transfer coefficients for a vertical tube in a fluidized bed. The predicted coefficients agreed quite closely with the measured heat transfer coefficients for the same system, providing the residence times were not vanishingly small. For short residence times, it is concluded [26] that the expression for packet thermal conductivity must be modified to

accommodate increased packet void fraction near the tube surface. The Ozkaynak modified packet renewal model successfully predicts heat transfer coefficients for a vertical tube, for both long and short packet residence times.

The heat transfer work at Lehigh then proceeded to an investigation of heat transfer from a horizontal tube in a shallow fluidized bed [27]. Heat transfer coefficients were experimentally measured. This data was compared to semi-empirical heat transfer correlations of Vreedenberg [28], Gelperin et al. [29], and Genetti et al. [30] for horizontal tubes. It was found that each of these correlations was grossly inadequate in predicting heat transfer data for the shallow bed system. Due to the previous success of the Ozkaynak modified packet model, a study was begun to determine if the modified packet model is equally accurate in predicting heat transfer coefficients for a horizontal tube in a shallow fluidized bed. The subject of this paper is to present the results of this investigation.

1.3 Scope of Present Investigation

This work considers the packet renewal mechanism for an immersed horizontal tube in a shallow fluidized bed. The object of this work is foremost to investigate the phenomenology of contacting packets at the tube surface. Local data around the circumference of the tube is generated for: 1) packet void fraction, 2) packet replacement frequency, 3) packet residence times and 4) packet

densities. Such data have not been available to date. From the data, an observation of the effectiveness of surface renewal around the circumference of the tube is possible for the first time. Secondly, local and average heat transfer coefficients are predicted from the data using the packet renewal model as modified by Ozkaynak [26]. These calculated packet renewal model heat transfer coefficients are compared to existing measured heat transfer data [27]. Finally, this comparison permits a discussion of the accuracy of a transient packet renewal model to describe heat transfer for horizontal tube geometry.

2. THEORY

2.1 Packet Renewal Concept

2.1.1 Temperature Profile in a Packet

According to the packet renewal model of Mickley and Fairbanks [16], heat is transferred from an immersed surface in a cold fluidized bed to "packets". A packet is an aggregate of solid particles and interstitial gas, which contacts the surface. Since these packets are intermittently transported to and from the surface by gas bubbles, heat conduction into these packets is transient. Heat transfer [16] is modeled by the one dimensional unsteady state conduction equation:

$$\rho_p c_p \frac{\partial T}{\partial t} = k_p \frac{\partial^2 T}{\partial x^2} \tag{1}$$

x is a measured positive outward from the surface, and ρ_p, c_p and k_p describe the thermal/physical properties of a packet.

The bed is essentially isothermal due to thorough gas/solids mixing. Accordingly, the temperature of the fresh packet as it newly arrives at the surface, is equal to the interior temperature of the bed,

$$T(x,0) = T_b \tag{2}$$

For brief packet contact times, only the portion of the packet directly adjacent to the tube surface undergoes a temperature change.

Thus the packet may be closely approximated by a semi-infinite slab [16] with the attendant boundary condition,

$$T(\infty,t) = T_b \tag{3}$$

If the second boundary condition is either: 1) $T_w(o,t)$ = constant or 2) $q_w(o,t)$ = constant, equation (1) can be readily solved. For constant wall temperature the solution of equation (1) is:

$$\frac{T(x,t)-T_b}{T_w - T_b} = \text{erfc}\left[\frac{x}{\sqrt{4\alpha_p t}}\right] \quad . \tag{4}$$

For constant wall heat flux,

$$T(x,t) - T_b = \frac{q_w}{k_p}\left\{\left[2\left(\alpha_p \frac{t}{\pi}\right)^{\frac{1}{2}} e^{\left(-\frac{x^2}{4\alpha_p t}\right)}\right] - x\,\text{erfc}\left[\frac{x}{2(\alpha_p t)^{\frac{1}{2}}}\right]\right\} \tag{5}$$

2.1.2 Local Heat Transfer Coefficient

To determine the local instantaneous conduction heat transfer coefficient for constant T_w, differentiate equation (4) and dividing by (T_w-T_b) yields

$$h_i = \sqrt{\frac{k_p \rho_p c_p}{\pi t}} \quad . \tag{6}$$

The mean local conduction heat transfer coefficient over one packet contact time θ_p, gives

$$h_{\theta p} = \frac{\int_o^{\theta_p} h_i \, d\theta}{\theta_p} = 2\sqrt{\frac{k_p \rho_p c_p}{\pi \theta_p}} \tag{7}$$

Averaging over all packet times, the mean local conduction heat transfer coefficient is for T_w = constant,

$$\bar{h} = \frac{\sum h_{\theta_p} \theta_p}{\sum \theta_p} = 2\sqrt{\frac{k_p \rho_p c_p}{\pi}} \quad \frac{\sum \sqrt{\theta_p}}{\sum \theta_p} \tag{8}$$

The expression for total local heat transfer also includes effects of 1) radiation, and 2) conduction to gas bubbles:

$$\bar{h}_L = h_o f_o + (1-f_o)(\bar{h}) + h_r \quad . \tag{9}$$

f_o is the fraction of time the local surface is covered by bubbles. For wall temperatures less than 800°C, radiative heat transfer is negligible. Furthermore, assume heat transfer to bubbles is by conduction, analogous to heat transfer to packets [26]. A comparison of the group $(k_p \rho_p)^{\frac{1}{2}}$ for both gas and packet reveals that h_o may be ignored. The total local heat transfer coefficient is therefore given by,

$$\bar{h}_L = (1-f_o)\ 2\sqrt{\frac{k_p \rho_p c_p}{\pi}} \quad \frac{\sum \sqrt{\theta_p}}{\sum \theta_p} \qquad T_w = \text{constant} \tag{10}$$

Defining the root square average packet residence time [26] as,

$$\theta_p' = \left[\frac{\sum \theta_p}{\sum \sqrt{\theta_p}}\right]^2 \quad , \tag{11}$$

The total heat transfer coefficient is finally expressed as

$$\bar{h}_L = (1-f_o)2\sqrt{\frac{k_p \rho_p c_p}{\pi}} \quad \frac{1}{\sqrt{\theta_p'}} \qquad T_w = \text{constant} \tag{12}$$

For the boundary condition of constant wall flux, from equation (5),

$$h_i = \frac{q_w}{(T(0,t)-T_b)} = \frac{\sqrt{k_p \rho_p c_p}}{2} \frac{\sqrt{\pi}}{\sqrt{t}} \tag{13}$$

Following the same procedure as equations (6) through (11), the total local heat transfer coefficient for constant wall heat flux is:

$$h_L = (1-f_o) \sqrt{k_p \rho_p c_p \pi} \frac{1}{\sqrt{\theta_p'}} \tag{14}$$

2.1.3 Packet Properties

2.1.3.1 Void Fraction

Mickley and Fairbanks assume packet void fraction, ε, is equal to the corresponding void fraction of a quiescent bed. The value of ε_q is approximately equal to the value of void fraction for a cubic or hexagonal prism lattice of spheres [16]. This suggested to Mickley and Fairbanks that each particle within a packet is in contact with six or eight particle neighbors. Because of this particle contact, the original renewal model assumes that the packet particles are loosely locked together and do not move in relation to one another. Accordingly, Mickley and Fairbanks [16] conclude that in the reference frame of the packet, non-mobile particles imply constancy of ε and all packet properties.

In this work, ϵ is measured for packets contacting the horizontal tube. The location of the packets varies circumferentially around the tube. An additional variable which influences ϵ, is gas fluidizing velocity, u. A list of run conditions is given in Table 1.

2.1.3.1 Packet Density

Packet density is considered to equal the density of a quiescent bed in the original packet renewal model of Mickley and Fairbanks. Therefore, packet density is expressed as [26]:

$$\rho_p = \rho_s (1-\epsilon_p) \quad . \tag{15}$$

since $\rho_s(1-\epsilon_p)$ is equal to the density of a loosely packed bed.

2.1.3.3 Packet Heat Capacity

The specific heat is assumed to equal the heat capacity of the solid material.

2.1.3.4 Packet Thermal Conductivity

Effective thermal conductivity of a packet is calculated from the correlation of Kunii and Smith [31], and Yagi and Kunii [32]. This model for two phase solid/gas thermal conductivity assumes that there are always particles in contact for even the loosest packing state of spheres.

According to this model,

$$k_p = k_e + \bar{k}_e \tag{16}$$

k_e is the contribution to effective conductivity arising from: 1) thermal conduction through solid; 2) thermal conduction through the contact surface between adjacent particles; 3) conduction through the stagnant fluid near the contact surfaces between particles; 4) radiation between solid surfaces; and 5) heat transfer through the fluid by radiation between and conduction in the void spaces. The term $\bar{k}_e$ is the effective contribution from heat transfer due to motion of the fluid.

In references [31], [32]

$$k_e = k_g \left[\varepsilon_p + \frac{\beta(1-\varepsilon_p)}{\phi + \gamma(\frac{k_g}{k_s})}\right] \quad . \tag{17}$$

Equation (17) neglects heat conduction through the contact surfaces of particles, and ignores heat transfer by radiation between solid surfaces and voids.

β refers to the ratio of the distance between the centers of two particles, divided by the particle diameter. It is here considered equal to unity [26].

The term ϕ is proportional to the effective thickness of gas slab through which heat is conducted between particles. The quantity ϕ is evaluated by the expression:

$$\phi = \frac{\frac{1}{2}\left(\frac{K-1}{K}\right)^2 \sin^2\theta_o}{\ell_n\{K-(K-1)\cos\theta_o\} - \frac{K-1}{K}(1-\cos\theta_o)} - \frac{2}{3}\frac{1}{K} \qquad (18)$$

K is the ratio k_s/k_g and θ_o relates to the angle subtended by the circumferential boundary of heat flow for a particle.

γ is proportional to the effective length of solid through which heat is conducted in a particle. The effective length is assumed to be equal to the length of a cylinder whose volume is equal to the volume of the given spherical particle. Accordingly,

$$\gamma = \frac{2}{3} \qquad (19)$$

To account for heat transfer due to the motion of gas within a packet,

$$\bar{k}_e = \alpha\beta D_p c_g G \quad . \qquad (20)$$

The product $\alpha\beta$ is taken to be equal to 0.12 for glass spheres.

A summary of particle properties is given in Table 2.

2.1.4 Ozkaynak Modified Packet Renewal Model

Ozkaynak and Chen [26] predicted heat transfer coefficients for a vertical tube in a fluidized bed according to equation (12) using correlation (17). The predicted values were compared to measured heat transfer coefficients. It was observed that for very short residence times, the predicted heat transfer coefficients significantly exceed the measured values for h. The

discrepancy is explained by the unaccounted increase in void fraction for packets of short contact time with the tube surface.

The temperature profile of a packet may be determined from either equation (4) or (5). The penetration depth is defined [26] as that distance $\bar{x}$ for which

$$\frac{T_w - T(\bar{x})}{T_w - T_b} = 0.9 \qquad (21)$$

If the penetration depth $\bar{x}$ into a packet is less than the particle diameter D_p, the packet cannot be assumed to have the properties of a packed bed. This is because for short residence times, i.e. small penetration depth, the total packet void fraction is dominated by the large void fraction of the portion of the packet adjacent to the wall. The effect of the wall is studied by Kimura et al. [33].

For the above packet, void fraction is described by Kimura:

$$\varepsilon = \varepsilon_q - .304 \ln \left(\frac{y}{D_p}\right) \qquad \frac{\bar{x}}{D_p} < 1 \qquad (22)$$

$$\varepsilon = \varepsilon_q \qquad \frac{\bar{x}}{D_p} \geq 1 \qquad (23)$$

Instead of averaging ε over the total length of a packet, Ozkaynak defines effective ε_p for void fraction evaluated at y equals $\frac{\bar{x}}{2}$. The increase in ε when $\bar{x}$ is less that D_p, decreases k_e according to equation (17). It follows that k and $\bar{h}_L$ also decrease. Including this effect of the wall for short packet residence times,

Ozkaynak recalculated values for $\bar{h}_L$, which now closely agreed with measured h [26].

Due to the success of the correction for Ozkaynak's investigation, the present study includes this modification for packets of short contact time, i.e. small penetration depth.

2.2 Proposed Modification

The data generated in this study indicates a further modification to the packet renewal model of Mickley and Fairbanks. This modification is the observation that packet properties are not constant but exhibit a time variation. The degree to which packet properties vary depends upon packet location on the tube surface and fluidizing gas velocity, as will be further discussed in Section 3.3.1. Because of this time dependence, the expressions for k_p and ρ_p as previously developed must be time averaged over the total time of contact before being used in equation (12) or (14).

3. EXPERIMENT

3.1 Test System and Experimental Procedure

3.1.1 Fluidized Bed Assembly

The fluidized bed vessel is a rectangular tank of .635 cm plexiglass with cross sectional area of .304 m x .152 m. A brass horizontal tube of .304 m length and 2.54 cm diameter is mounted at each end on teflon tracks on the inside of the side walls. The vertical position of the tube is .152 m above the distributor plate which is made of sintered steel of average porosity of 10 microns.

The fluidizing gas is air which is provided by one of two compressors of maximum capacity 3.74×10^{-2} m^3/sec and 5.85×10^{-2} m^3/sec respectively. The flow circuit from either compressor to the bed distributor plate includes passing air through: 1) a dehumidifier, 2) a nullmatic pressure regulator to maintain constant upstream pressure of approximately 2.06×10^5 N/m^2, and 3) one of three Shutte and Koerting rotameters to measure air flow. The type and maximum flow rate for the meters used is listed below:

METER	TUBE NO.	FLOAT NO.	MAXIMUM FLOW RATE
C	5-HCF	54-J	1.88×10^{-2} m^3/sec
E	6-HCF	64-J	2.94×10^{-2} m^3/sec
D	8-HCF	83-J	6.27×10^{-2} m^3/sec

Pressure drop measurements in the bed are made by positioning taps axially along the length of the bed. The taps are connected to a water manometer.

A schematic drawing of the fluidized bed is given in Fig. 1.

The solid material is a .22 m static bed of glass spheres. The properties of this material are listed in Table 2.

3.1.2 Capacitance Measurements

The capacitance probe in this work [25] incorporates a design feature not applied before to a horizontal tube geometry, Fig. 2. This feature is the implantation of two small condenser plates flush with the surface of the tube, which are connected in series with a Boonton capacitance bridge. The angular position of the plates is variable through 360° by rotating the brass tube in the teflon guides at the side walls.

Optimal condenser plate dimensions and the optimal separation distance between the plates are determined on a trial and error basis. The dimensions must be as small as possible to insure that the area of both plates is commensurate with an area equal to or less than the contact area of only one packet. At the same time, the plate dimensions must be large enough to provide a readable capacitance output signal. The chosen plate dimensions are .388 cm by .19 cm with separation distance equal to .127 cm. Magnitude of the capacitance signal is .01 pF.

A local value of capacitance provided by the condenser plates is proportional to the value of the dielectric constant of the solid material between the plates:

$$C = \eta_{dielectric} A/d \qquad (24)$$

However, η varies as the amount of solid material between the plates changes. A consequence of this is that capacitance vs. time information for the probe at any angle, can be directly related to local time variations in solids density. Determining the time variation in solids density from the capacitance time history, respective packet and bubble dwell times can be identified in the signal according to the methods of Section 3.1.4.

3.1.3 *Digital Processing*

The capacitance data is digitized and processed by a PDP-8 mini computer. The analog capacitance signal from the capacitance bridge is digitized by an analog to digital converter. The digitized signal is sampled at a rate of 100 capacitance points per second. Capacitance points are collected for fifteen seconds at a given probe angle and gas fluidizing velocity. The 15 second sampling is then repeated five times for the same angle and velocity.

The angular position of the condenser plates varies from 0° to 180° in 45° intervals measured from the vertical. At each of these probe angles, capacitance data is sampled for a total of 90

seconds for each of the air velocities 0.060 m/sec, .125 m/sec, 0.265 m/sec and .781 m/sec. Capacitance data for angles 180° to 360° is not collected. This is because symmetry of fluid dynamic and heat transfer behavior is assumed on both sides of the tube in the direction of gas flow.

The PDP-8 performs the calculations necessary for determining: 1) packet void fraction, 2) the number of packet to bubble exchanges, 3) bubble fraction time, f_0, 4) root mean square residence time, 5) average packet density and 6) time averaged density. The capacitance data is stored on paper tapes, for the purpose of submitting it to a CDC computer with plotting capability. Typical capacitance vs. time plots are given in Figures 3 to 27.

3.1.4 Analysis of the Signal

The capacitance signal is analyzed by first calibrating the signal according to an upper and lower bound. The upper bound is the capacitance value at any given probe angle corresponding to the plates fully covered by a static bed of particles. The lower bound is the capacitance value corresponding to the probe fully exposed to air. The capacitance difference between these two limits is normalized. Therefore the capacitance value representing a fully packed condition is 1.0, and that for a bubble is 0.0.

The capacitance signal oscillates between the two bounds. The excursion of the signal means that the probe is successively

exposed to packets or bubbles and intermediate conditions between these two limits. The attitude of this work is to neglect the possibility of intermediate conditions. The value of the capacitance signal is considered at all times to represent either a packet or a bubble only.

This binary interpretation demands a definition of packet in terms of a capacitance value between 0.0 and 1.0. The choice of capacitance value represents a "cutoff" between bubble and packet condition. Whatever capacitance level is chosen, capacitance values equal to or exceeding this level correspond to packet, and capacitance values less than this level correspond to bubble. The choice of capacitance definition for packet is arbitrary. Therefore, three definitions are successively employed to determine the sensitivity of the values of the calculated quantities to the arbitrary choice of packet definition. These packet definitions are the normalized capacitance levels: 0.333, 0.500, and 0.667, as shown in Figure 2.

The justification for this binary approach is the fact that it has successfully been used elsewhere. For example in boiling heat transfer the gas and liquid phases are considered to be completely disparate, describing a separated model. In boundary layer theory, the effect of viscosity exists on only one side of the boundary layer, and not the other.

Finally, this binary approach is justified on the basis of providing a simple and workable model. From this model, at the very least, qualitative information and trends for comparison purposes can be inferred, as will be discussed in Sections 3.3.2-3.3.3. Moreover, considering the order of magnitude of calculated average and local heat transfer coefficients, indicates that, at least for this study, useful quantitative information can be derived from a binary approach.

3.2 Results

3.2.1 Capacitance Signals

Capacitance vs. time data is plotted in Figures 3 to 27 for all run conditions listed in Table 1. Examination of the plots reveals three types of signal patterns which are described below.

First a "constant" capacitance signal approximately equal to 1.0 in value is displayed by the probe in Figures 3, 4 and 8. This flat signal occurs when the probe is at or near the twelve o'clock position for low fluidizing velocities. The degree of "noise" to the signal increases with gas velocity until, as in Figure 7, the signal no longer has a flat character.

The second pattern, as in Figure 23 is a signal which rapidly oscillates between 1.0 and 0.0 on the normalized capacitance scale. The mean capacitance value is noticeably lower than the constant capacitance value for the first type of signal.

Thirdly, the last type of signal includes all patterns intermediate to the first two patterns. This signal as in Figure 15 does not oscillate as vigorously as the second type, but is not as "flat" as the first. The mean capacitance value is bounded by the mean capacitance values of the other two signal categories.

3.2.2 *Void Fraction*

The time avaraged void fraction of the reduced capacitance vs. time signal is plotted in Figure 28, corresponding to the following conditions:

RUN	PROBE ANGLE (DEGREE)	VELOCITY (M/SEC)
1,2,3	0°	0.060, 0.265, 0.783
4,5,6	45°	0.060, 0.265, 0.783
7,8,9	90°	0.060, 0.265, 0.783
10,11,12	135°	0.060, 0.265, 0.783
13,14,15	180°	0.060, 0.265, 0.783

At the top of the tube, for probe angles 0°, 45° and 315°, the void fraction successively increases as gas velocity increases. For probe angle 315°, identical behavior to that at probe angle 45° is assumed and plotted accordingly. Henceforth in all polar plots, all points from 180° to 360° are assumed identical to corresponding points between 0° and 180°, as discussed in Section 3.1.3.

For the probe oriented at an angle of 90°, there is a minimum void fraction for the intermediate velocity of .265 m/sec. As at

the top of the tube, maximum void fraction occurs for the highest gas velocity of .783 m/sec.

For probe angle 135°, a minimum void fraction occurs for the intermediate velocity as for the 90° case. However, distinct from the other angles considered thus far, the maximum void fraction occurs for the smallest gas velocity of .060 m/sec.

At the bottom of the tube for probe angle 180°, the void fraction successively decreases as gas velocity increases.

3.2.3 Replacement Frequencies

The number of packet to bubble exchanges is plotted in Figures 29, 30 and 31 for the probe angle positions and gas velocities listed in Section 3.2.2. In addition, for each angle and velocity condition, the replacement frequency is calculated according to all three packet definitions, Section 3.1.4.

As gas velocity increases for probe angles 0° and 45°, the number of packet to bubble exchanges increases from 0 to a finite value, depending upon the packet criterion used. Since the number of packet to bubble exchanges is proportional to the number of bubbles, this trend is consistent with the increase in void fraction at these angles, as discussed in 3.2.2.

For angles 90° and 135°, the minimum replacement frequency as well as minimum void fraction, Section 3.2.2, occurs for the

intermediate velocity .25 m/sec. This means that when the minimum number of bubbles occurs, the void fraction is minimum.

The maximum replacement frequency for both 90° and 135° occurs at the minimum gas velocity. For this same minimum velocity, the void fraction is maximum at 135°, corresponding to the maximum number of bubbles at the probe. However at 90° for the minimum velocity .060 m/sec, the void fraction is not correspondingly a maximum, Section 3.2.2. The reasons will be discussed in Section 3.2.4.

The greatest effect of the choice of packet definition on the particular value of replacement frequency occurs at the 180° position for the lowest gas velocity. Using the "0.333" packet criterion the number of packet to bubble exchanges continuously decreases as gas velocity increases. This is paralleled by the decrease in void fraction as velocity increases, Section 3.2.2. Using the "0.500" packet criterion, the number of packet to bubble exchanges remains approximately constant for the range of gas velocities considered. For the "0.667" packet definition criterion, the number of packet to bubble exchanges continuously increases as gas velocity increases.

These three different trends are the result of three different packet definitions arbitrarily applied to a type 2 signal at 180° and velocity .060 m/sec. The capacitance signal, Figure 23, is highly oscillatory with low mean capacitance, or density, value.

Thus, the number of times the signal traverses the 0.333 normalized capacitance level is much greater than the number of times the signal crosses the 0.667 capacitance level. This produces the disparity between the 0.333 and 0.667 criteria replacement frequency shown in Figure 29. Therefore the contradictory trends in replacement frequency vs. velocity are artifacts of the analysis. Any interpretations of conditions at 180° for low gas velocity should begin with the fundamental observation of highly fluctuating density of low mean value.

3.2.4 Fractional Contact Times

f_o, the fraction of the total sample time that the probe is covered by bubbles, is plotted in Figures 32 to 36 for the run conditions listed in Table 1.

At probe angle 0°, f_o increases directly as velocity increases above a "critical" velocity of .267 m/sec. Below this velocity as discussed in Section 3.2.3 and indicated in Figure 29, there are zero packet to bubble exchanges. From Figures 3 and 4, it is seen that at 0° for velocities 0.60 and .120 m/sec, the probe is continuously exposed to packet, using any of the three packet criteria. Accordingly, there are no bubbles and f_o is zero at these velocities.

For the probe oriented at 45°, f_o increases continuously as gas velocity increases, similar to the 0° case. A zero value of f_o at 45° for velocity .060 m/sec is consistent with Figure 29, discussed

in 3.2.3, and shown in Figure 8.

In Figure 34, a minimum value of f_o for probe angle 90°, occurs at gas velocity .267 m/sec. This is consistent with: 1) the observation of minimum number of bubbles at 90° for gas velocity .267 m/sec, Figure 30, and 2) the observation of minimum void fraction at 90° for gas velocity .267 m/sec, Figure 28.

As mentioned in Section 3.2.3, the maximum void fraction for probe angle 90° does not occur at velocity .060 m/sec, Figure 28, although the number of packet to bubble exchanges is maximum at this velocity, Figure 29. In fact, the maximum void fraction occurs for velocity .765 m/sec, Figure 28, since f_o, for the velocity range .060 m/sec to .765 m/sec, is greatest at velocity .765 m/sec, Figure 34.

For probe angle 135°, f_o asymptotically increases with gas velocity, Figure 35. It was previously observed that the maximum void fraction, Figure 28, and maximum number of bubbles, Figure 29, prevails for velocity .060 m/sec. However, in Figure 35, it appears that the minimum value of f_o at .060 m/sec is inconsistent with maximum void fraction and maximum replacement frequency. When a fourth variable is considered, i.e. average packet density, Figure 45, it is seen that packets are less dense at velocity .060 m/sec than at velocity .765 m/sec. This accounts for larger void fraction at .060 m/sec than void fraction corresponding to .765 m/sec, Figure 29.

For probe angle 135° at velocity .267 m/sec: 1) void fraction is minimum, Figure 28, and 2) replacement frequency is minimum, Figure 30. These observations are consistent with minimum f_o, for the velocity range .267 to .765 m/sec, corresponding to velocity .267 m/sec, Figure 35.

f_o asymptotically decreases as gas velocity increases for probe angle 180°, Figure 36. This is paralleled by the decrease in void fraction with increasing velocity, Figure 28. This trend is also consistent with the decrease in replacement frequency for the 0.333 packet criterion with increasing velocity, Figures 29 to 31.

3.2.5 Residence Times

In Figures 37 and 38 for probe angles 0° and 45°, the root mean square residence time, equation 11, decreases as gas velocity increases. This is because the number of bubbles increases dramatically as velocity increases, indicated by Figures 29-31. The implication of more bubbles in the total span of the sample time is that packets are carried more frequently to and from the probe. The greater the packet replacement frequency, the smaller θ_p'.

Similarly in Figure 39, the variation of θ_p' with velocity for angle 90° is inversely proportional to the variation of replacement frequency with velocity, Figures 29 to 31.

Distinct from the previous cases, at angle 135°, the root mean square residence time vs. velocity behavior, Figure 40, is not

inversely proportional to the replacement frequency vs. velocity behavior, Figures 29 to 31.

The maximum residence time at 135° occurs for velocity .060 m/sec. This is because, as Figure 18 indicates, the individual dwell times of the packets are small. Vanishingly small packet dwell times produce a small value for the denominator, $\Sigma\theta_p$, for the expression θ_p'. The result is a large numerical value for θ_p' at velocity .060 m/sec.

For the probe at 180°, the asymptotic increase in root square residence time with increasing velocity, Figure 41, is inversely proportional to the variation in replacement frequency.

3.2.6 Average Packet Densities

As a result of the flat or tending to flat capacitance signals, Figures 3 to 12, the average packet density at 0° and 45° are high and relatively invariant with velocity, Figures 42 and 43.

For both 90° and 135°, Figures 44 and 45 indicate a local maximum in packet density corresponding to velocity .267 m/sec. This is consistent with the minimum void fraction at 90° and 135° each occurring at velocity .267 m/sec.

In Figure 49, void fractions for 90° and 135° at .765 m/sec are greater than the respective minimum values at .267. However in Figures 44 and 45, packet densities at .765 m/sec are equal to

or greater than the corresponding densities at .267 m/sec. The inconsistency arises from void fraction calculations integrating over the total capacitance signal, and packet density calculations integrating over the "packet" portion of the capacitance signal only. If the bubble durations, Figures 34 and 35, are considered, the void fraction and packet density behavior at 90° and 135° are compatable.

The increase in packet density at 180° as velocity increases, Figure 46, parallels the decrease in void fraction, Figure 28.

3.3 Applications to Heat Transfer Model

3.1.1 Packet Properties

The expression for heat transfer coefficient according to the packet renewal model, equation 12, is a function of certain thermal/physical quantities of a packet. These quantities include the following: 1) time averaged packet density, 2) thermal conductivity, equation 17, based on time averaged packet density, 3) fractional bubble contact time and 4) root mean square residence time.

The mutual variation of k_p, ρ_p, θ_p' and f_o vs. probe angle for gas velocity held constant at .060 m/sec, .265 m/sec, and .765 m/sec respectively, is plotted in Figures 47 to 49. The increase in f_o for increasing probe angle tends to decrease $\bar{h}_L$, equation 12. However, the decrease in θ_p' vs. angle tends to increase $\bar{h}_L$. The effect of decreasing thermal conductivity and packet density for

increasing angle is to decrease $\bar{h}_L$.

The variation of k_p, ρ_p, θ_p' and f_o with increasing velocity for fixed probe angle of 0°, 90°, and 180° respectively, is plotted in Figures 50 to 52. The opposite trends in f_o and θ_p' with increasing velocity oppositely effect $\bar{h}_L$ according to equation 12. Time averaged packet density and packet thermal conductivity generally increase with increasing velocity, tending to increase $\bar{h}_L$.

In summary, depending upon the fluid dynamic behavior of the bed at any given angle on the tube surface for any given gas velocity, one of the effects of ρ_p, θ_p' or f_o is dominant. Whichever of these effects is dominant, primarily determines the value of local heat transfer coefficients.

3.3.2 *Local Heat Transfer Coefficients*

Using the generated data for root mean square residence time, time averaged packet density, and packet thermal conductivity, local heat transfer coefficients are predicted by the packet renewal model, equation 12. The experimental error associated with these calculations is approximately 20%.

Figure 59 is a plot of calculated heat transfer coefficients for maximum gas velocity u = .783 m/sec. An approximately uniform distribution of heat transfer coefficients is obtained around the tube, for any of the three packet criteria. At each of the angles

considered, the percent deviation in calculated heat transfer coefficient for the three different packet criteria is less than 33%. Qualitatively, this predicted heat transfer behavior for a horizontal tube with high fluidizing gas velocity supports experimental observation [34,35,36].

For intermediate and low gas velocities, there are results from previous experimental work to measure heat transfer coefficients around a horizontal tube [34,35,36]. The results of this work show that the site for maximum heat transfer activity on the tube surface is the 90° position. Moreover the local minima in heat transfer coefficients exist in the upstream and downstream positions. However the local minimum at 0° has been measured to be smaller than that at 180°.

In the present study, predicted heat transfer coefficients for intermediate velocity u = .521 m/sec are shown in Figure 56. Heat transfer coefficients for the 0.500 and 0.667 packet criteria confirm the experimental findings [34,35,36] discussed above. For u = .52 m/sec, the maximum percent variation in heat transfer coefficient predicted for the three packet criteria is 40%.

Calculated heat transfer coefficients for u = .265 m/sec are plotted in Figure 55. Heat transfer coefficients for the 0.667 packet criterion, produce the trend predicted by the measurements of earlier experimental work [34,35,36]. The maximum percent variation in heat transfer coefficients calculated for the three

packet definitions is 95%, at gas velocity .265 m/sec.

For u = .125 m/sec and u = .060 m/sec, experimental heat transfer data for approximately the same fluidized bed system as used in the present study is available [27,37]. The differences between the two systems include: 1) a difference of .076 m in static bed height and 2) a difference of .076 m in tube elevation. Both the static bed height and tube height are lower for the bed used by Chandran [37] and Baker [27].

Predicted and measured heat transfer coefficients for u = .125 m/sec are plotted in Figure 54. For probe angles 0° and 45°, the packet renewal model underpredicts heat transfer coefficients. At 90°, the predicted and measured heat transfer coefficients show agreement to within 10% for the 0.667 packet definition. However, the packet renewal model overpredicts heat transfer at 135°, as shown in Figure 54. Similarly, heat transfer coefficients at 180° for the 0.333 and 0.500 packet definitions are overpredicted by the packet renewal model. But, for the 0.667 packet criterion at 180°, the calculated heat transfer coefficient underestimates heat transfer. The maximum percent variation in local heat transfer coefficients using the three packet definitions is 77% at 180°.

For u = .060 m/sec, the packet renewal model underpredicts heat transfer at 0°, 45°, 90°, and 180° as shown in Figure 53. At 135°, the packet renewal model overestimates heat transfer for

the 0.500 and 0.667 packet criteria, but underestimates for the 0.33 criterion. The maximum percent variation in calculated heat transfer coefficients using the three packet criteria is 179% at 135°.

3.3.3 Average Heat Transfer Coefficients

Average heat transfer coefficients for a horizontal tube immersed in a fluidized bed are measured by Baker [27] and Chandran [37]. The differences in these respective fluidized beds and the present system used in this study are noted in Figure 58.

Using the packet renewal model, average heat transfer coefficients for the entire tube surface are calculated assuming constant tube temperature. The variation in average heat transfer coefficient vs. velocity is plotted in Figure 58. Baker's and Chandran's data are included in Figure 58, and compared to the calculated heat transfer coefficients.

The calculated average heat transfer coefficients are bounded above by Chandran's extrapolated data. The calculated points are bounded below by Baker's data. Figure 58 suggests, at least for this study, that the packet renewal model does give reasonable order of magnitude prediction for average heat transfer coefficients. However, the agreement between predicted and measured data does not necessarily suggest that the model is physically correct. The reasonable values for calculated average heat transfer

coefficients may be the fortuitous result of cancellation of errors of the predicted local heat transfer coefficients as they are averaged around the tube.

4. CONCLUSIONS

4.1 Character of Fluidization

4.1.1 Interdependence of Properties

The fluid dynamic properties of void fraction, packet replacement frequency, fractional bubble contact time, root mean square residence time, and average packet density vary dependently around the circumference of the tube. These properties are a strong function of angular position on the tube surface and gas fluidizing velocity. Moreover these properties mutually influence heat transfer characteristics.

4.1.2 Bubble Production

The data for packet replacement frequency, described in Section 3.2.3 is explained by two sources of bubble production.

Source 1 arises from the obstructed gas pocket at the bottom of the tube [38]. The gas film is shed at the sides of the tube in the form of bubbles.

In Section 3.2.2, it was shown that at 180°, void fraction decreases with velocity and packet density increases with velocity. This means that the gas pocket of Source 1 becomes more dense and less effective for shedding bubbles. A result is the decrease in the number of packet to bubble exchanges as velocity increases at 180°.

Source 2 for bubbles is the distributor grid [39]. The number of bubbles evicted from the distributor varies with velocity according to:

$$uA = u_{mf}A + n\bar{V}_b \quad .$$

The increase in number of bubbles with velocity explains the increase in bubble activity at 0° and 45°.

It is seen that these two bubble sources behave oppositely with increasing velocity. Therefore it is possible that the competition of the two will produce a minimum amount of bubble activity for some intermediate gas velocity. This is in fact the case at 90° and 135°, as discussed in Section 3.2.3.

4.1.3 Regimes of Fluidization

The signal 1 pattern of capacitance vs. time behavior, Section 3.2.2, corresponds to an environment of: 1) high density, 2) low void fraction, 3) negligible to zero bubble activity, and 4) maximally large residence times. This kind of environment pertains to 0°, 45° and 315° for low velocities. A fluidized regime with these characteristics is described as solids-dense.

The signal 2 pattern of capacitance vs. time behavior, Section 3.2.3, corresponds to another type of fluidized regime. This regime is characterized by: 1) highly fluctuating density of low mean value, 2) high void fraction, 3) extensive bubble activity,

and, 4) vanishingly small root mean square residence time. These characteristics describe a disperse zone or lean emulsion of gas and single particles. This regime prevails at the bottom of the tube for low velocities.

The third type of capacitance vs. time signal, Section 3.2.1, refers to a third fluidized regime. This regime includes all fluidized states intermediate to 1) a highly solids-dense condition and 2) a low density, gaseous emulsion condition. All the intermediate states exhibit, in combination, both features 1) and 2) in varying strengths. Therefore all these states are characterized by some degree of inhomogeneity. At 90°, for intermediate and high gas velocities, the character of fluidization is greatly inhomogeneous.

The above argument for three regimes is paralleled by the flow pattern in a heated vertical channel. In the single phase liquid region at the lower entrance to the channel, the mass quality equals zero. Here the liquid is heated to the boiling point temperature. The quality increases as more heat is absorbed by the liquid as it flows upward through the channel. Bubbly flow, slug flow, and annular flow successively occur at higher elevations in the channel. Eventually as the quality approaches unity, drop flow is established.

In this present study, the fluidized analogy to the single phase liquid region is the dense zone on top of the tube.

Fluidized states of varying inhomogeneous character of the third type of regime, correspond to the bubbly flow, slug flow, and annular flow regions. Lastly, the disperse emulsion zone at the bottom of the tube corresponds to drop flow in the heated vertical channel.

4.2 Validity of Packet Renewal Model

4.2.1 Character of Packets

The capacitance vs. time plots indicate that the capacitance signal is not constant during any defined packet contact time. The variation in capacitance reflects a time variation in packet density. Changes in packet density are the result of changes in packing state of the component particles. But any variation in packing state is produced by relative particle motion within the packet. This relative particle motion physically suggests "squirming" packets in contact with the tube surface.

Originally, Mickley and Fairbanks assumed that a packet is a loosely locked aggregate of particles of zero relative velocity and constant void fraction [16]. Therefore, a squirming packet is a significant departure from the previous notion of a packet.

The expression for local heat transfer coefficient is derived by summing heat transfer to individual packets. Since packet density and packet thermal conductivity vary during the time of heat

conduction to these packets, the appropriate values to use in equation 12 are the time averaged values for ρ_p and k_p.

The case for time varying packet properties is suggested in Reference [24]. However the argument in the present study is stronger because of the improved capacitance probe used.

Packet properties ρ_p, k_p, and θ_p' are sensitive to the choice of packet definition. This study indicates that the minimum density value which defines a "packet" is not a matter of arbitrary choice.

4.2.2 Heat Transfer and Regimes of Fluidization

Qualitatively, heat transfer coefficients calculated by the packet renewal model compare favorably with observed trends for intermediate and high velocities. This observation holds true for packets defined by the 0.667 criterion.

At low velocities, measured heat transfer data is available for comparison with calculated heat transfer coefficients. It is observed that calculated local heat transfer coefficients favorably agree with measured values when the local regime of fluidization is relatively inhomogeneous, as at 90° for velocity .120 m/sec. However, calculated local heat transfer coefficients do not agree with measured data when the local regime of fluidization is solids-dense or lean emulsion condition.

This lack of agreement arises from the assumptions inherent in the expression for heat transfer coefficient based upon a packet renewal mechanism. The analysis for local heat transfer coefficient, Section 3.3.2, includes the unsteady conduction of heat into packets of finite contact time with the surface. The contact time is assumed finite since packets are presumably knocked off the surface by bubbles. If the fluidized environment does not display the characteristics of surface renewal behavior as for type 1 and 2 regimes, then this analysis for $\bar{h}_L$ is not valid.

At the top of the tube for low velocities, heat transfer coefficients calculated by the packet renewal model underpredict heat transfer. This is because the calculated heat transfer coefficient is based upon a packet renewal mechanism, yet no packet renewal mechanism exists at the top of the tube for low velocities. As discussed in Section 4.1.3, the type 1 fluidized regime which prevails at the top of the tube, is a dormant, dense zone of solid particles.

At the bottom of the tube for low velocities, most of the calculated heat transfer coefficients overpredict heat transfer. Again, this is because no packet renewal mechanism takes place. Instead, the environment is a type 2 fluidized regime of lean, gaseous emulsion.

In summary, the packet renewal mechanism applies to the fluid-

ized regime at only certain local positions around the horizontal tube. Only at these sites, does the packet renewal model adequately predict heat transfer coefficients. In spite of this limited applicability, the packet renewal model, at least for this work, appears to reasonably predict average heat transfer coefficient. This may be due to a fortunate cancellation of errors in the expressions for local heat transfer coefficient as they are averaged around the tube.

5. RECOMMENDATIONS

5.1 Heat Transfer Mechanism of Homogeneous Regimes

The results of this work suggest further topics of inquiry relating to the mechanism of heat transfer for a horizontal tube in a fluidized bed. In order to successfully predict heat transfer coefficients, it is necessary to determine the processes around the tube by which transfer of heat is achieved. The present study indicates that heat transfer by packet renewal takes place at only certain tube positions for certain velocities. This study does not investigate the mechanism of local heat transfer from those sites on the tube exposed to solids-dense or lean emulsion fluidized environments. Descriptions of these mechanisms are required to formulate a physically complete and accurate analytical model. Therefore, investigation of the mode of heat transfer to the homogeneous zones is recommended.

5.2 Multiphase Thermal Conduction

The calculation of heat transfer coefficient by the packet renewal model requires an expression for packet thermal conductivity. This thermal conductivity must necessarily be calculated for a multiphase medium since a packet is composed of solid particles and interstitial gas.

The model of Kunii and Smith [31] and Yagi and Kunii [32] was

used in this work, Section 2.1.3.4. This model evaluates thermal conductivity for a gas/solid two phase medium. In this medium, Kunii's model assumes there is always some extent of particle to particle contact, which depends upon the particular packing state.

The present work concludes that packets at the bottom of the tube are dilute with high void fraction. For these cases, the thermal conductivity of a very low density packet may not be adequately described by the Kunii model based on touching particles. Specifically, if the particles are not in contact with each other, the terms ϕ and β in equation (17) are increased. Both ϕ and β will increase since they are a measure of gas thickness between neighboring particles.

The refinement of Kunii's model for a dilute medium will effect the values for heat transfer coefficients at the sites exposed to dilute packets. Moreover, the use of different existing models for two phase k_e will influence the final values for calculated heat transfer coefficients. These effects should be investigated, since an accurate model for two phase k_e is required for accurately predicting heat transfer coefficients.

TABLE - 1

TEST RUN CONDITIONS

Runs	Fluidizing Agent	Fluidizing Solid	Static Bed Height	Probe Height	Probe Angle From Vertical	Range of Air Velocities m/sec				
1-5	Air	Glass Spheres GT-2	.228 m	.152 m	0°	0.060	0.125	0.265	0.521	0.781
6-10	Air	Glass Spheres GT-2	.228 m	.152 m	45°	0.060	0.125	0.265	0.521	0.781
11-15	Air	Glass Spheres GT-2	.228 m	.152 m	90°			0.265	0.521	0.781
16-20	Air	Glass Spheres GT-2	.228 m	.152 m	135°	0.060	0.125	0.265	0.521	0.781
21-25	Air	Glass Spheres GT-2	.228 m	.152 m	180°	0.060	0.125	0.265	0.521	0.781

TABLE - 2

PROPERTIES OF SOLID PARTICLES

Quality of Particles	GT-2 Tech. Qual. Glass Beads
Mean Particle Diameter (cm)	0.024
Variance (cm^2) U.S. Sieve Size	6.01×10^{-4}
Particle Thermal Conductivity (watt/m°K)	0.89
Particle Heat Capacity (J/kg°K)	0.75
Particle Density (kg/m^3)	2467.0
Bed Void Fraction	
Loose Packed	0.390
Dense Packed	0.352
Bed Density (kg/m^3)	
Loose Packed	1504.0
Dense Packed	1598.0
Minimum Fluidization Velocity (m/sec)	0.058

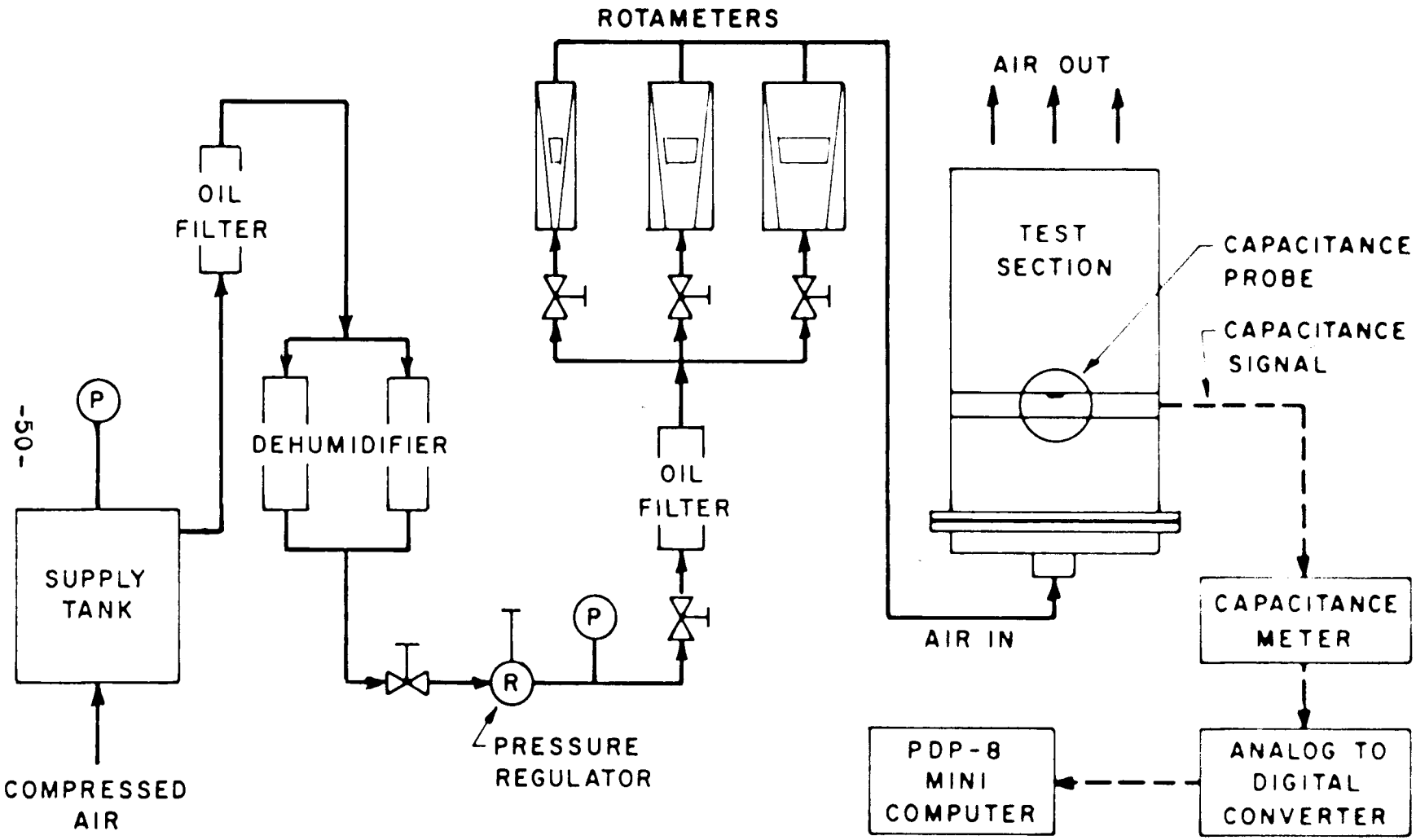

Figure 1 - Flow diagram of the experimental apparatus and instrumentation

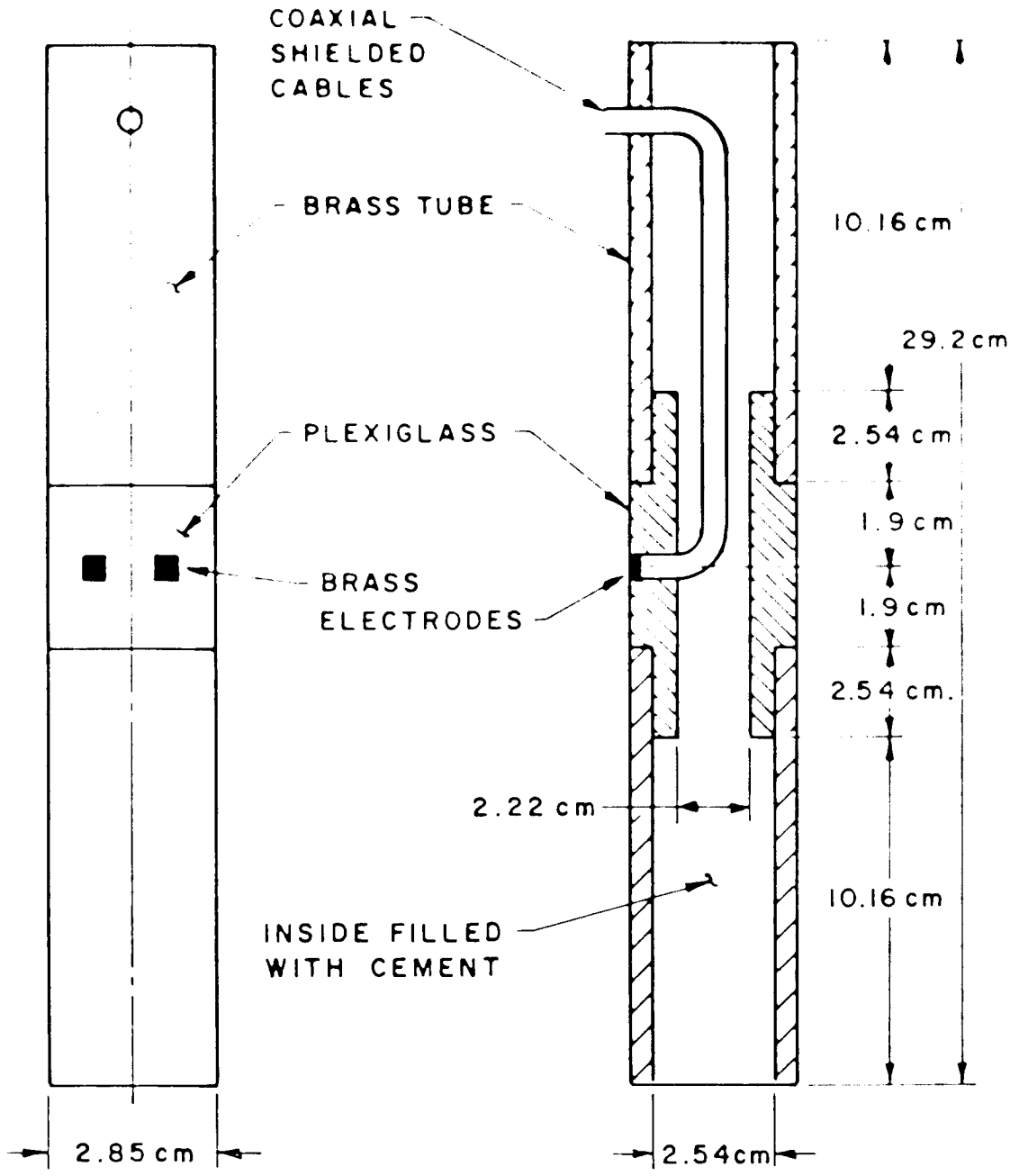

Figure 2 - Capacitance probe

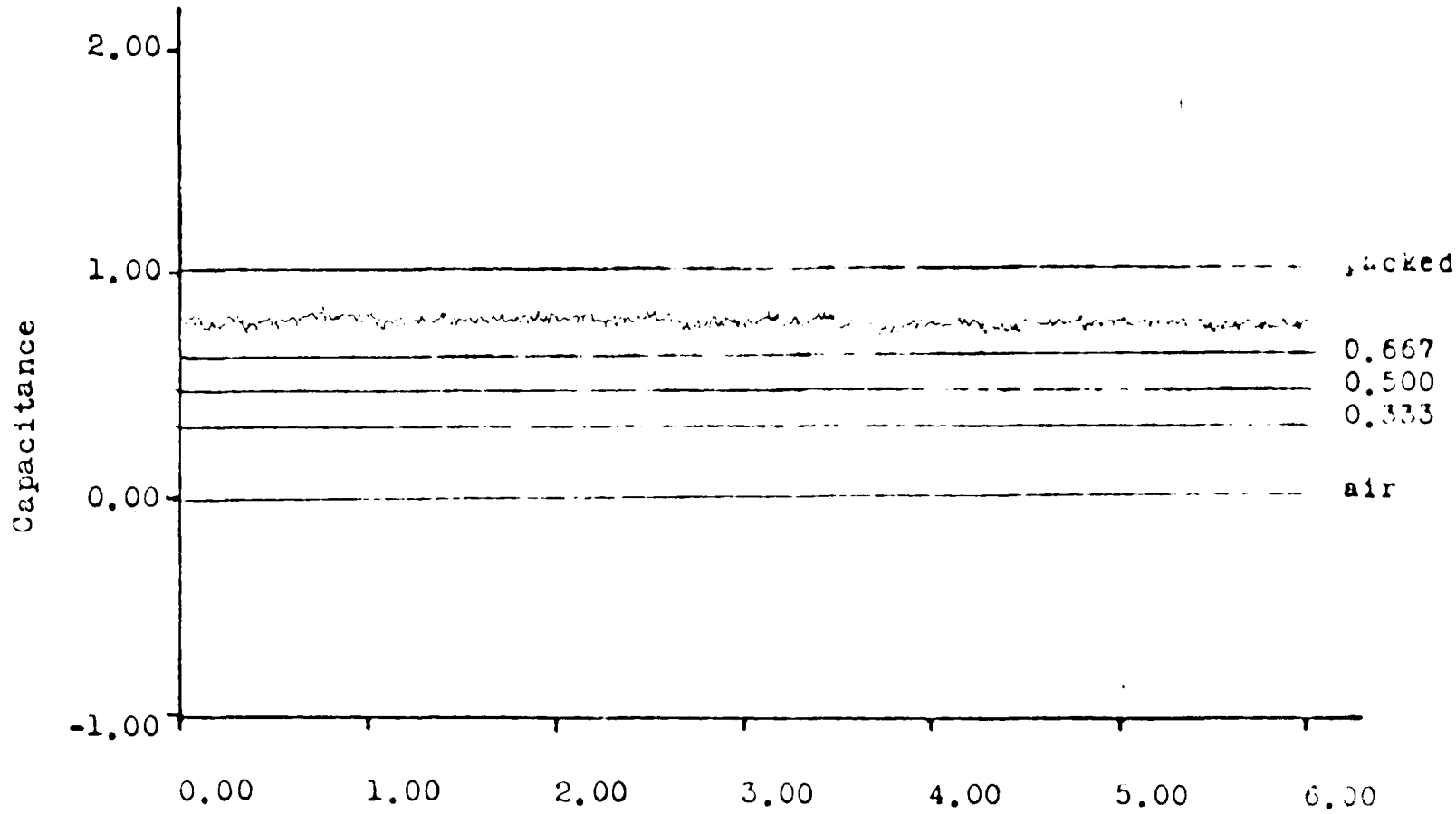

Angle=0^{o} Velocity=0.06 c/sec

Figure 3 - Capacitance Signal vs. Time

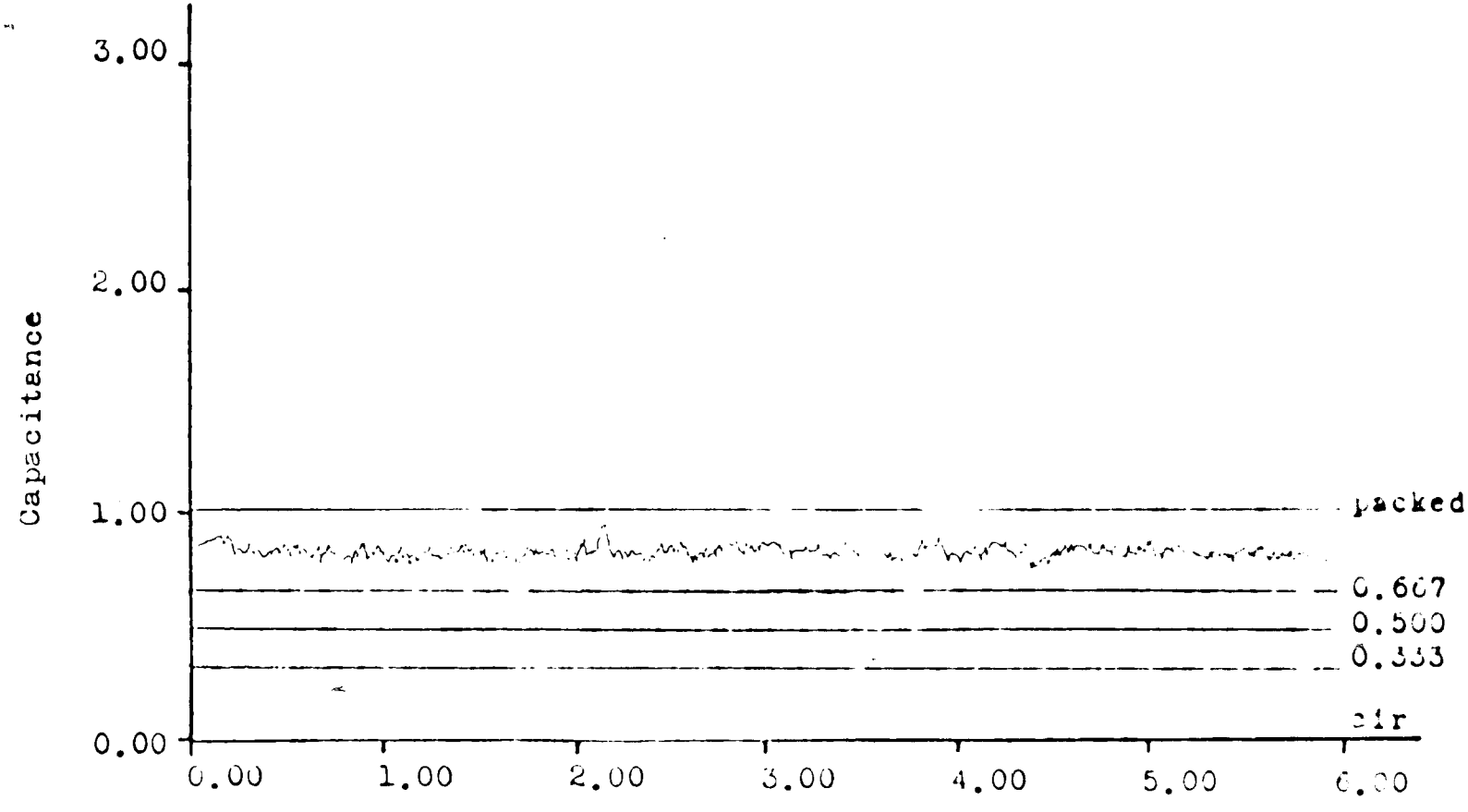

Angle=0° Velocity=0.125 cm/sec

Figure 4 - Capacitance Signal vs. Time

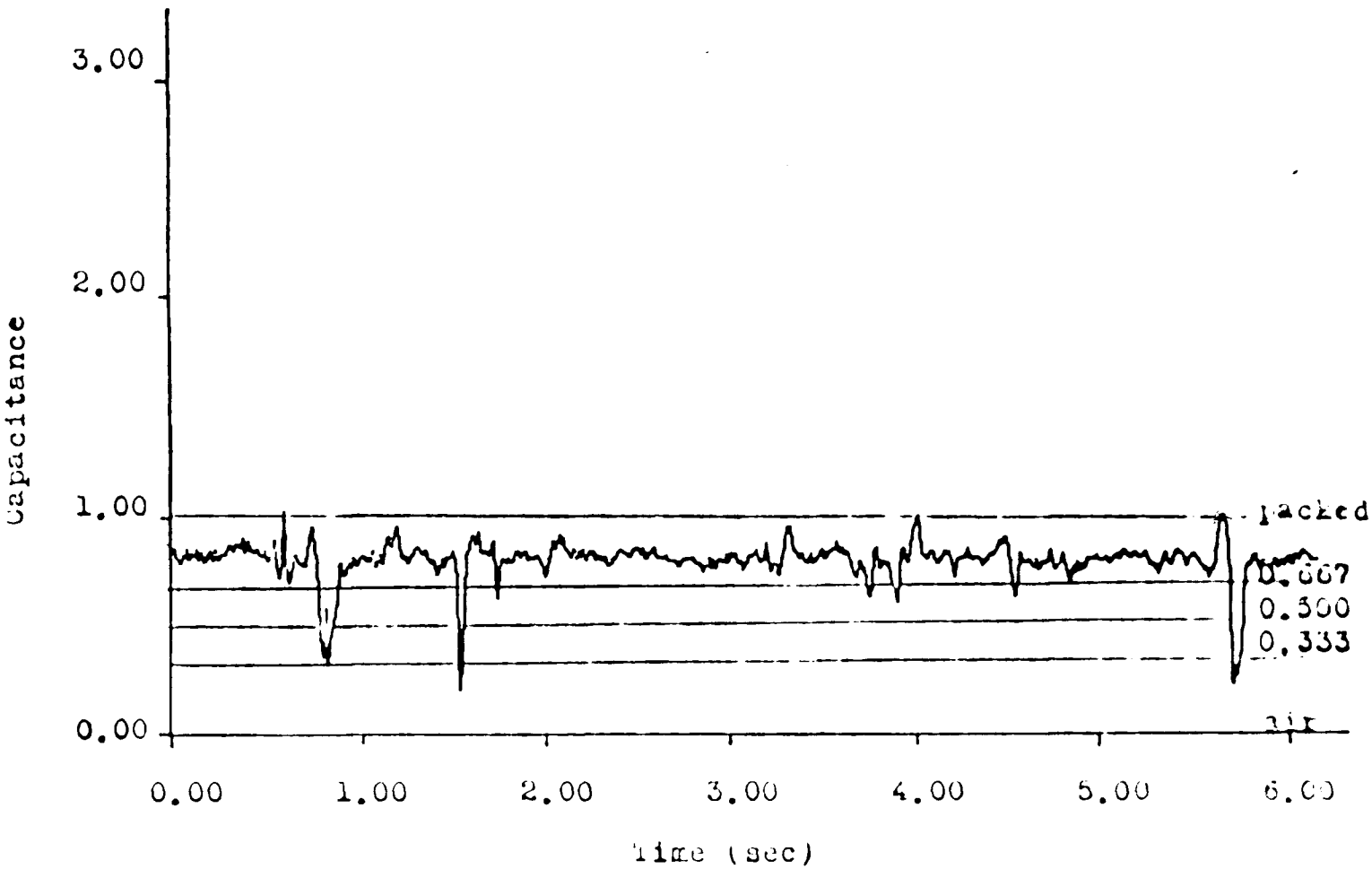

Angle=0° Velocity=0.265 m/sec

Figure 5 - Capacitance Signal vs. Time

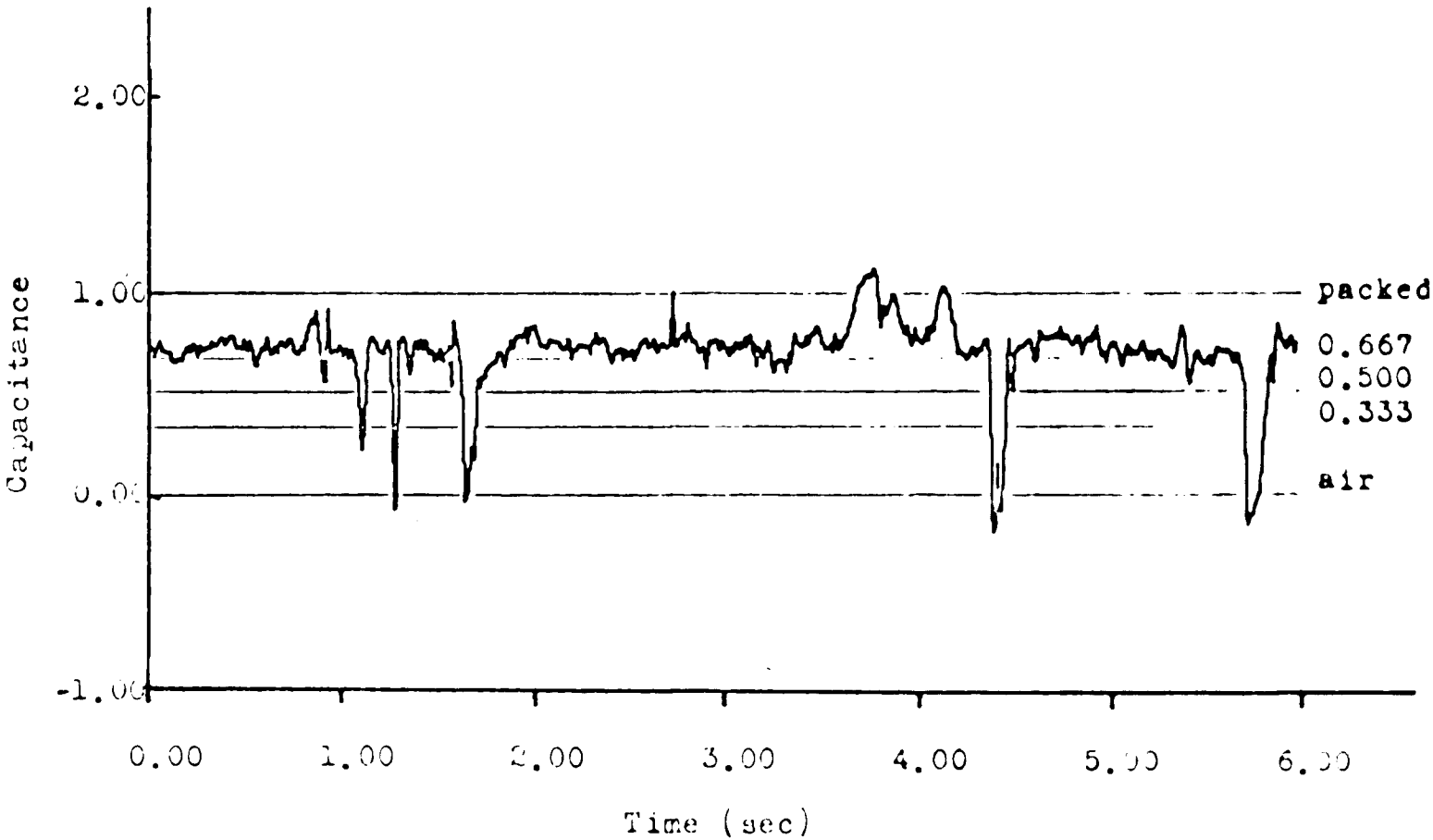

Angle=0° Velocity=0.521 m/sec

Figure 6 - Capacitance Signal vs. Time

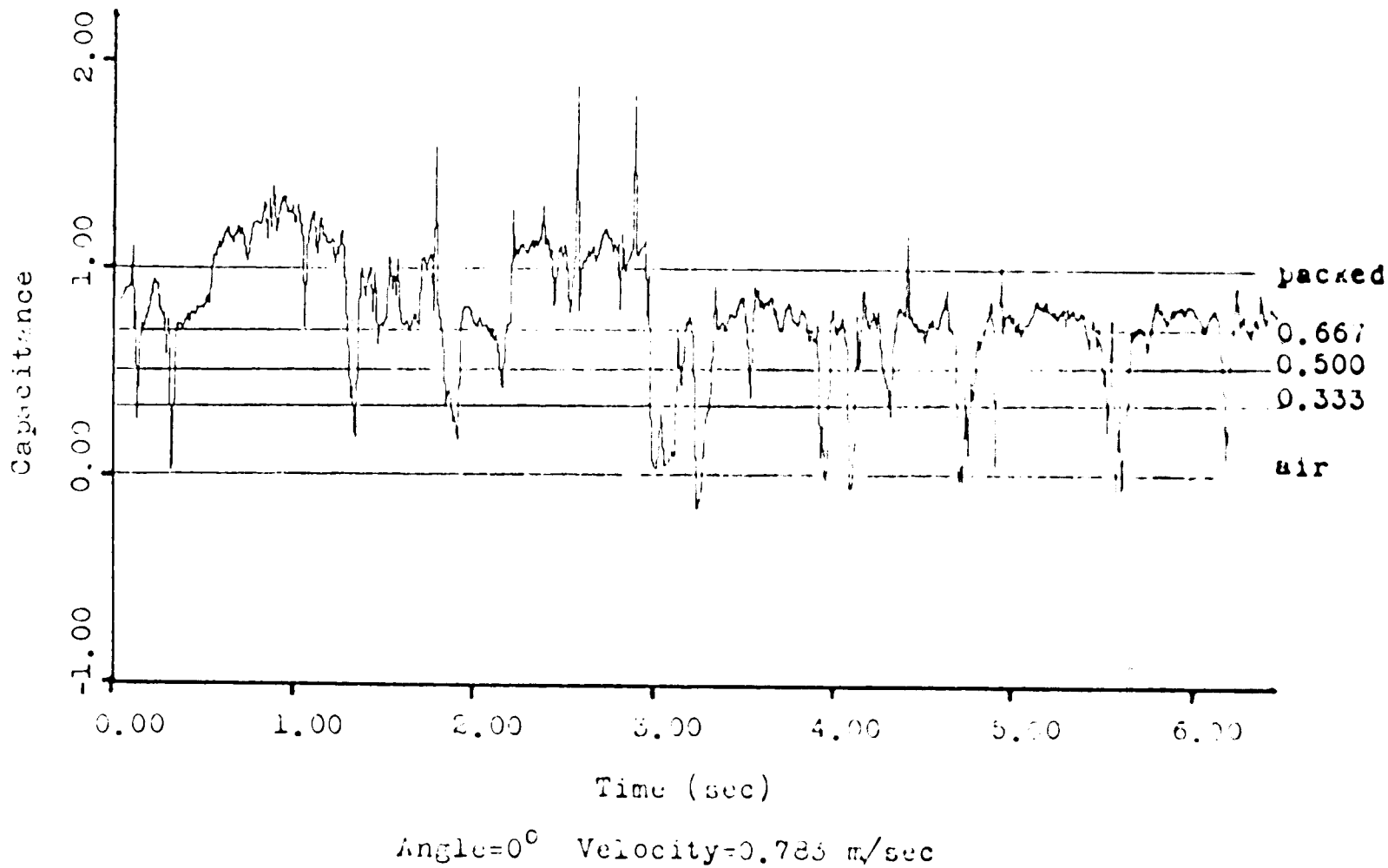

Figure 7 - Capacitance Signal vs. Time

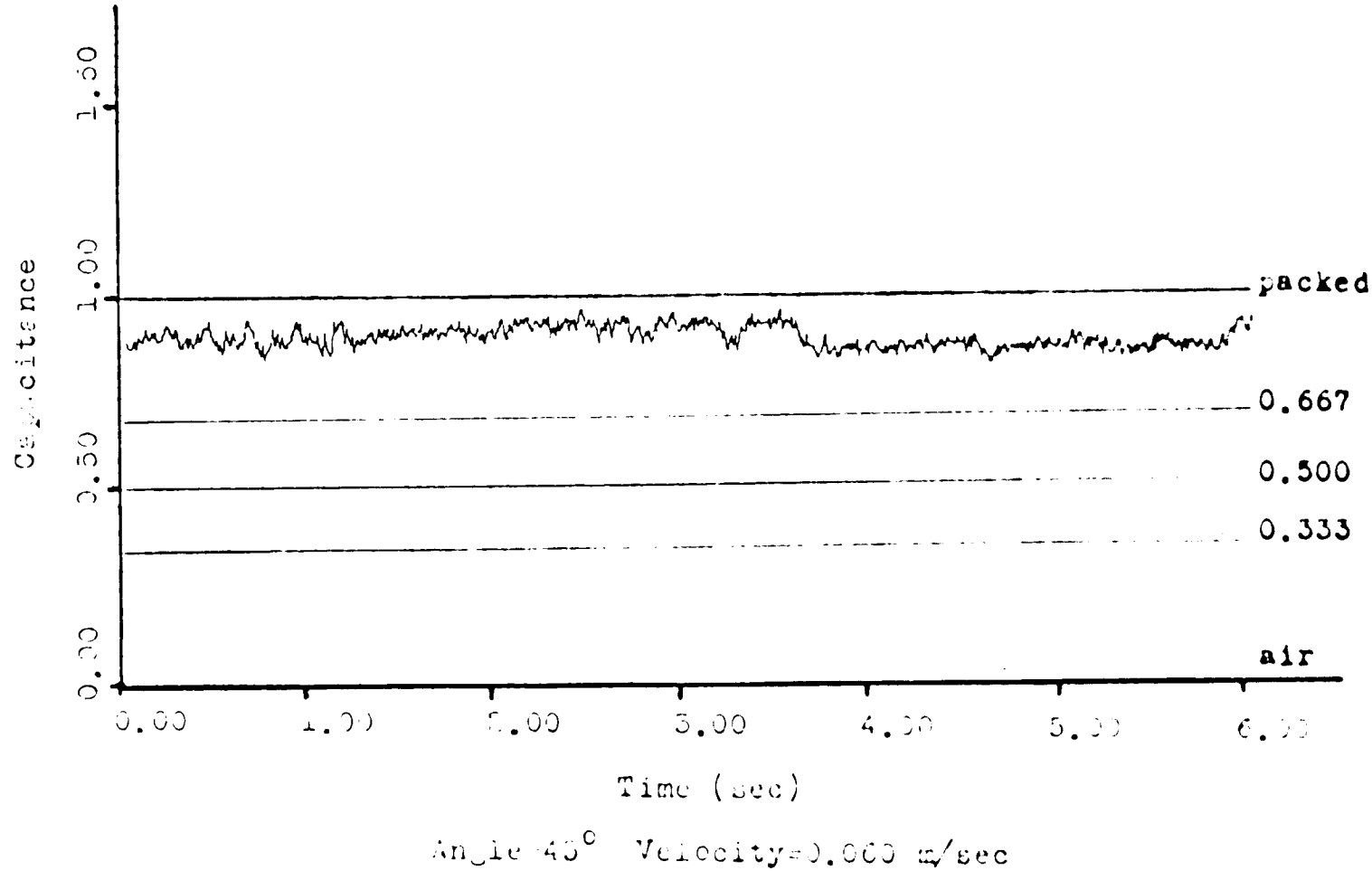

Figure 8 - Capacitance Signal vs. Time

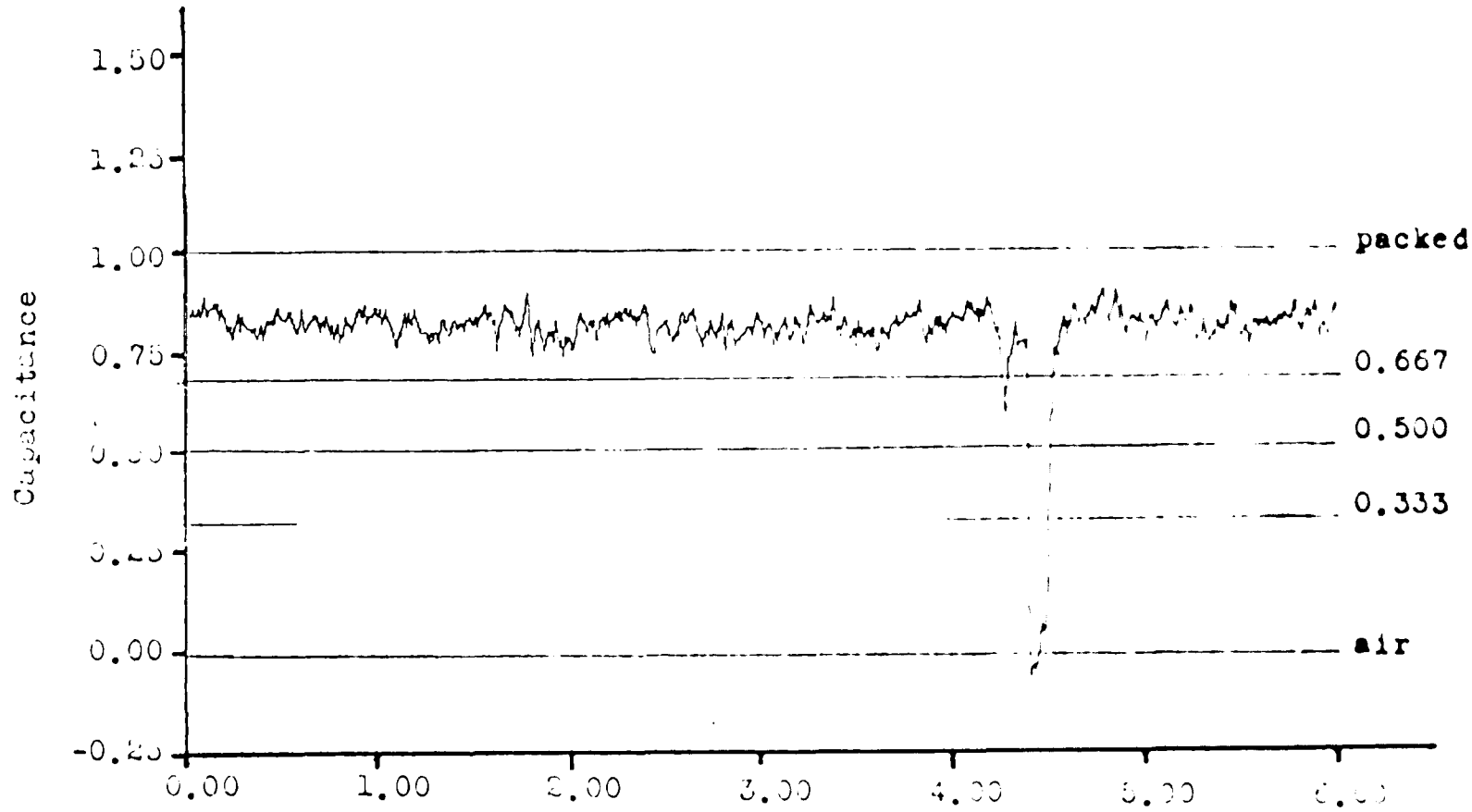

Angle=45° Velocity=0.1[illegible] in/sec

Figure 9 - Capacitance Signal vs. Time

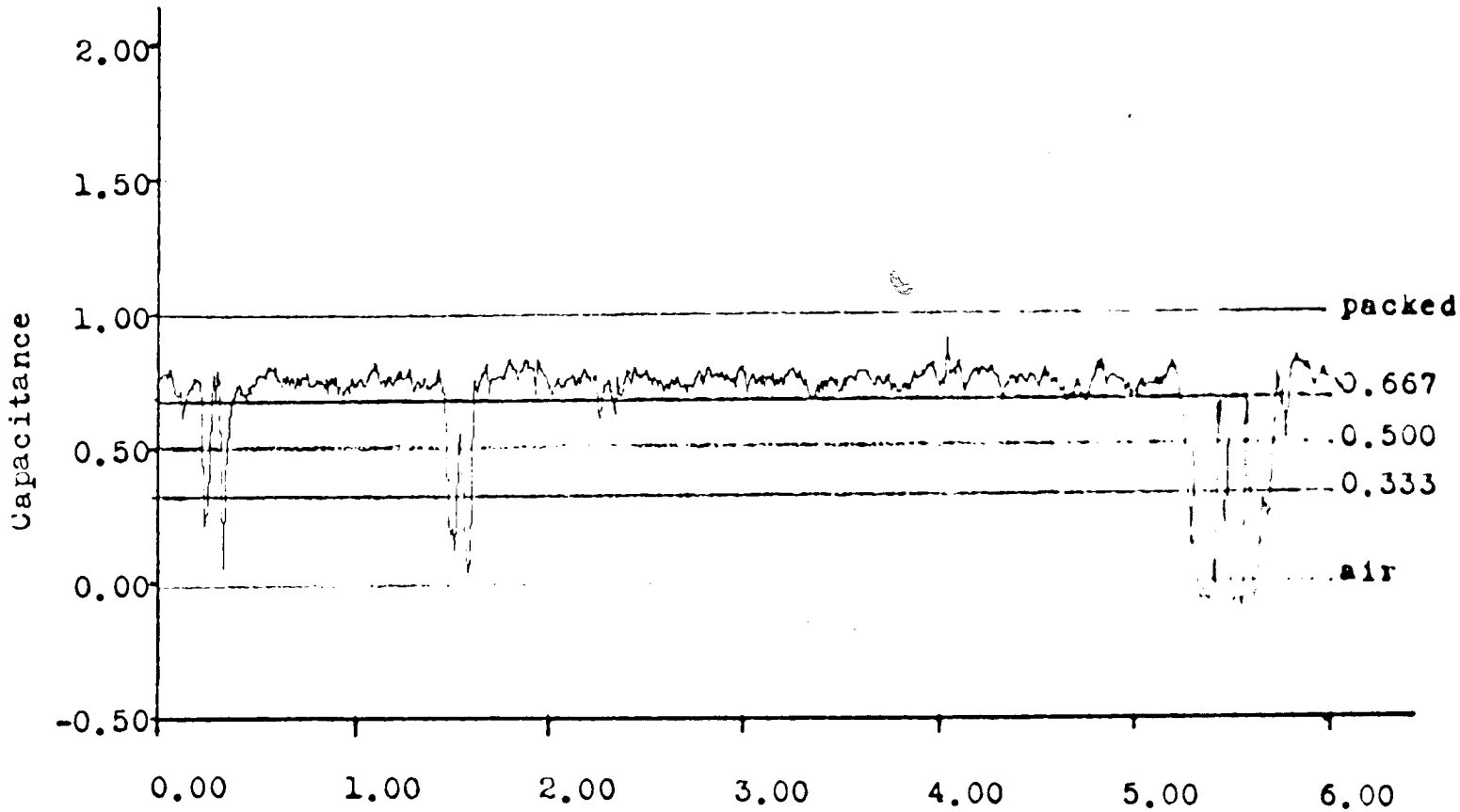

Angle=45° Velocity=0.265 m/sec

Figure 10 - Capacitance Signal vs. Time

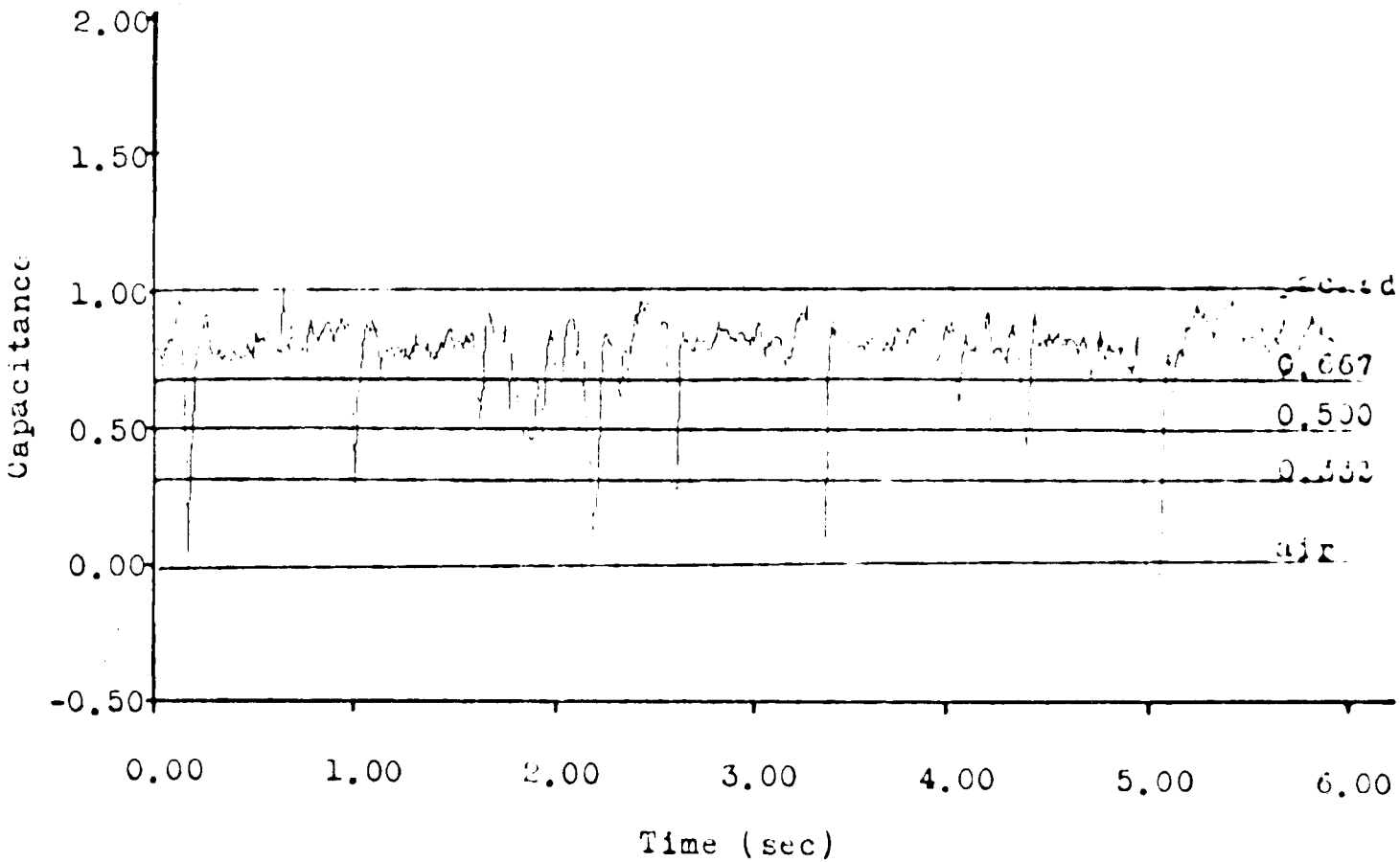

Angle=45° Velocity=0.521 m/sec

Figure 11 - Capacitance Signal vs. Time

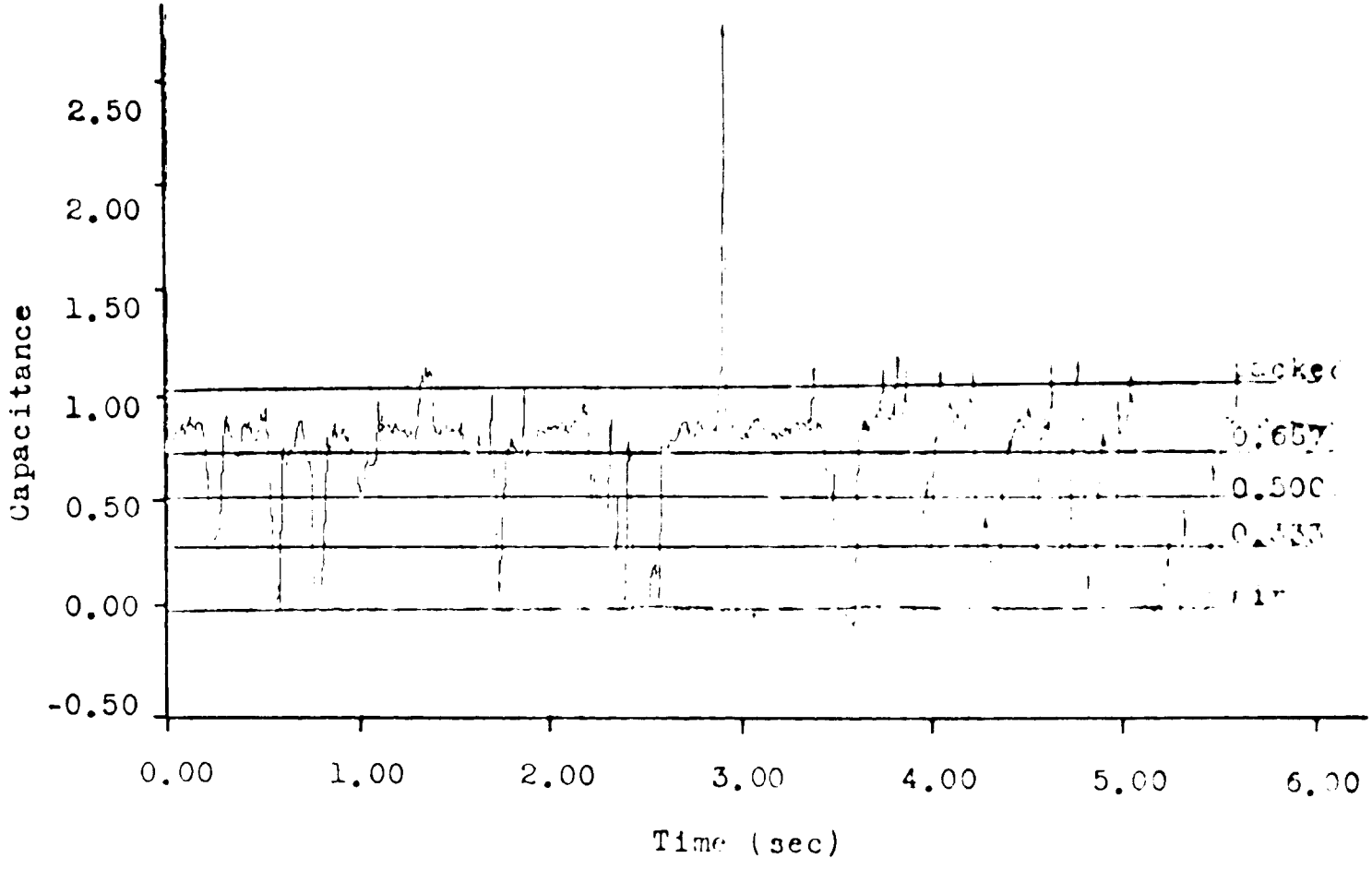

Angle=45° Velocity=0.783 m/sec

Figure 12 - Capacitance Signal vs. Time

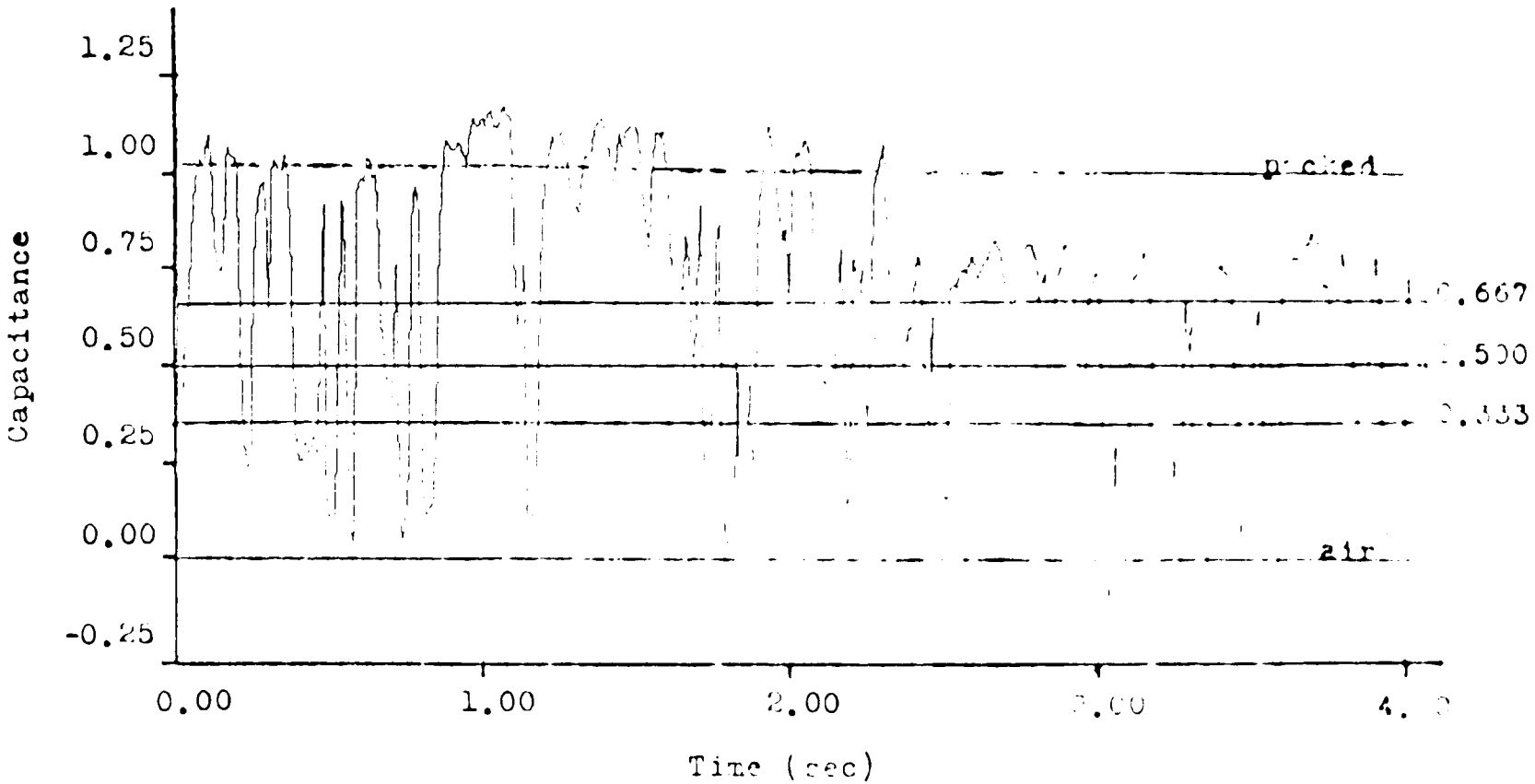

Angle=90° Velocity=.066 m/sec

Figure 13 - Capacitance Signal vs. Time

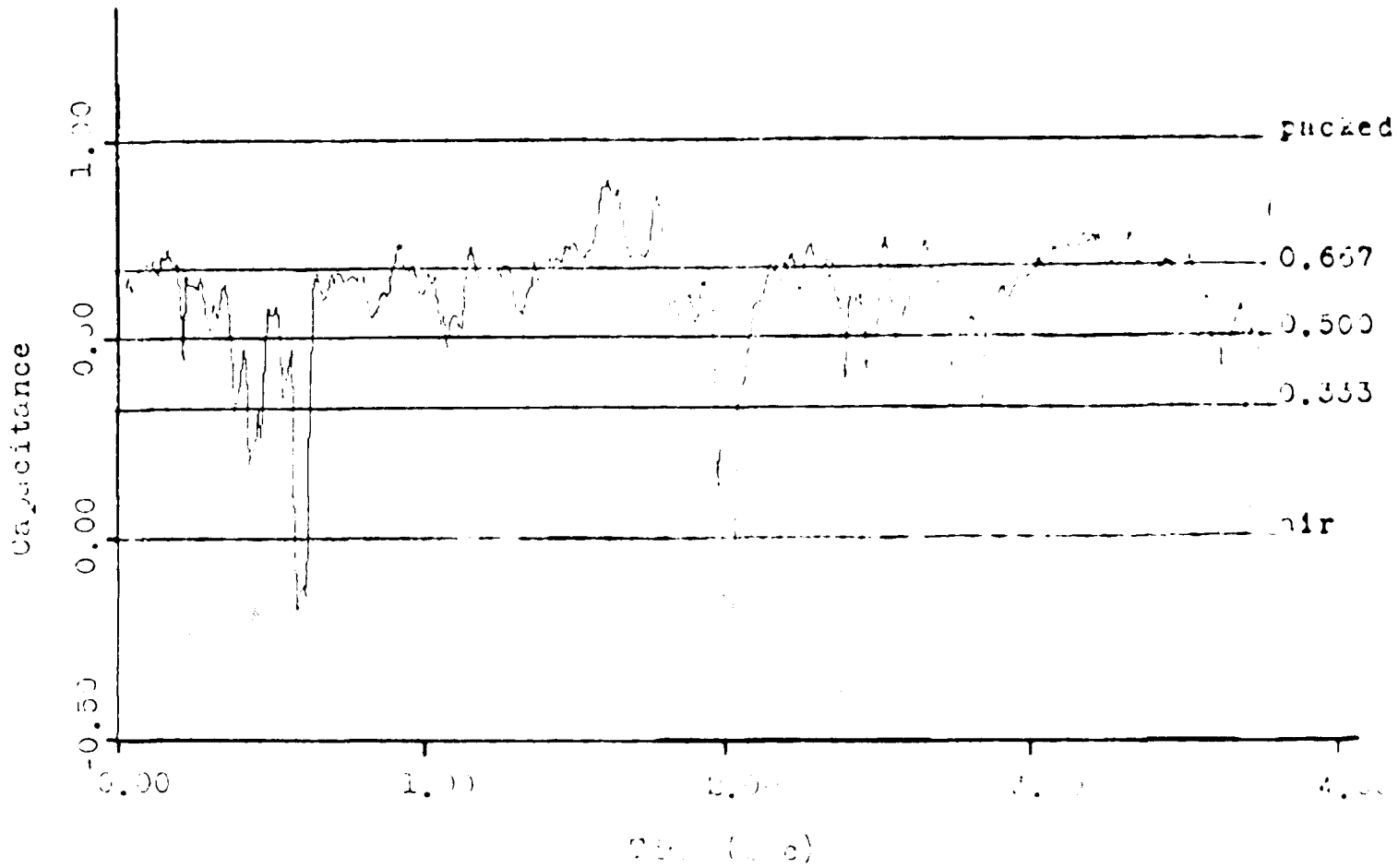

Figure 14 - Capacitance Signal vs. Time

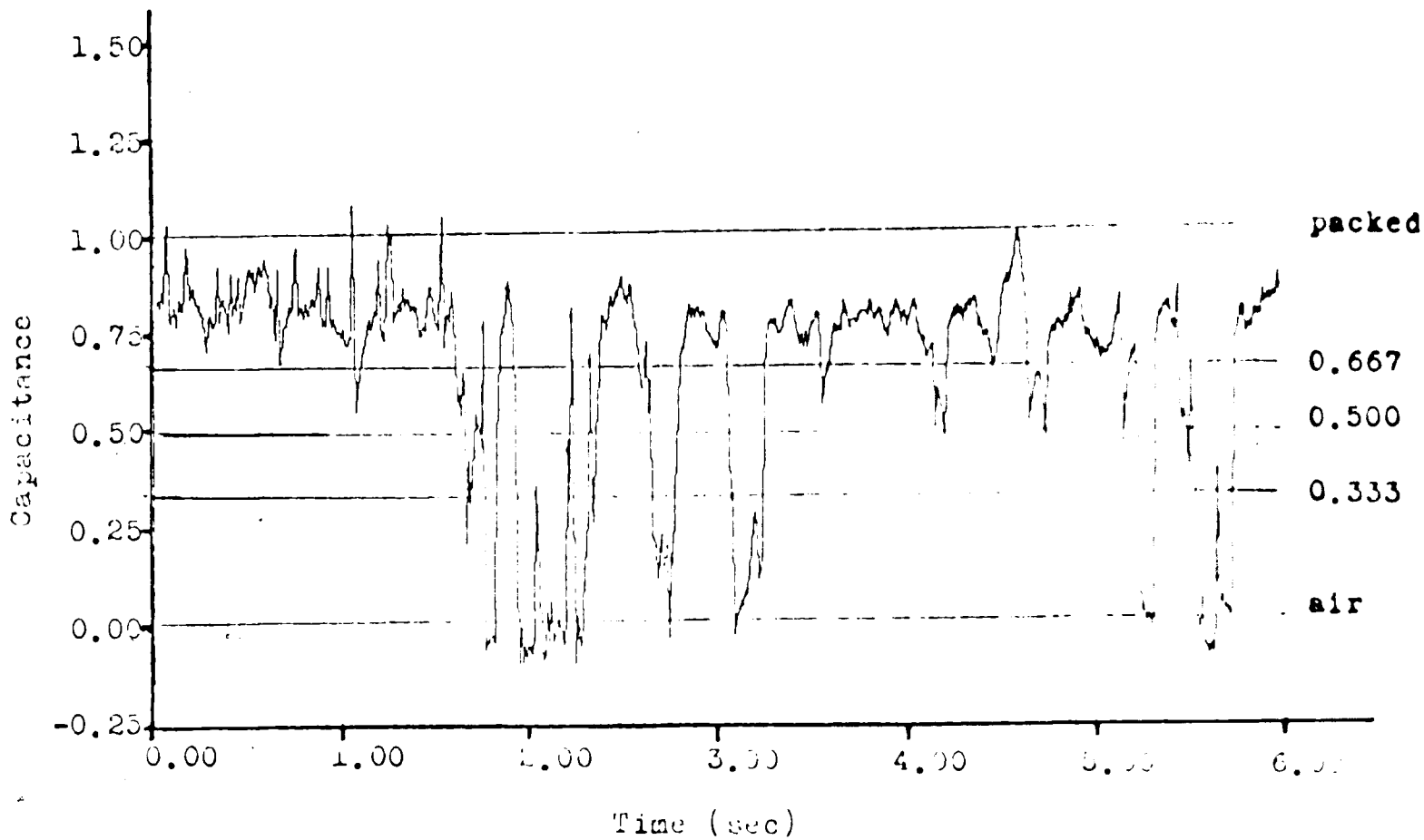

Angle=90° Velocity=0.265 m/sec

Figure 15 - Capacitance Signal vs. Time

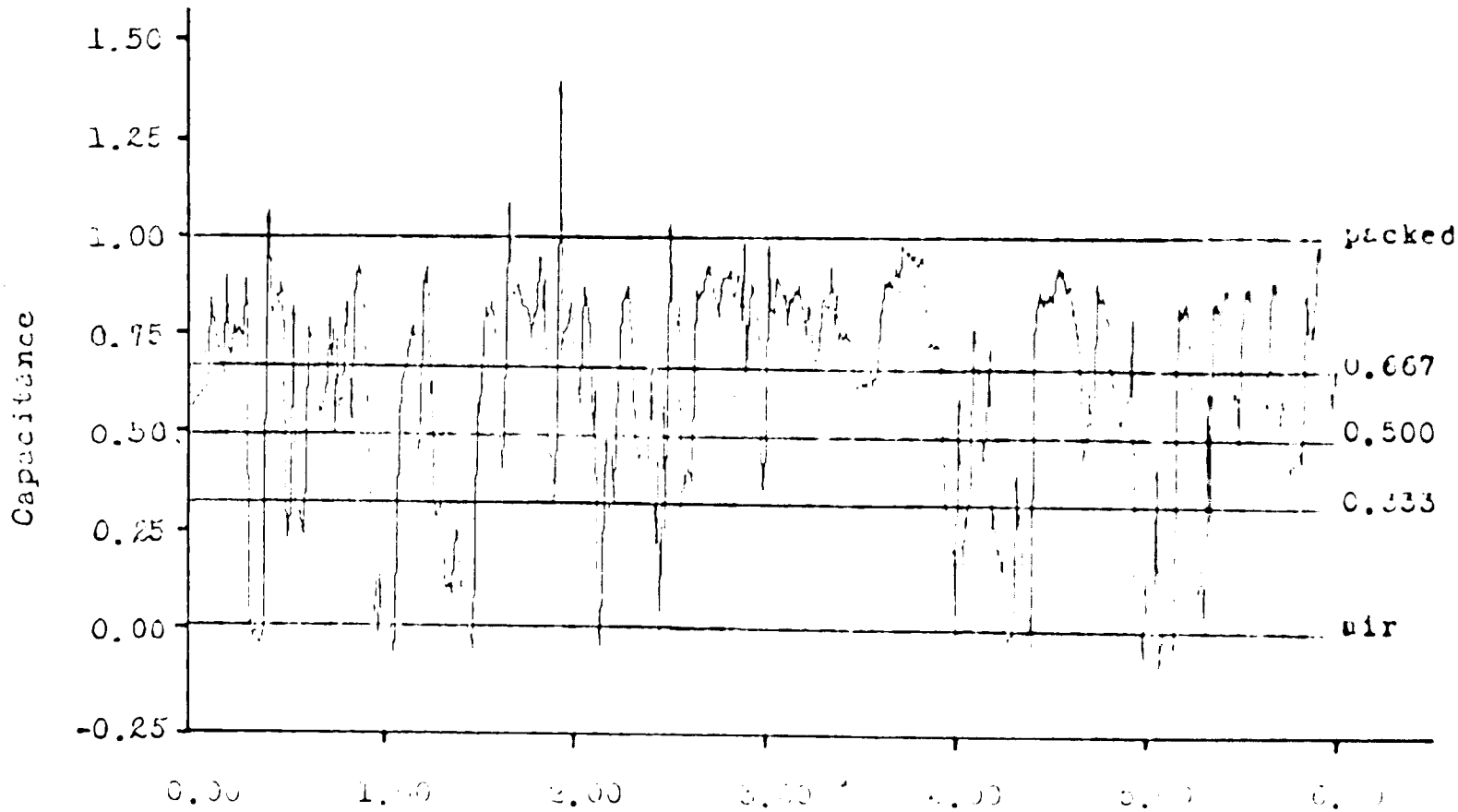

Figure 16 - Capacitance Signal vs. Time

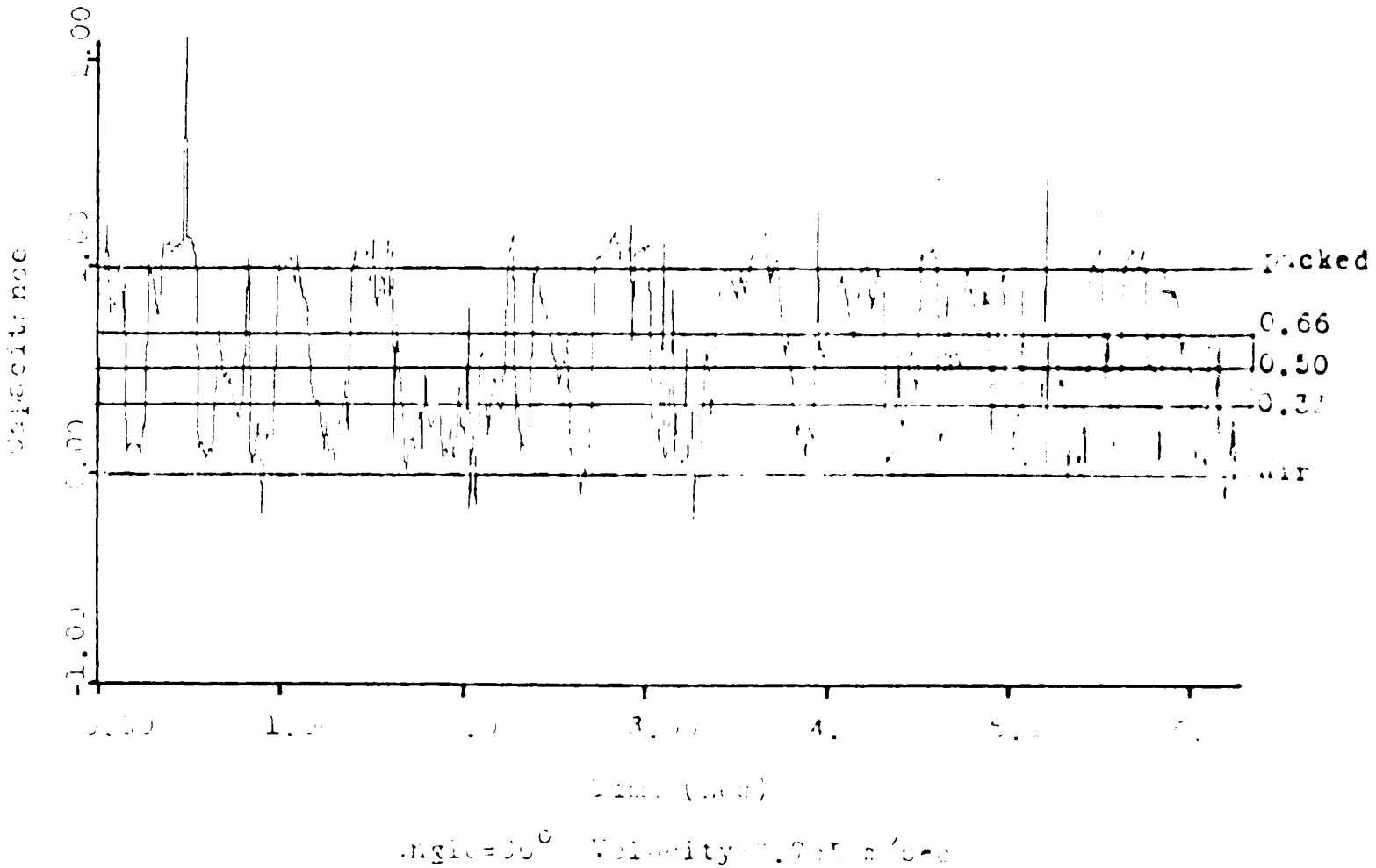

Figure 17 - Capacitance Signal vs. Time

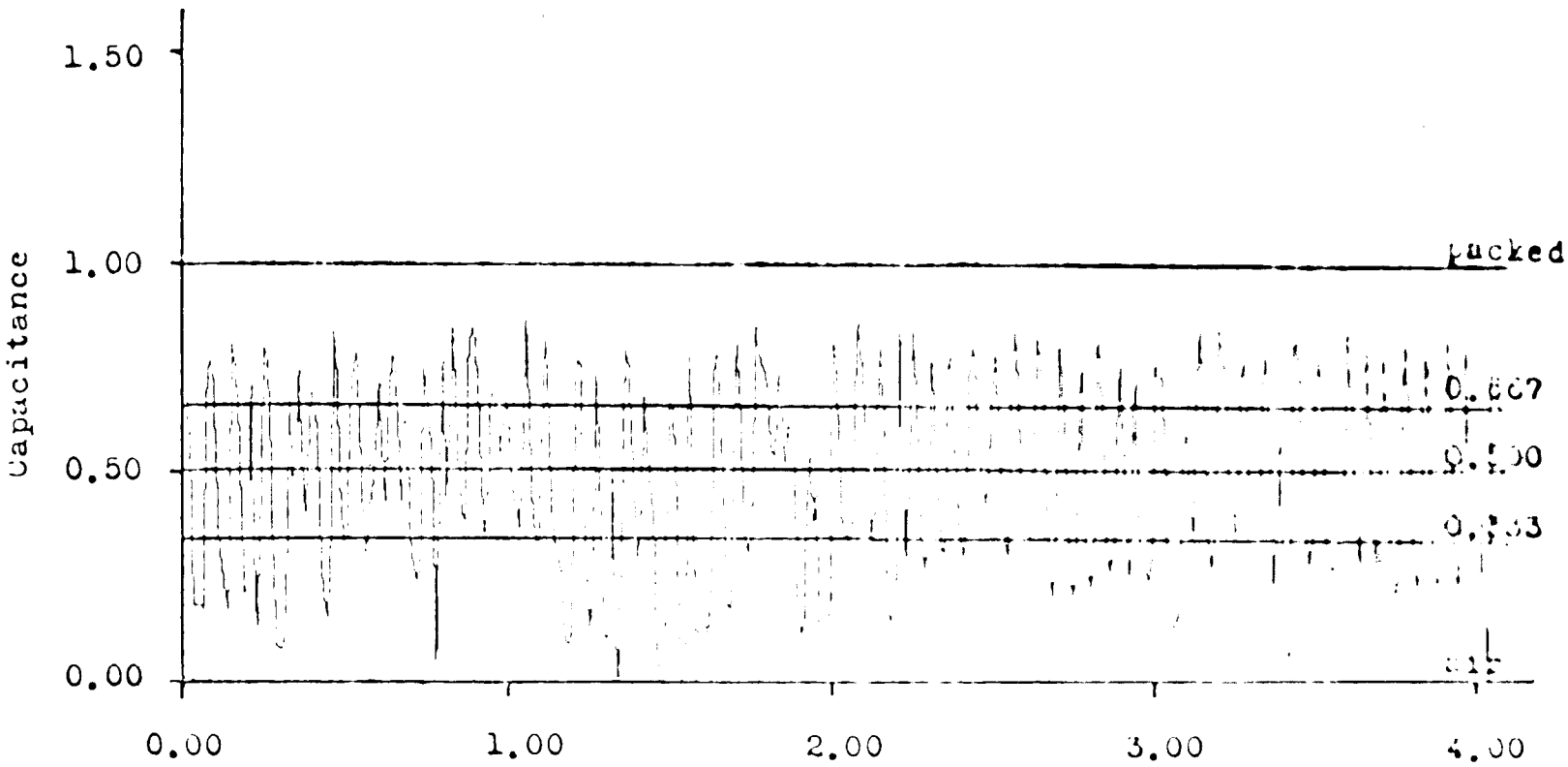

Angle=135° Velocity=0.060 m/sec

Figure 18 - Capacitance Signal vs. Time

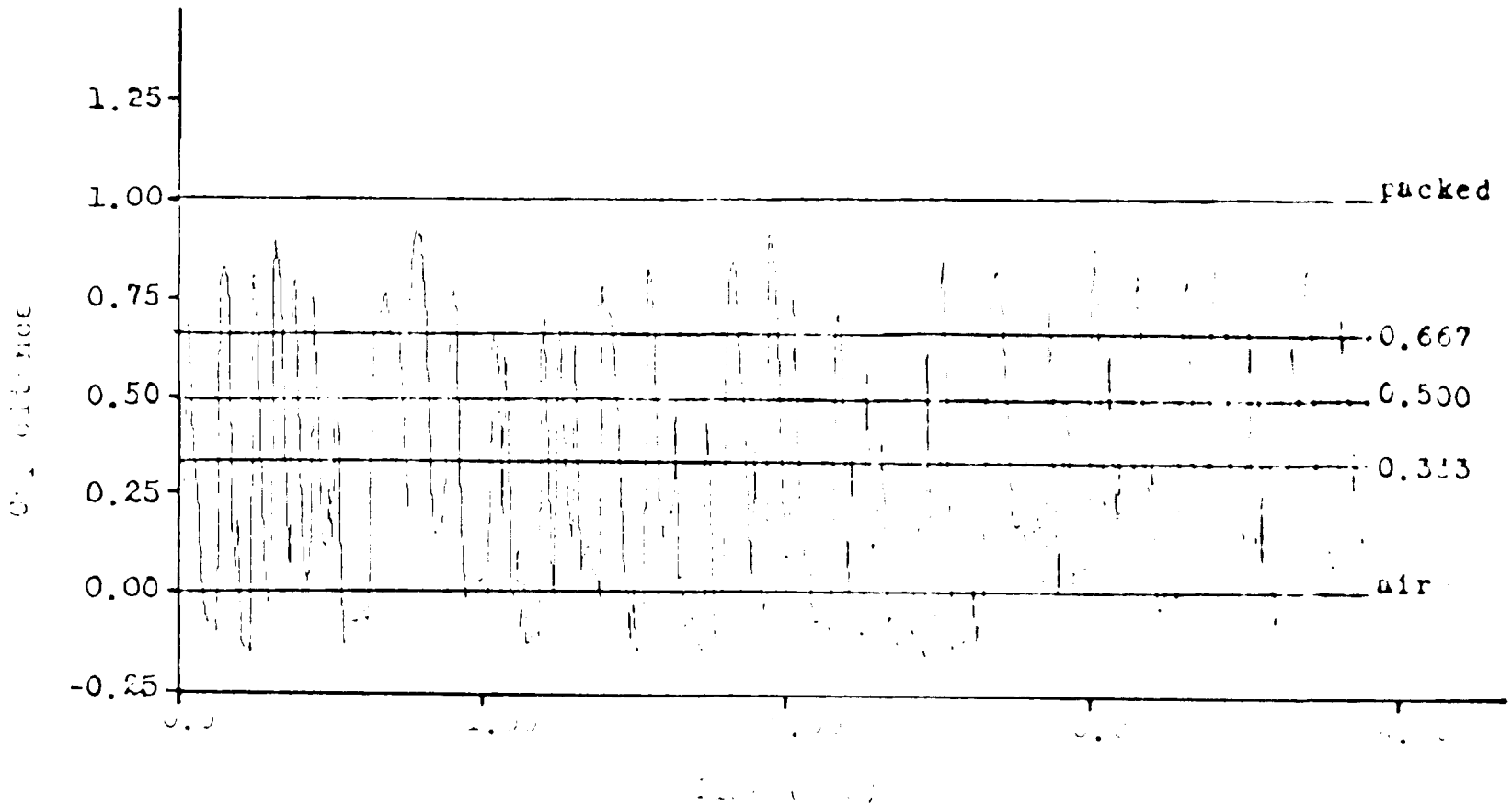

Angle 135° Velocity 0.125 m sec

Figure 19 - Capacitance Signal vs. Time

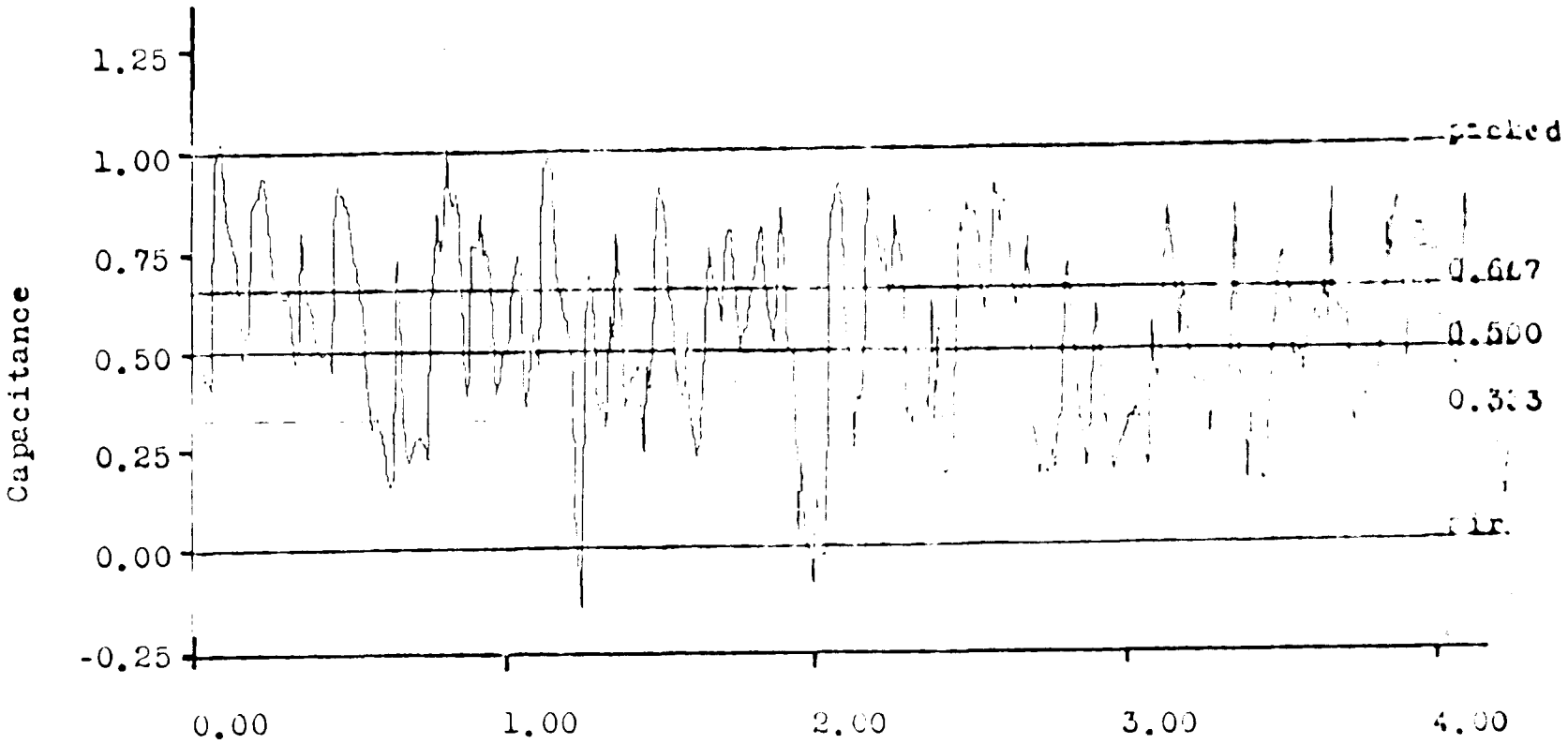

Angle=135° Velocity=0.265 m/sec

Figure 20 - Capacitance Signal vs. Time

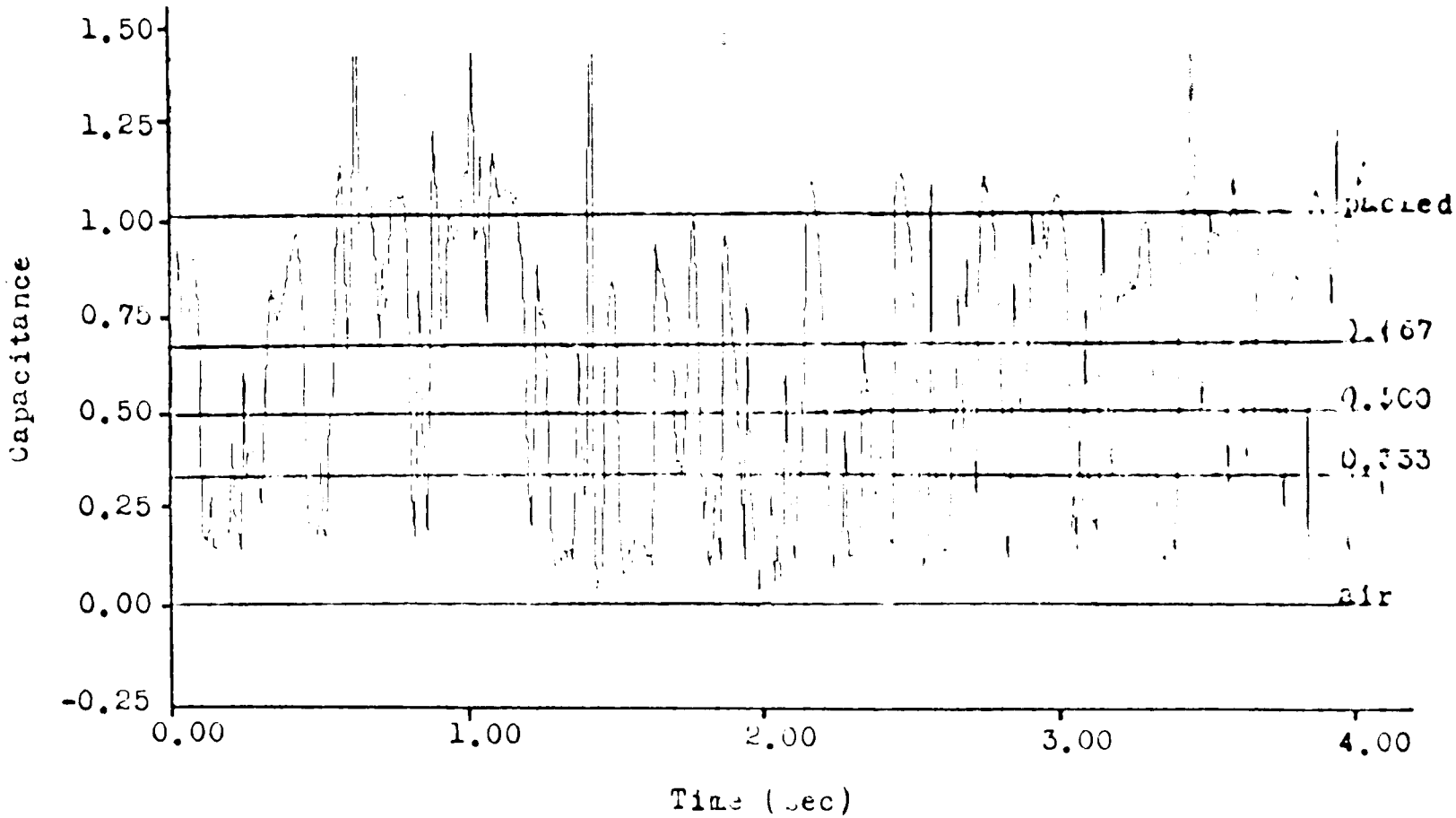

Angle=135° Velocity=0.521 m/sec

Figure 21 - Capacitance Signal vs. Time

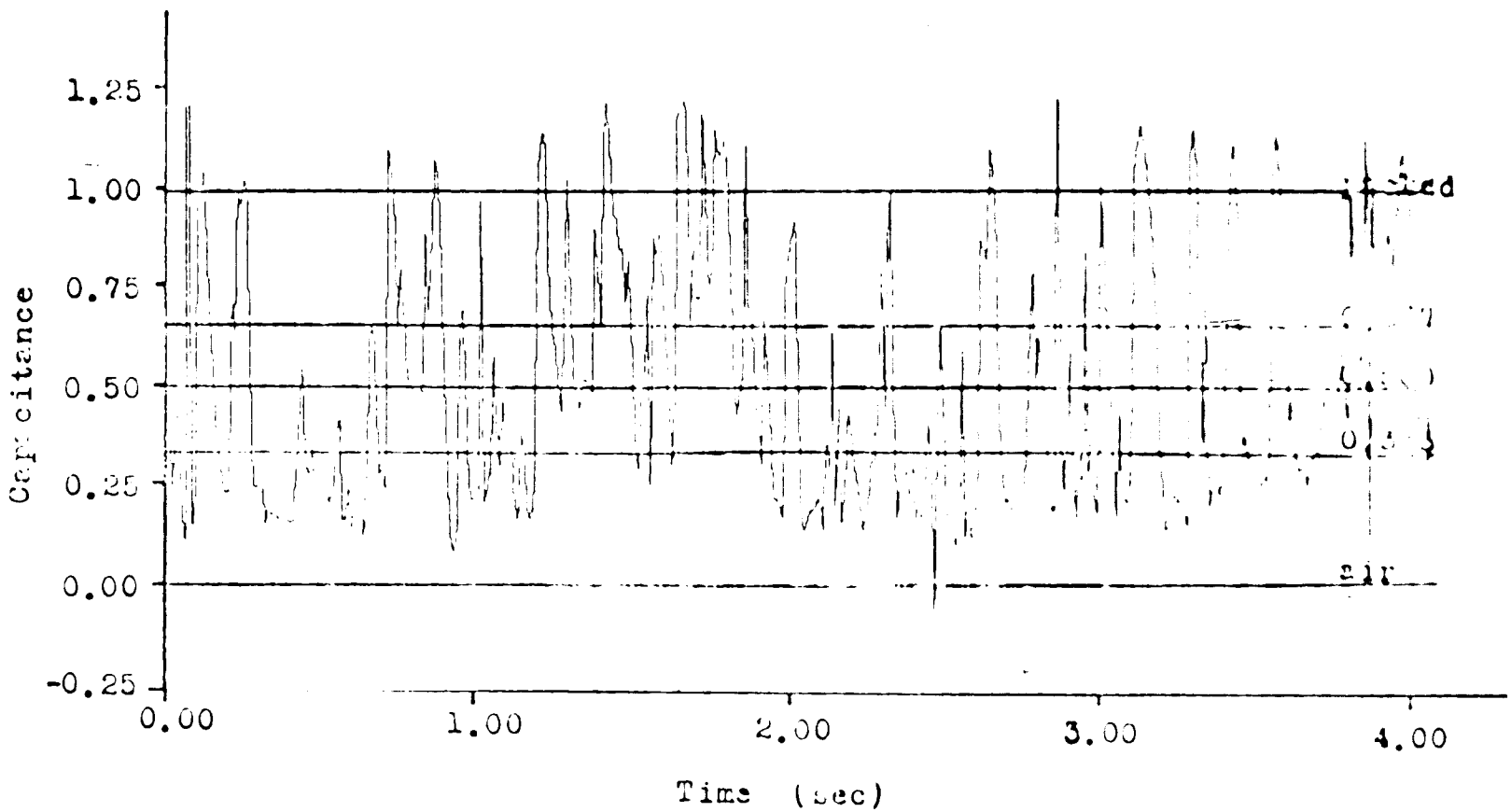

Angle=135° Velocity=0.783 m/sec

Figure 22 - Capacitance Signal vs. Time

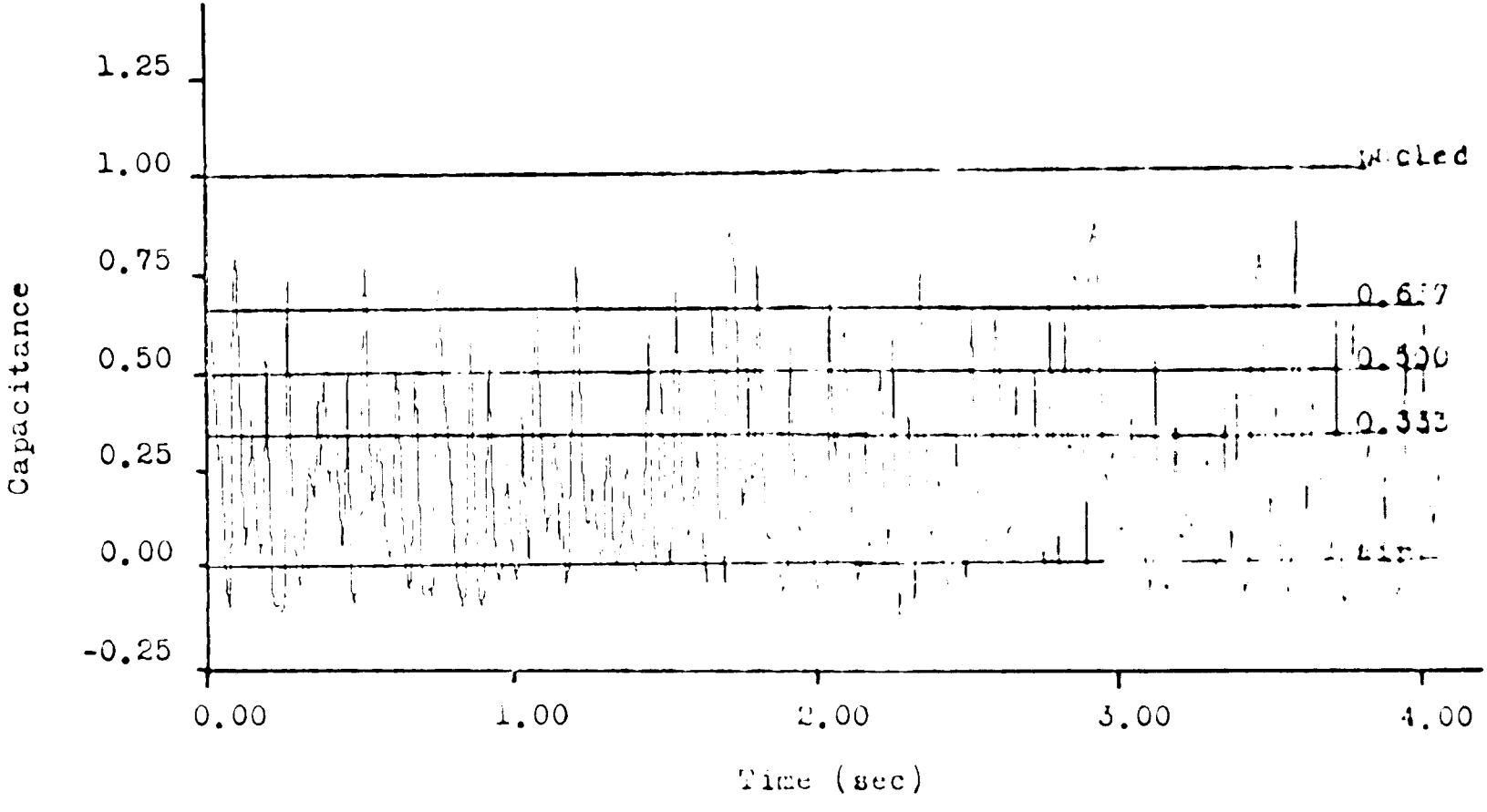

Angle=180° Velocity=0.06 m/sec

Figure 23 - Capacitance Signal vs. Time

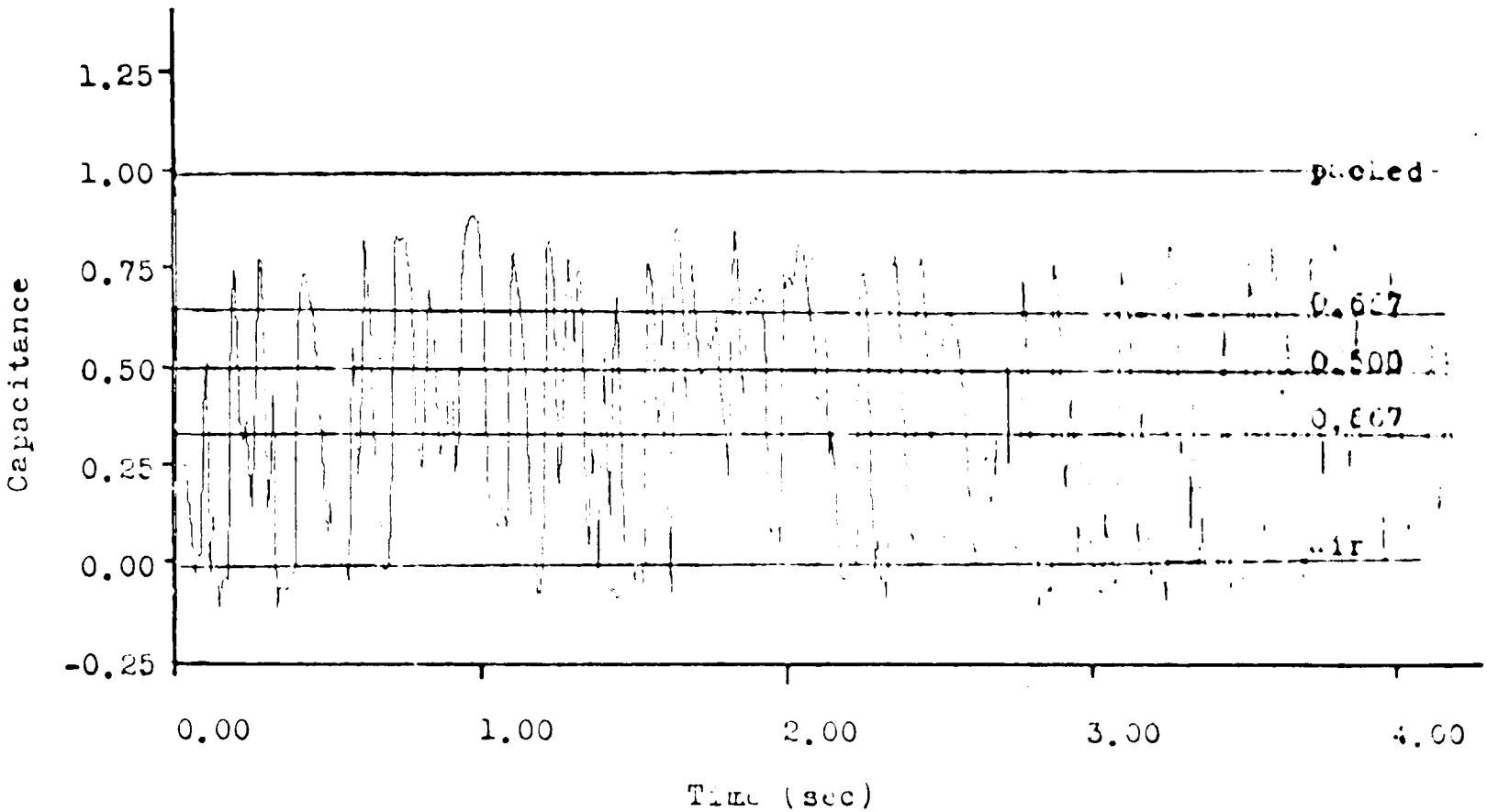

Angle=180° Velocity=0.125 m/sec

Figure 24 - Capacitance Signal vs. Time

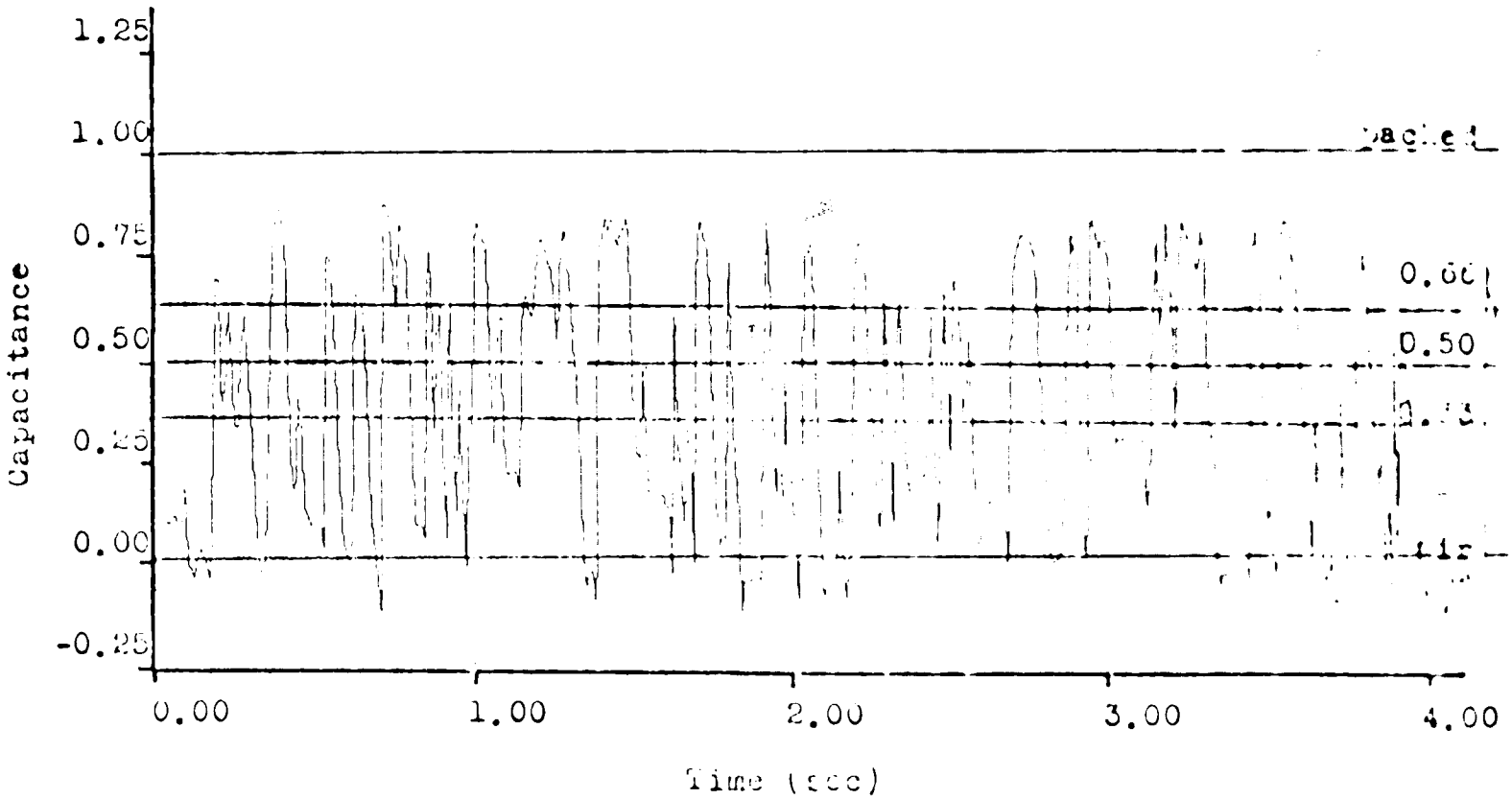

Angle=180° Velocity=0.265 m/sec

Figure 25 - Capacitance Signal vs. Time

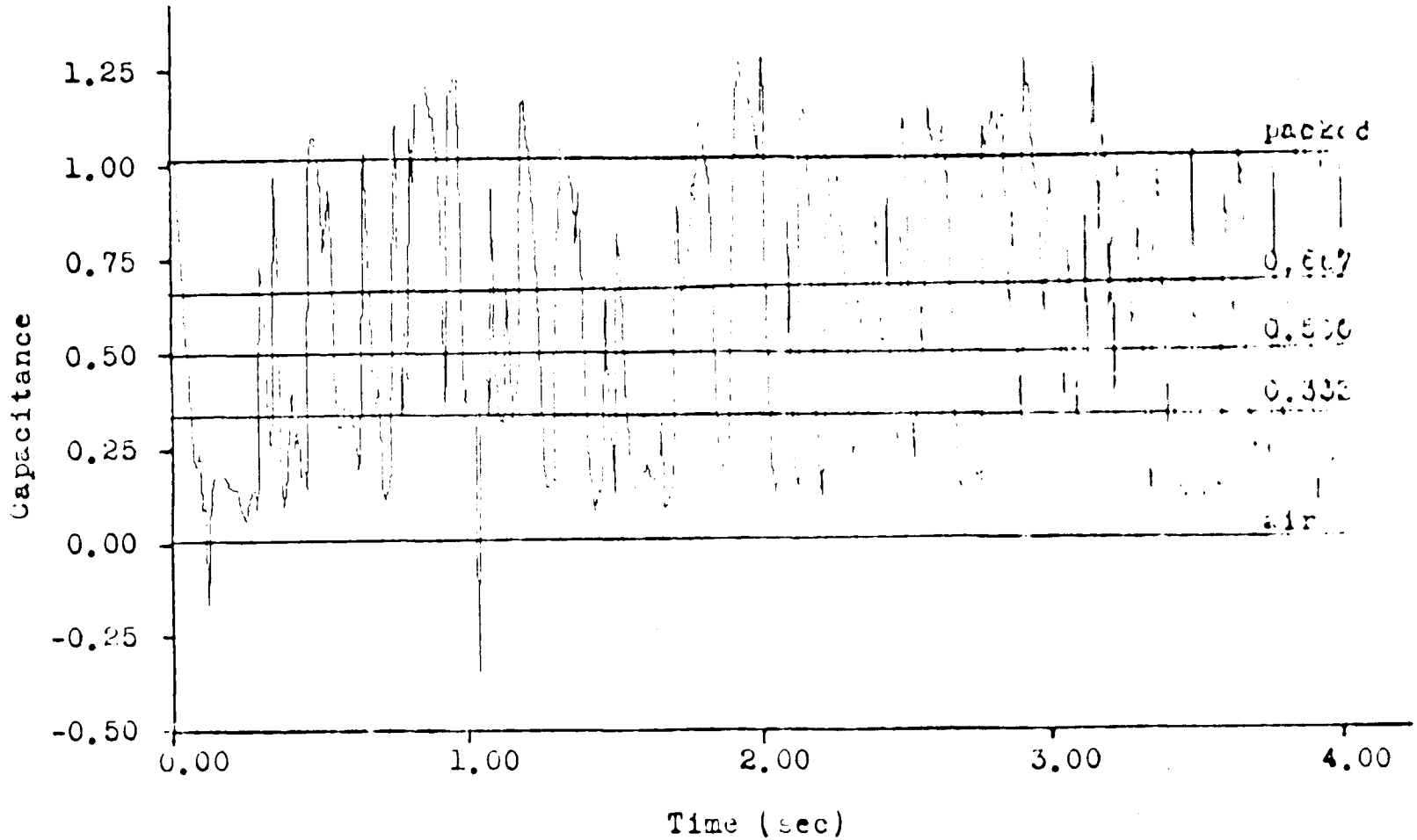

Angle=180° Velocity=0.521 m/sec

Figure 26 - Capacitance Signal vs. Time

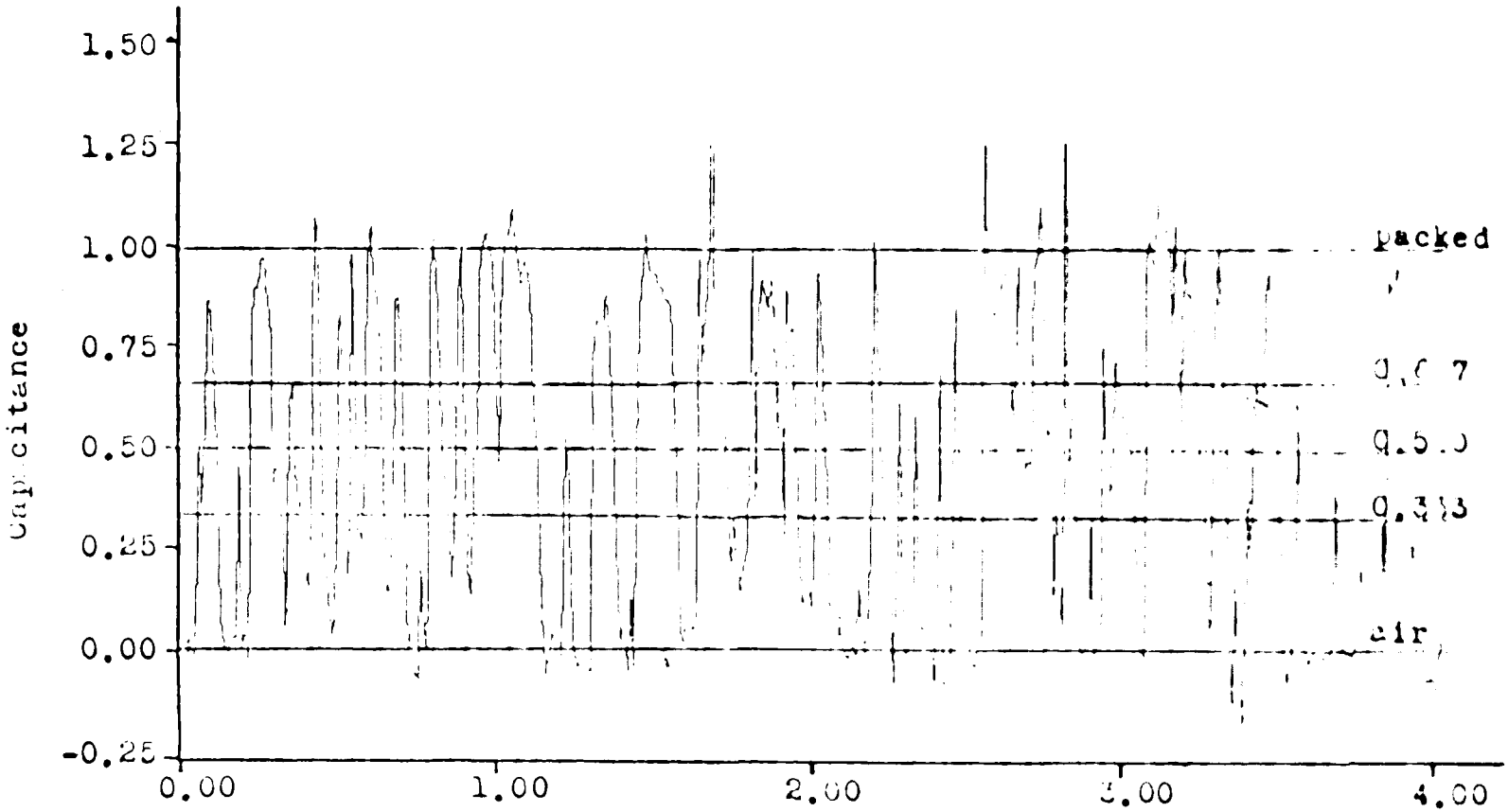

Angle=180° Velocity=0.783 m/sec

Figure 27 - Capacitance Signal vs. Time

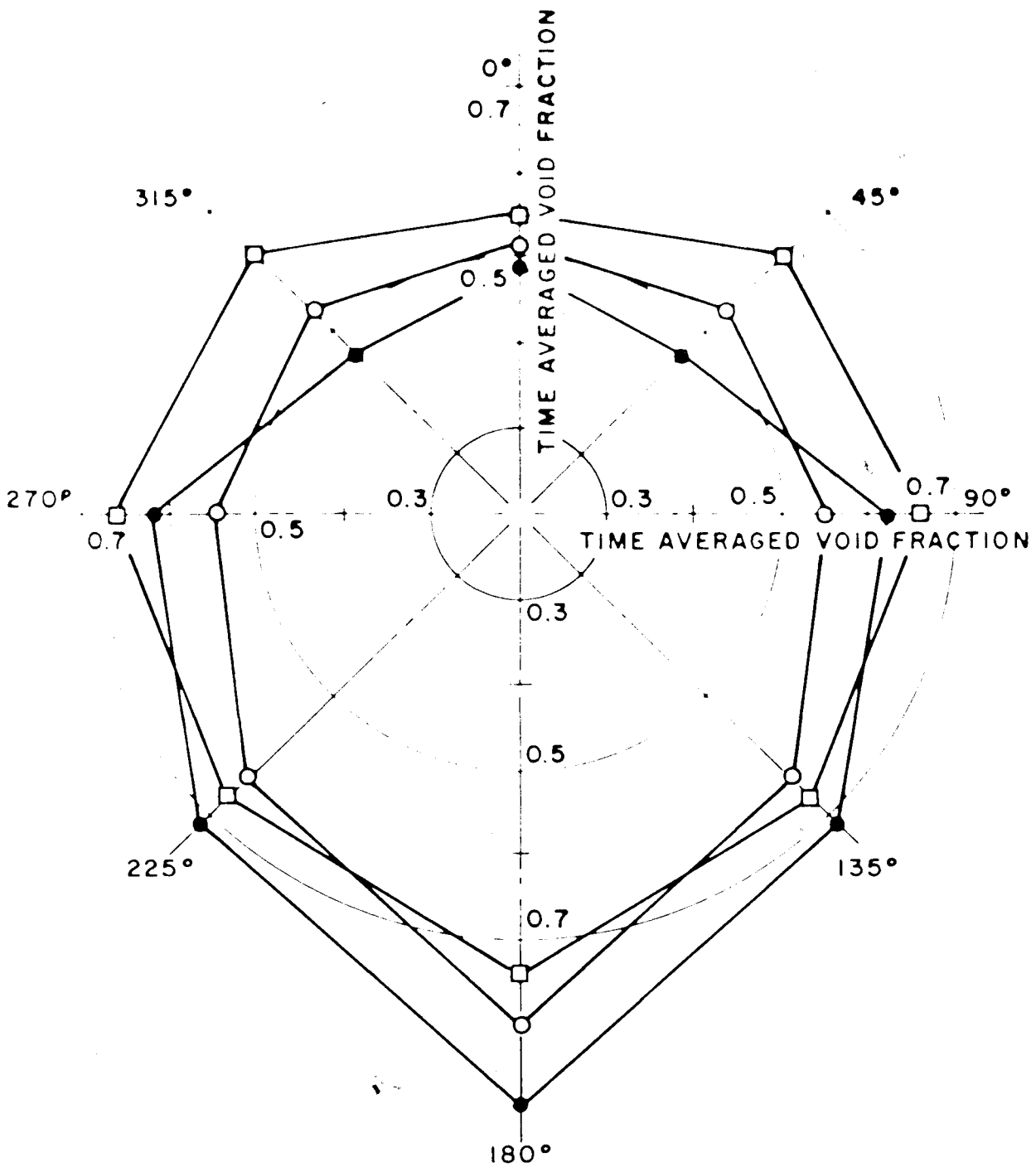

GT-2 GLASS SPHERES
STATIC BED HEIGHT = 0.228 m
TUBE ELEVATION = 0.152 m

VELOCITY:
● = 0.060 m/SEC
○ = 0.263 m/SEC
□ = 0.783 m/SEC

Figure 28 - Effect of angular position on time averaged void fraction

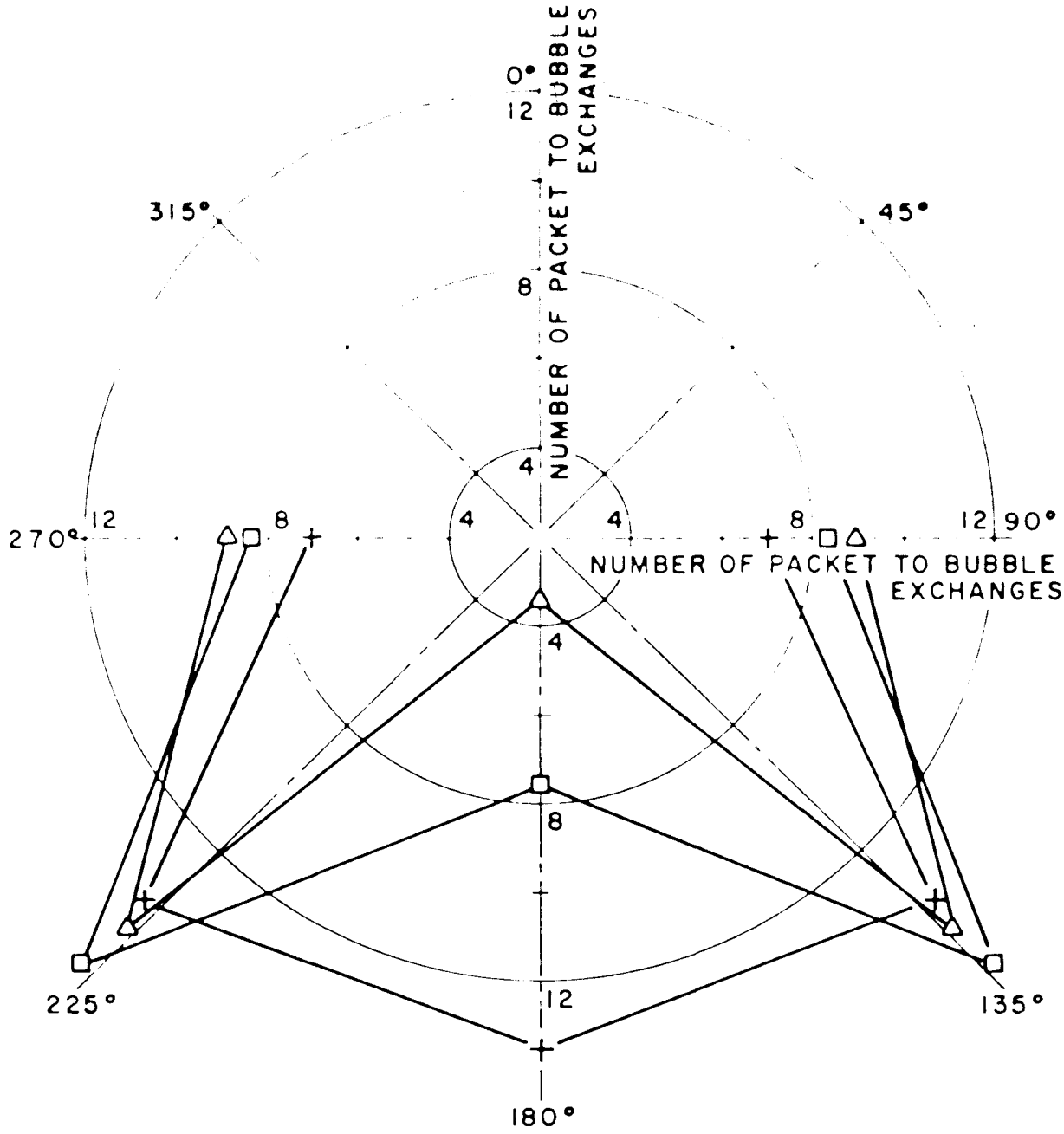

GT-2 GLASS SPHERES

STATIC BED HEIGHT = 0.228 m
TUBE ELEVATION = 0.152 m
VELOCITY = 0.060 m/SEC

0.333 PACKET CRITERION = +
0.500 PACKET CRITERION = □
0.667 PACKET CRITERION = O

Figure 29 - Effect of angular position on number of packet to bubble exchanges

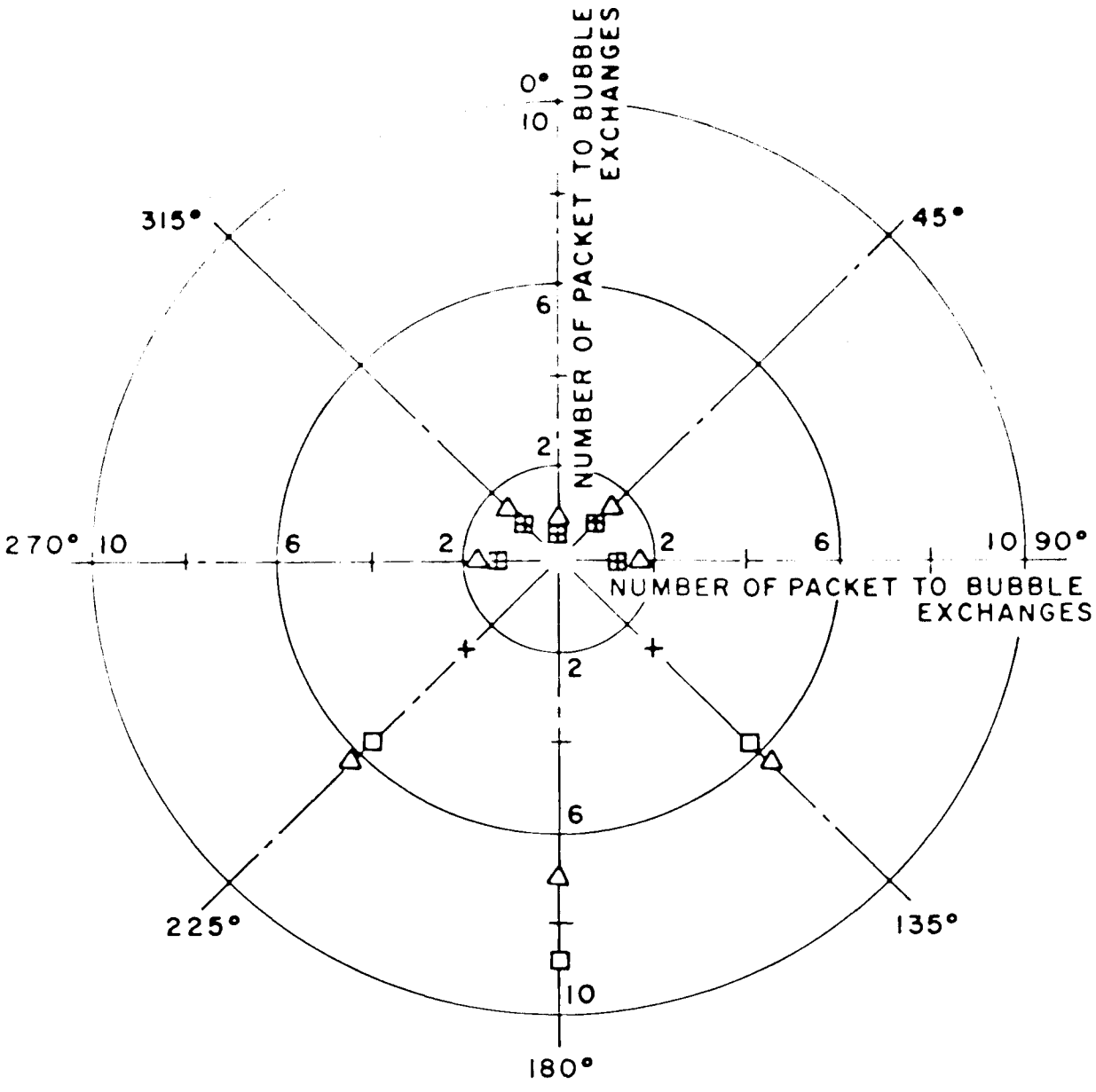

GT-2 GLASS SPHERES

STATIC BED HEIGHT = 0.228 m
TUBE ELEVATION = 0.152 m
VELOCITY = 0.265 m/SEC

0.333 PACKET CRITERION = +
0.500 PACKET CRITERION = □
0.667 PACKET CRITERION = △

Figure 30 - Effect of angular position on number of packet to bubble exchanges

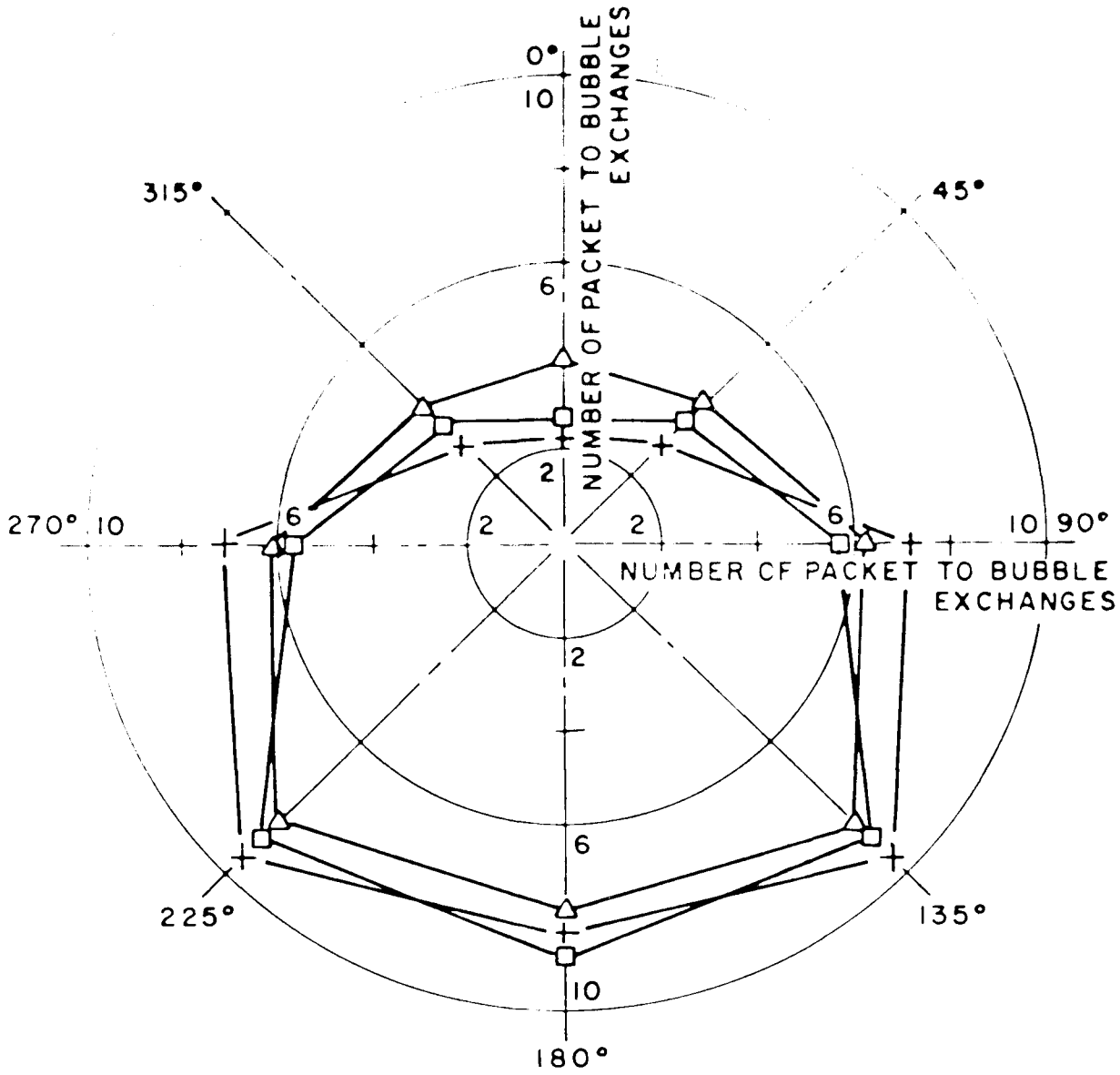

GT-2 GLASS SPHERES

STATIC BED HEIGHT = 0.228 m
TUBE ELEVATION = 0.152 m
VELOCITY = 0.783 m / SEC

0.333 PACKET CRITERION = +
0.500 PACKET CRITERION = □
0.667 PACKET CRITERION = △

Figure 31 - Effect of angular position on number of packet to bubble exchanges

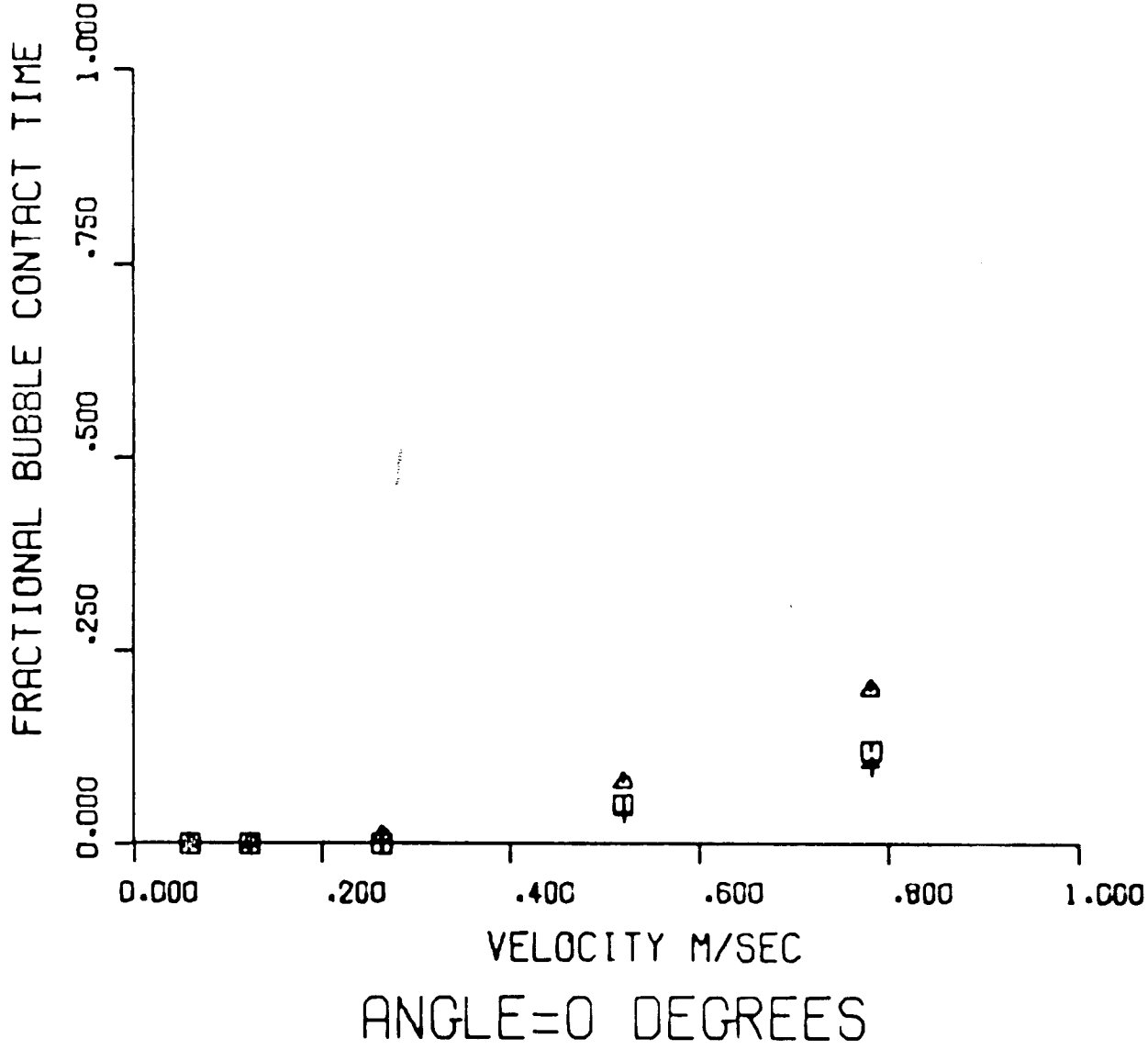

Figure 32 - Effect of Velocity on Fractional Bubble Contact Time

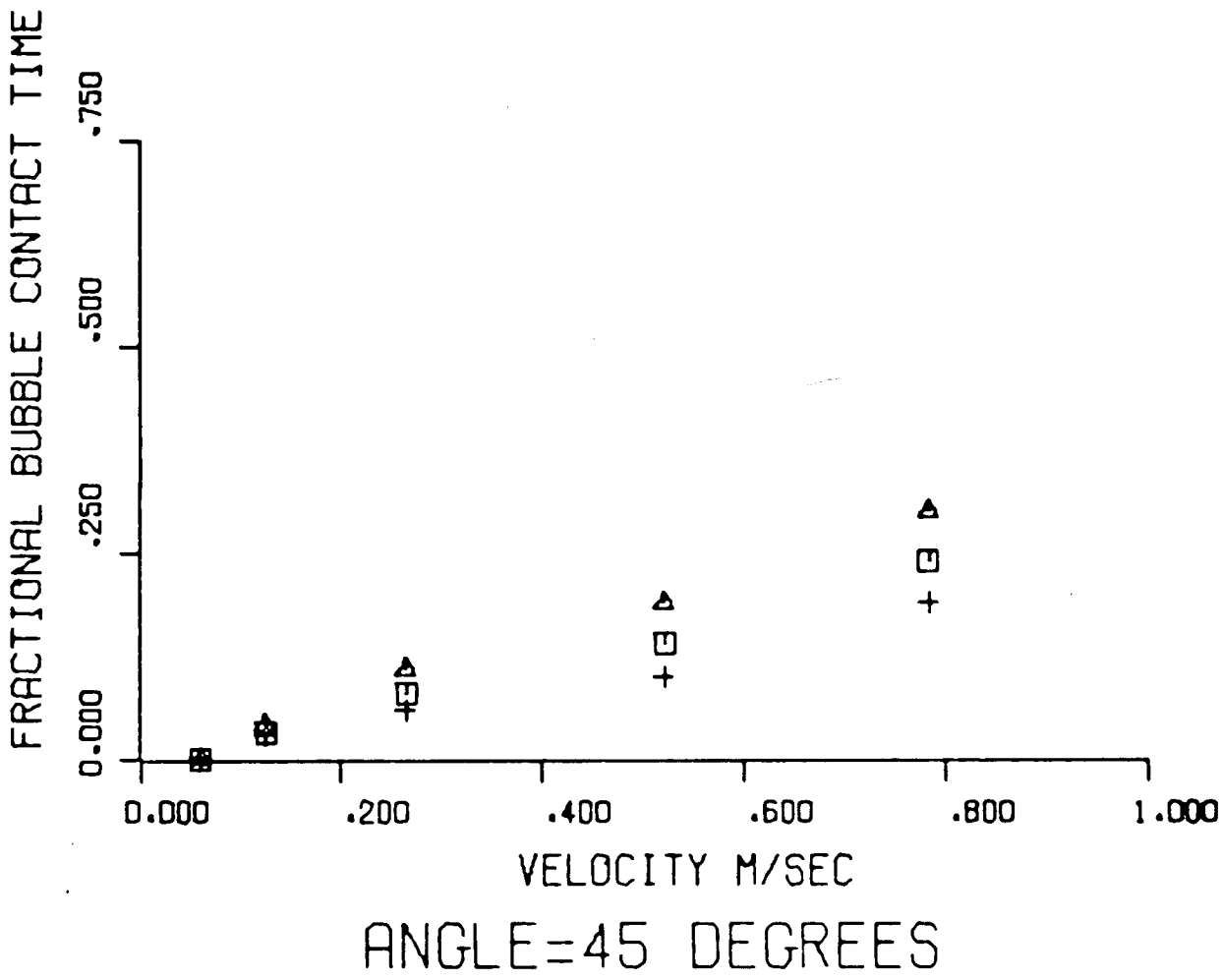

Figure 33 - Effect of Velocity on Fractional Bubble Contact Time

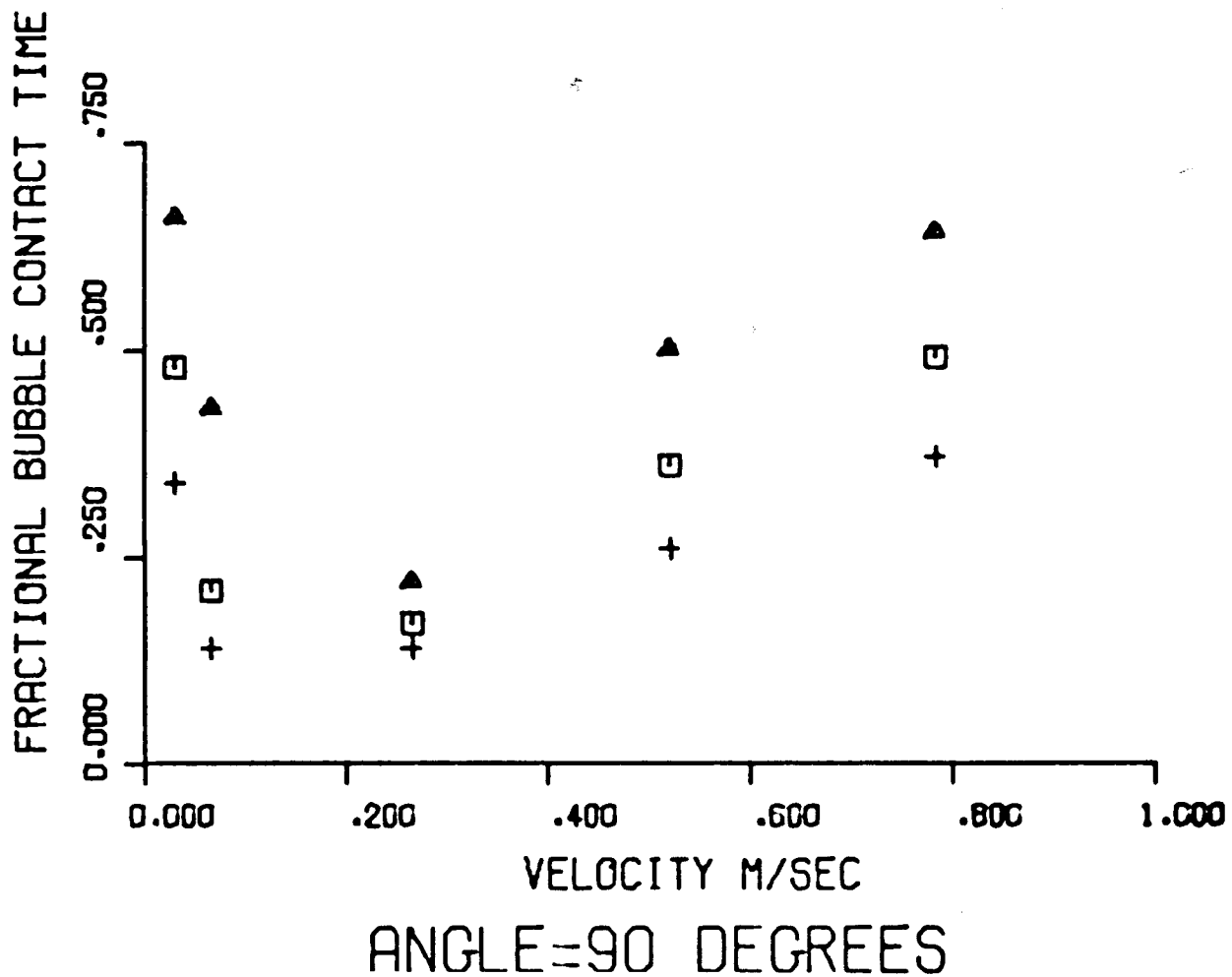

Figure 34 - Effect of Velocity on Fractional Bubble Contact Time

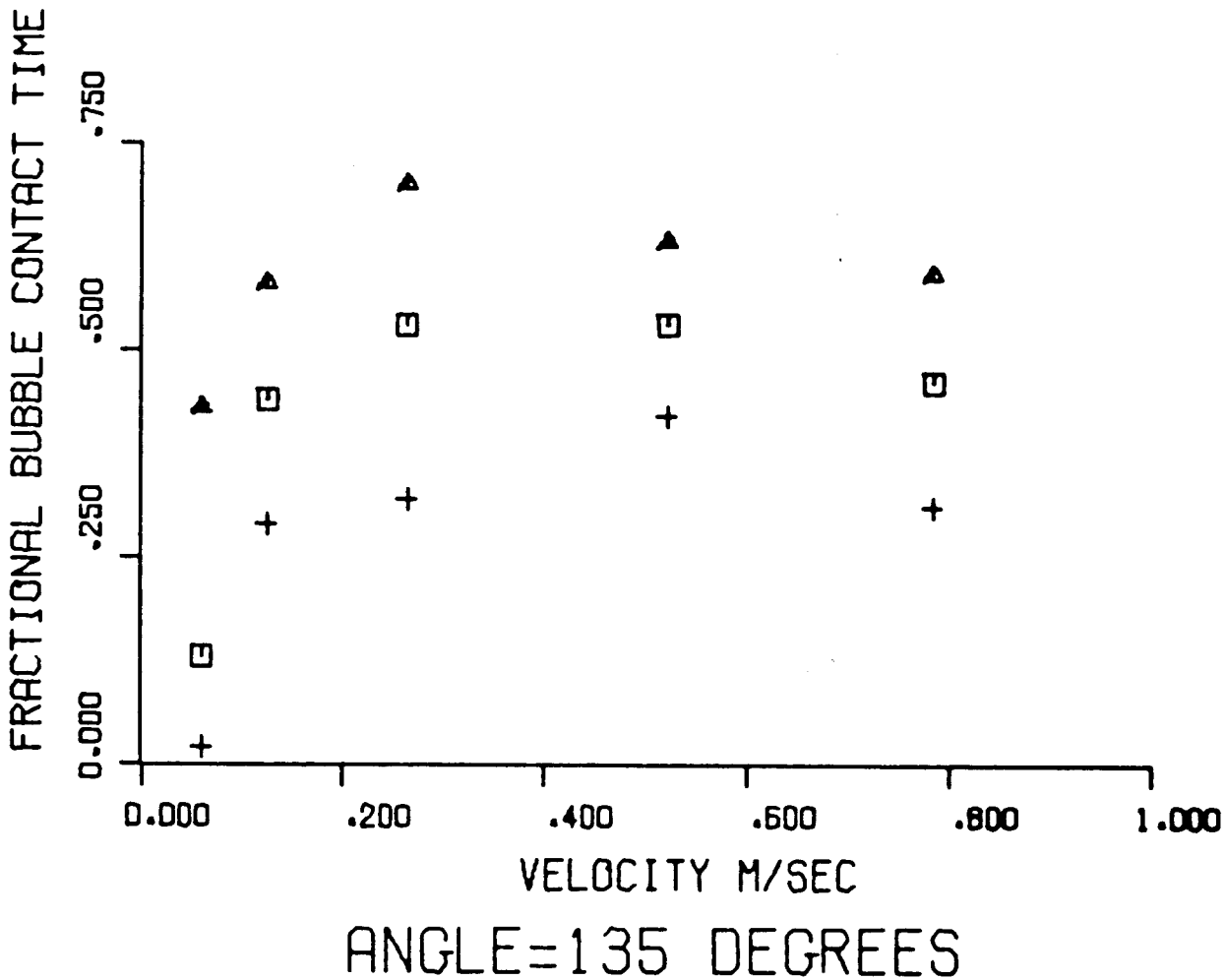

Figure 35 - Effect of Velocity on Fractional Bubble Contact Time

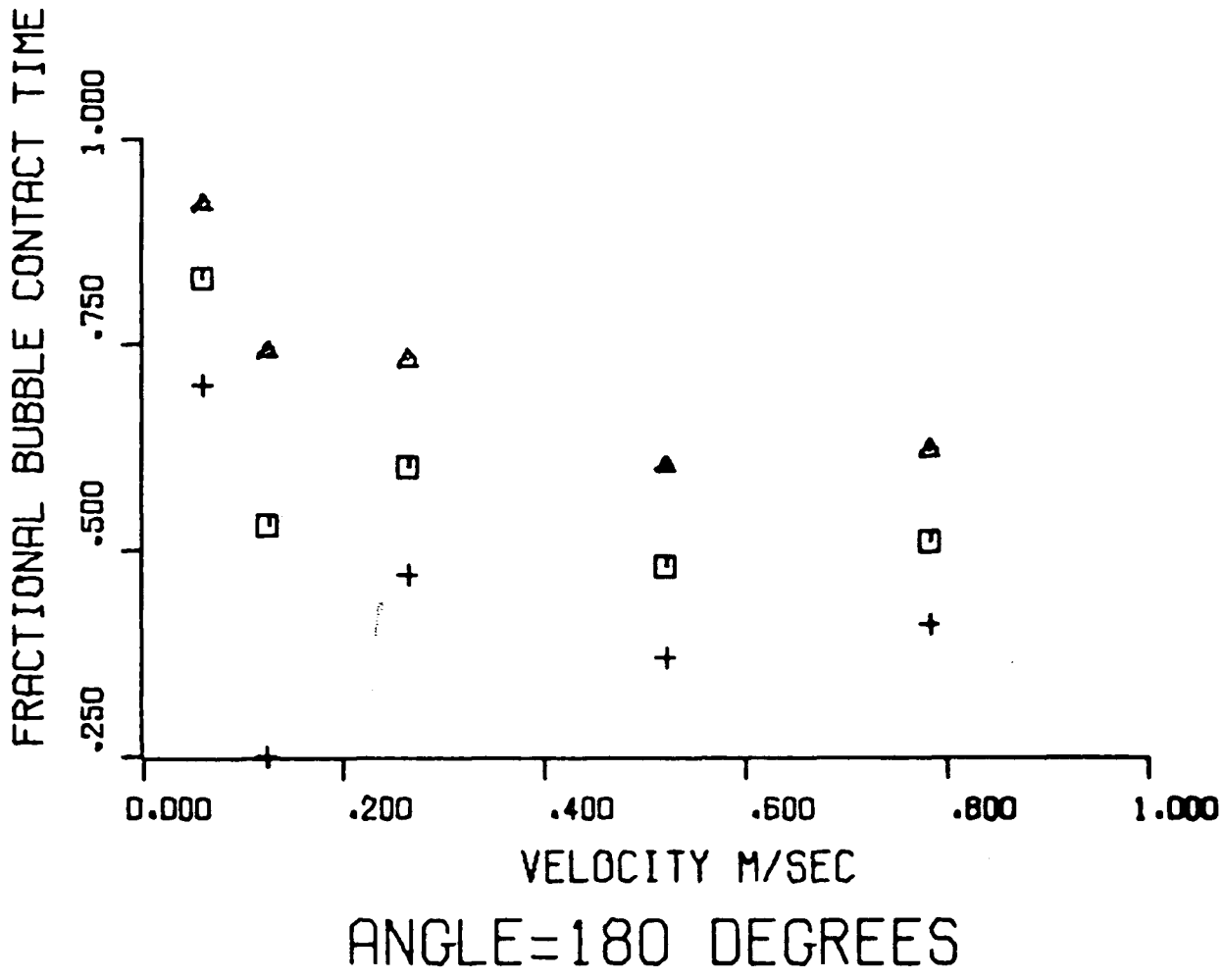

Figure 36 - Effect of Velocity on Fractional Bubble Contact Time

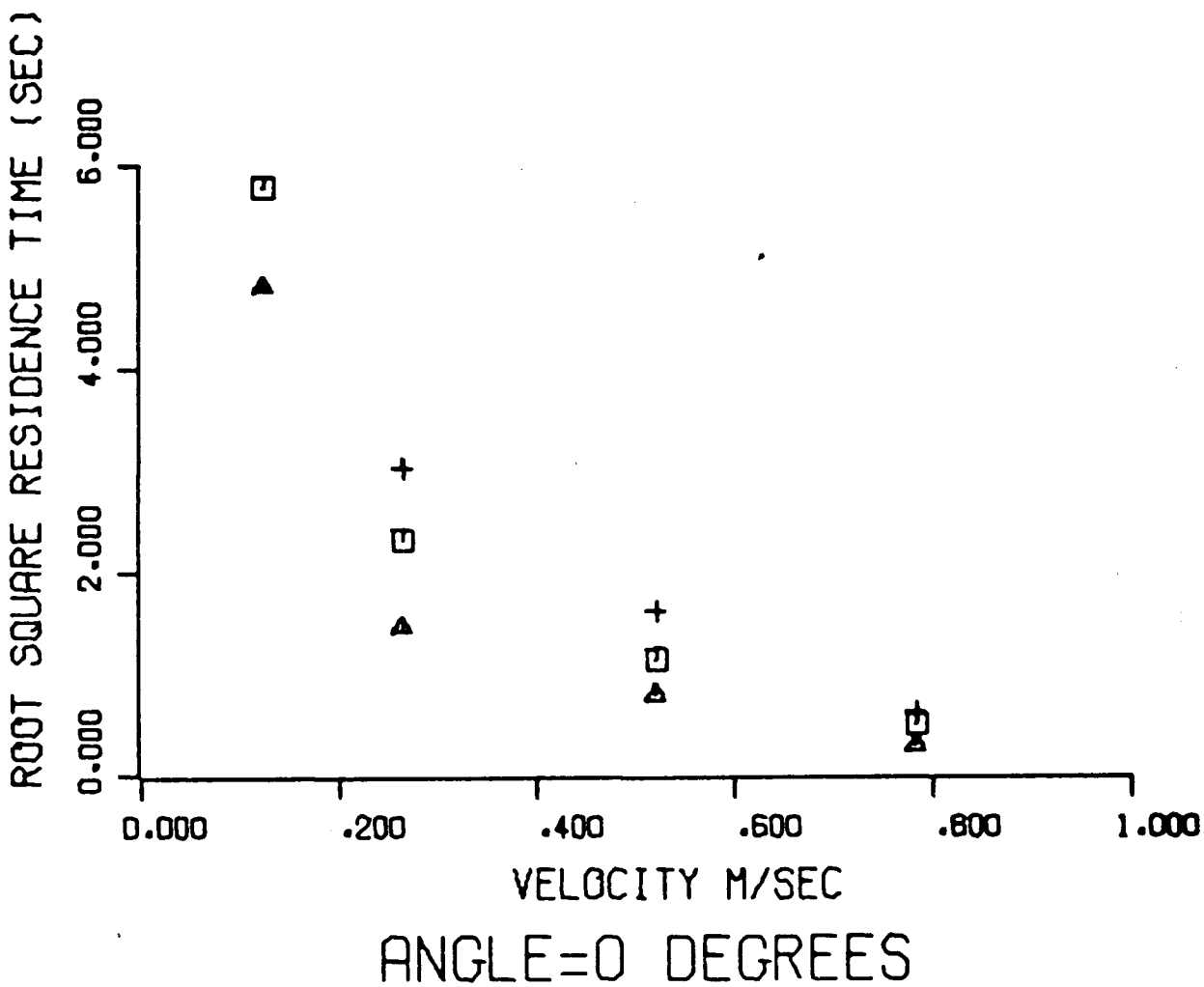

Figure 37 - Effect of Velocity on Root Square Average Packet Residence Time

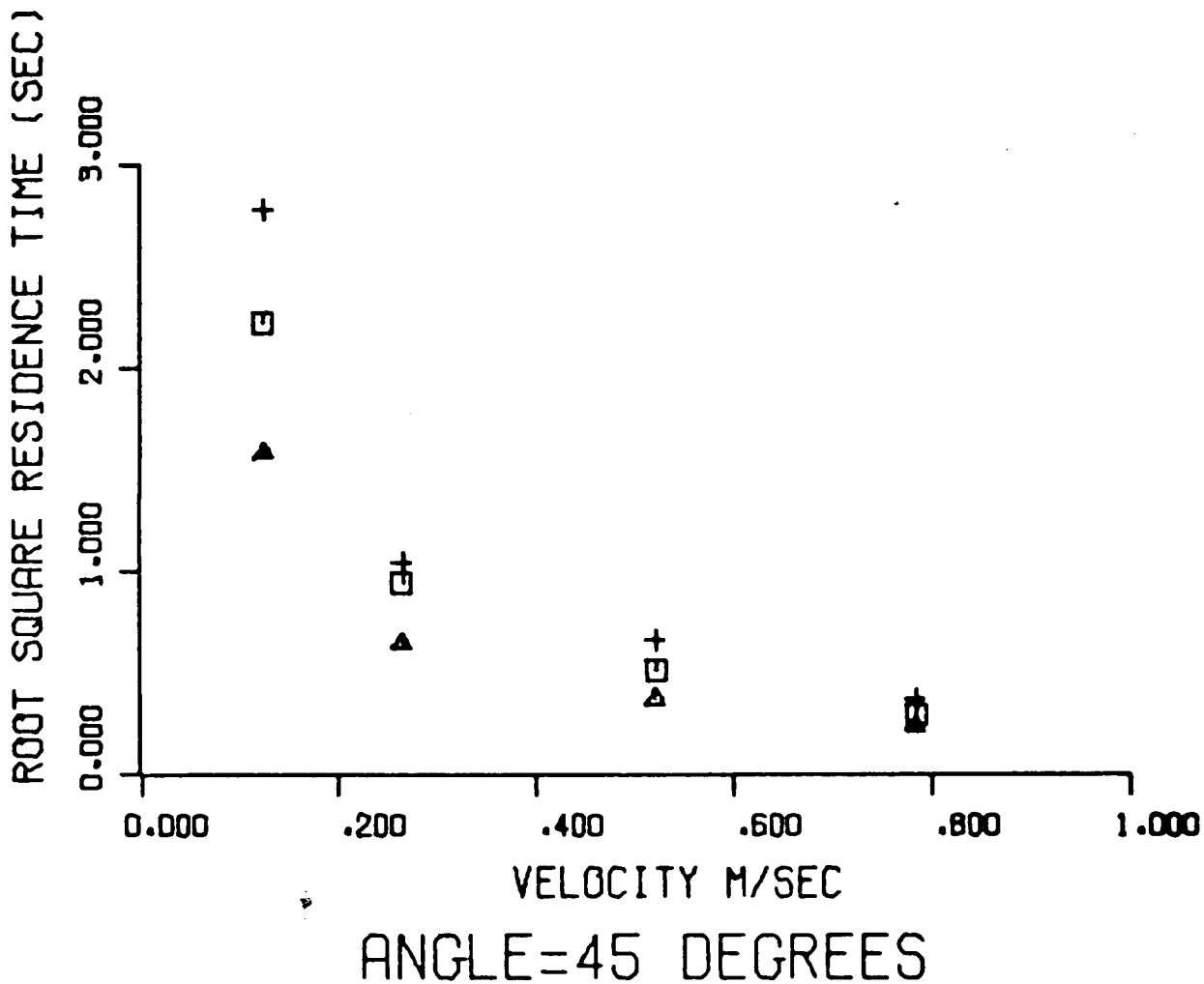

Figure 38 - Effect of Velocity on Root Square Average Packet Residence Time

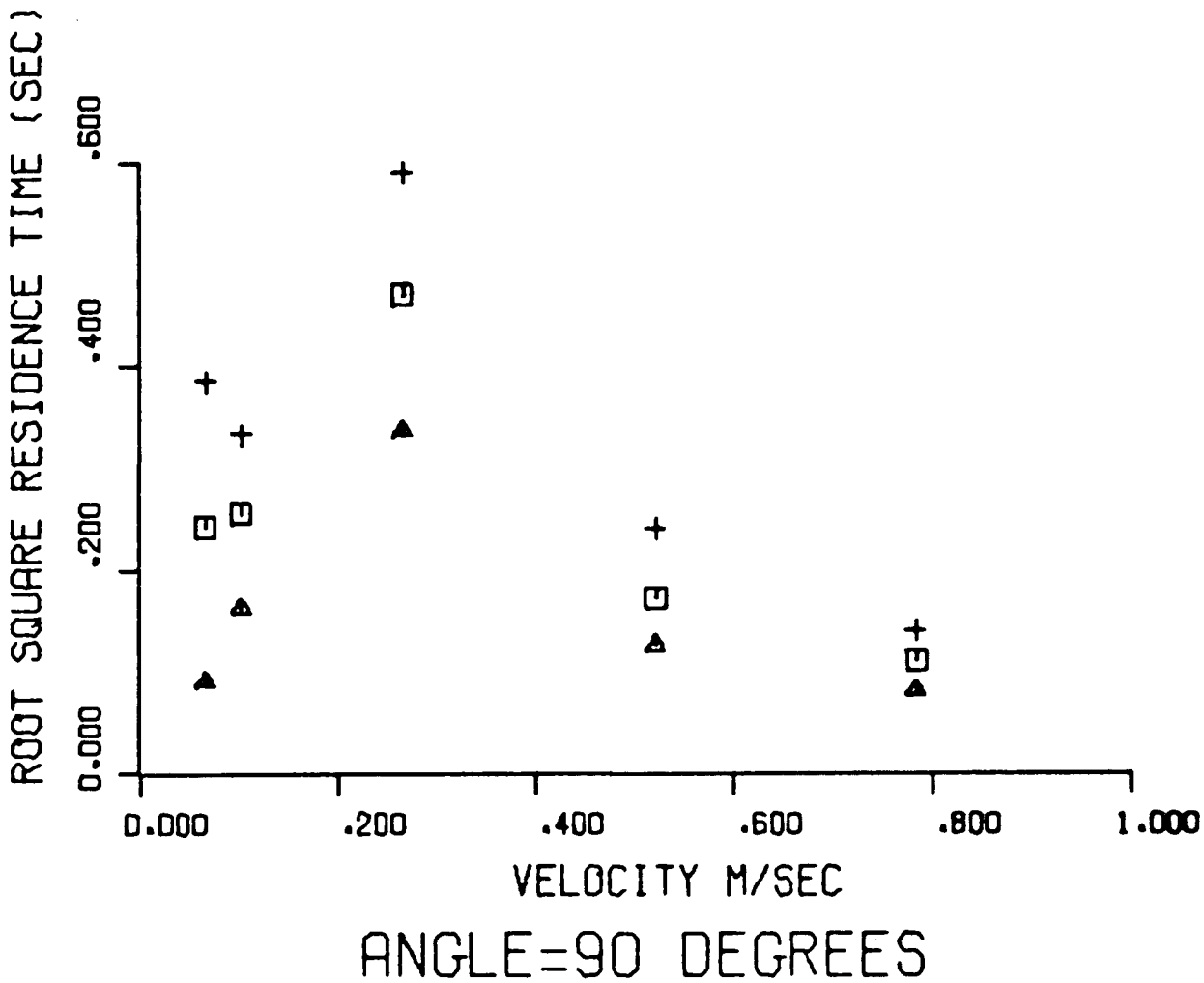

Figure 39 - Effect of Velocity on Root Square Average Packet Residence Time

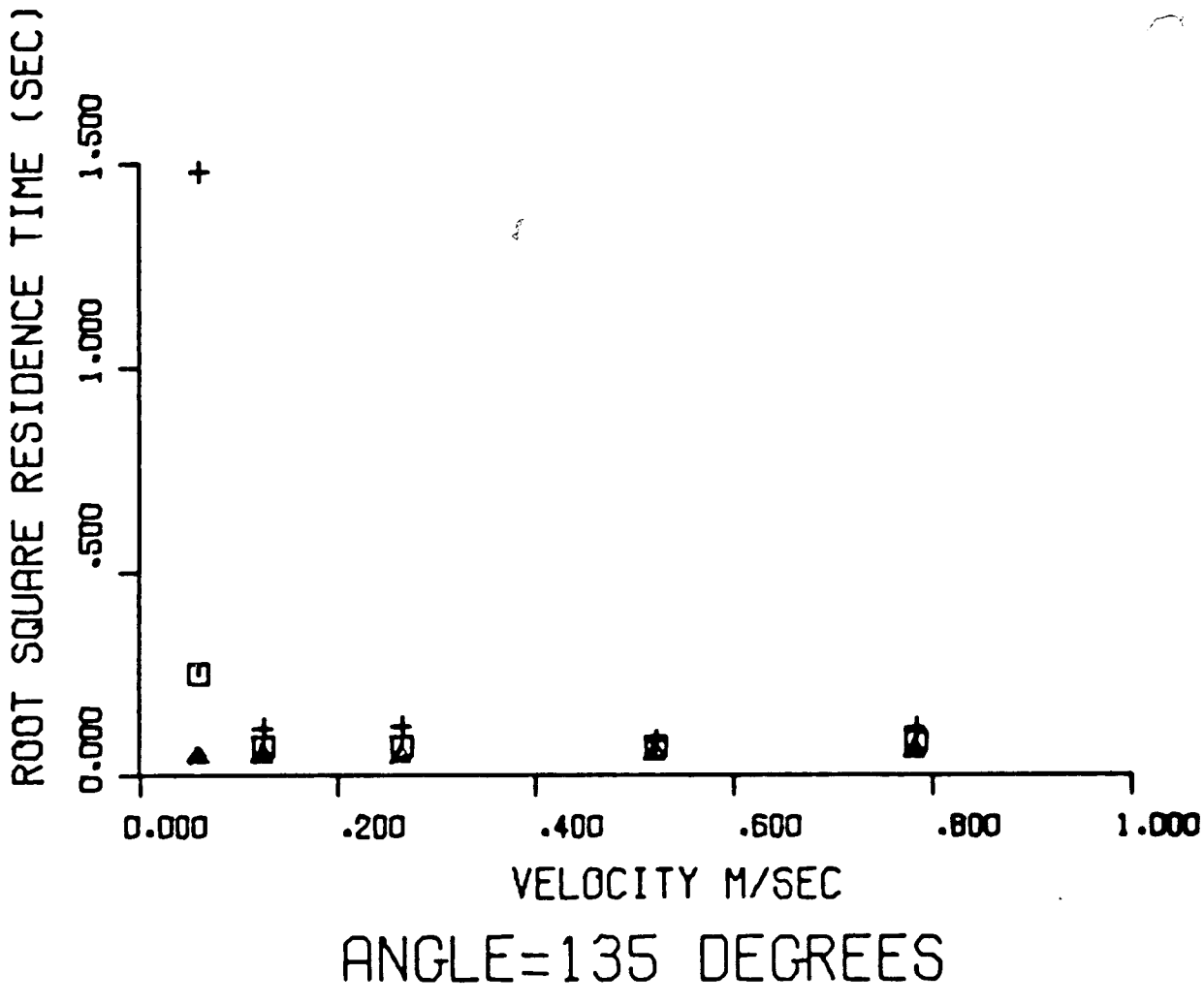

Figure 40 - Effect of Velocity on Root Square Average Packet Residence Time

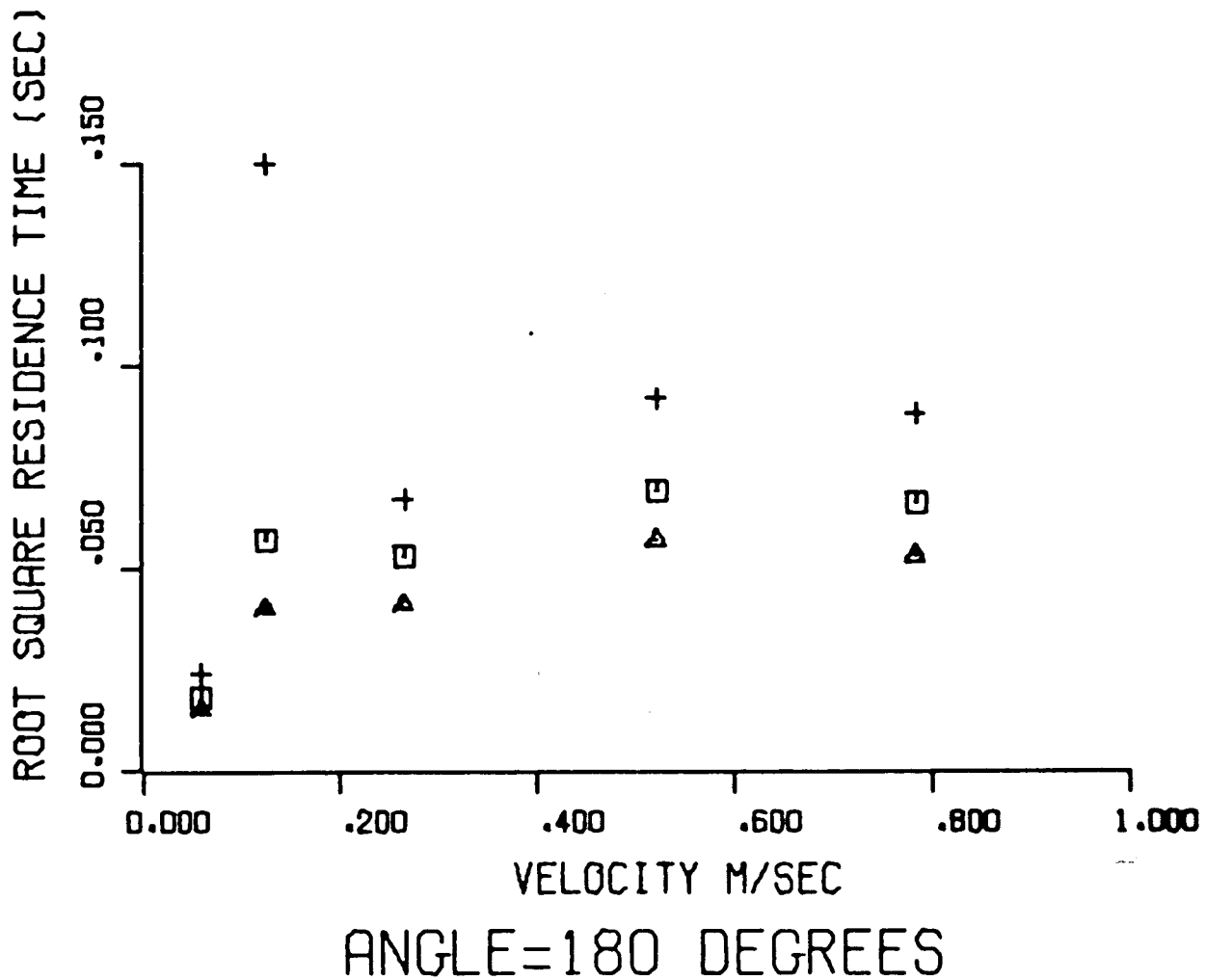

Figure 41 - Effect of Velocity on Root Square Average Packet Residence Time

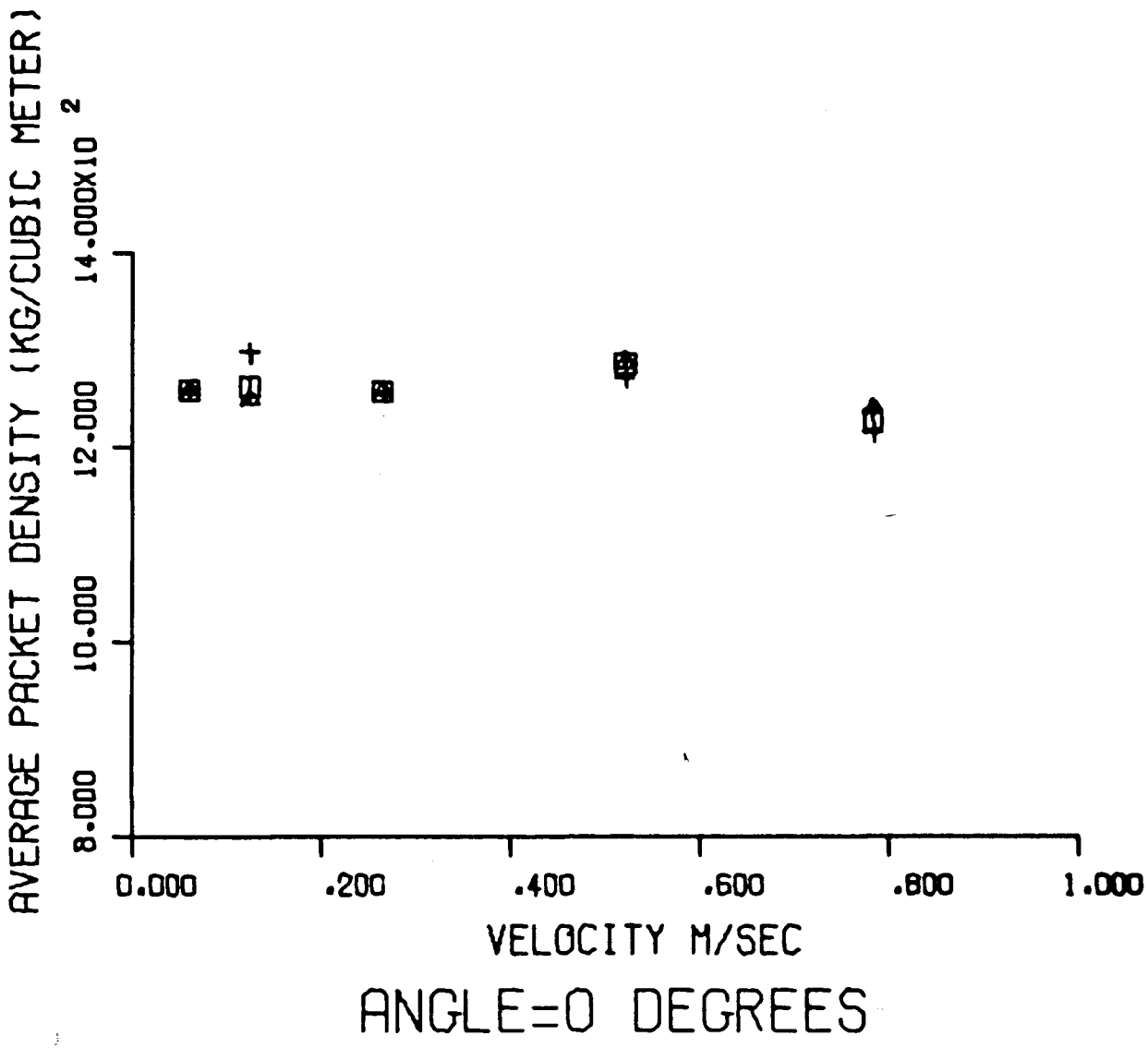

Figure 42 - Effect of Velocity on Average Packet Density

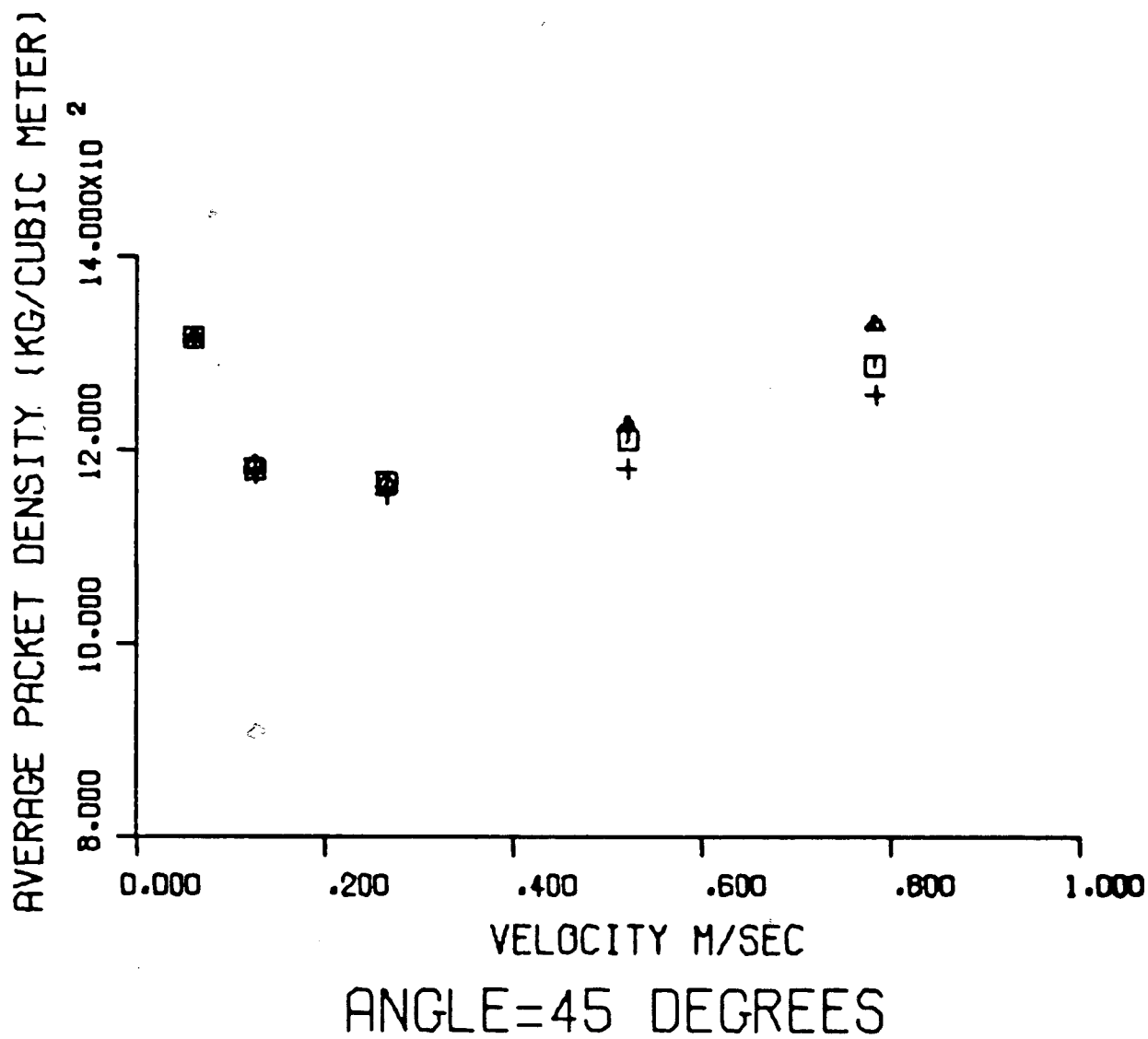

Figure 43 - Effect of Velocity on Average Packet Density

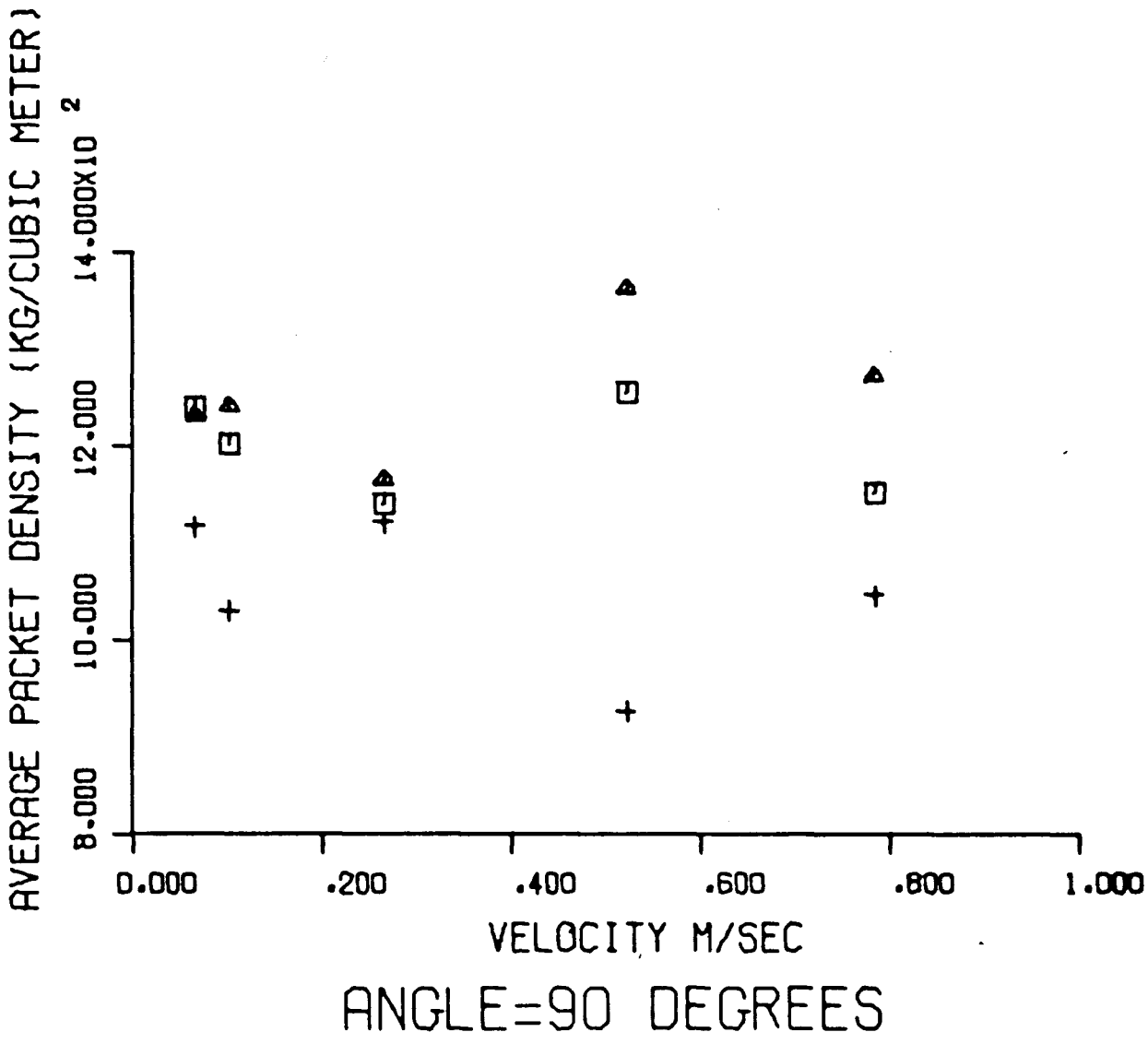

Figure 44 - Effect of Velocity on Average Packet Density

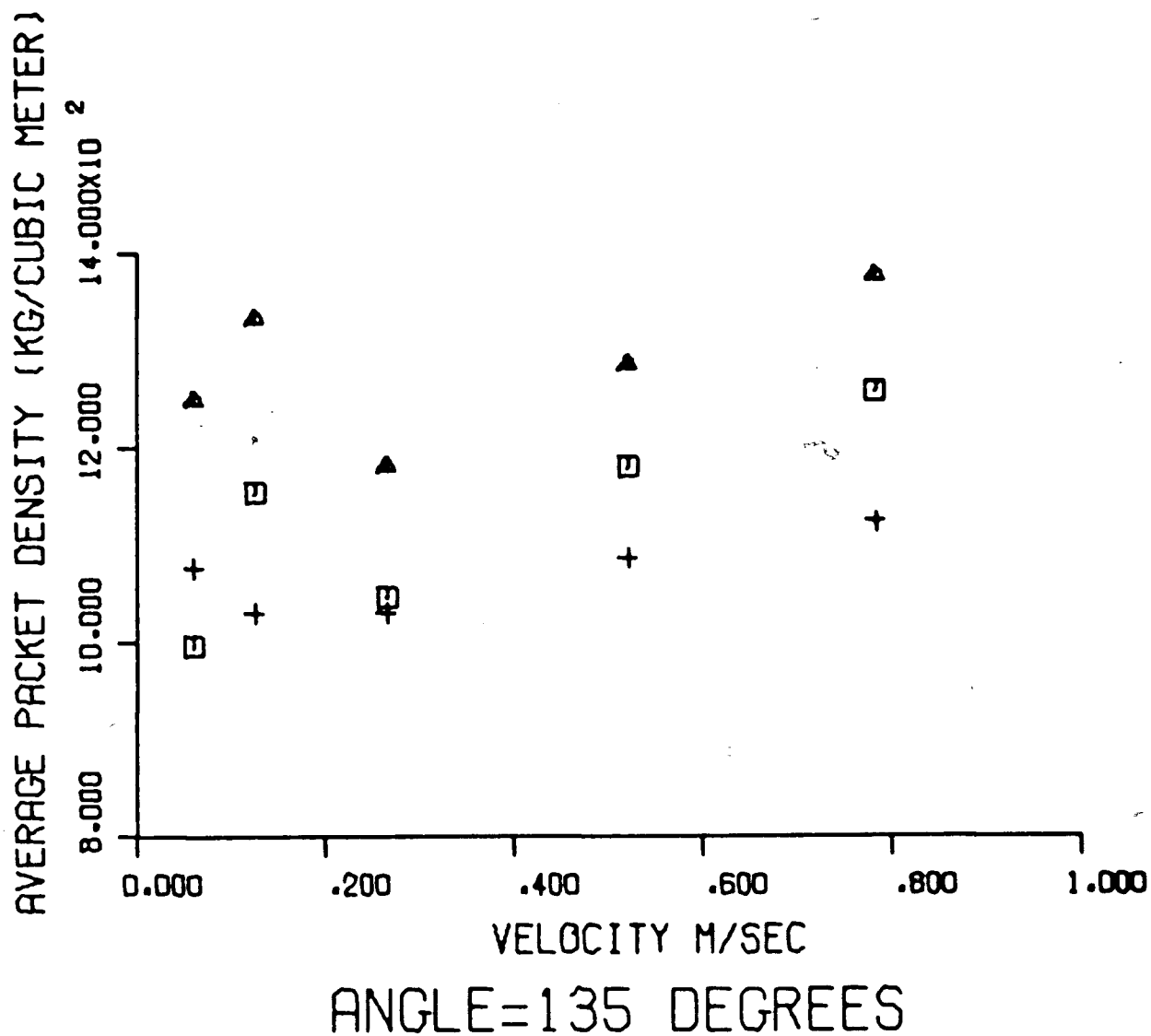

Figure 45 - Effect of Velocity on Average Packet Density

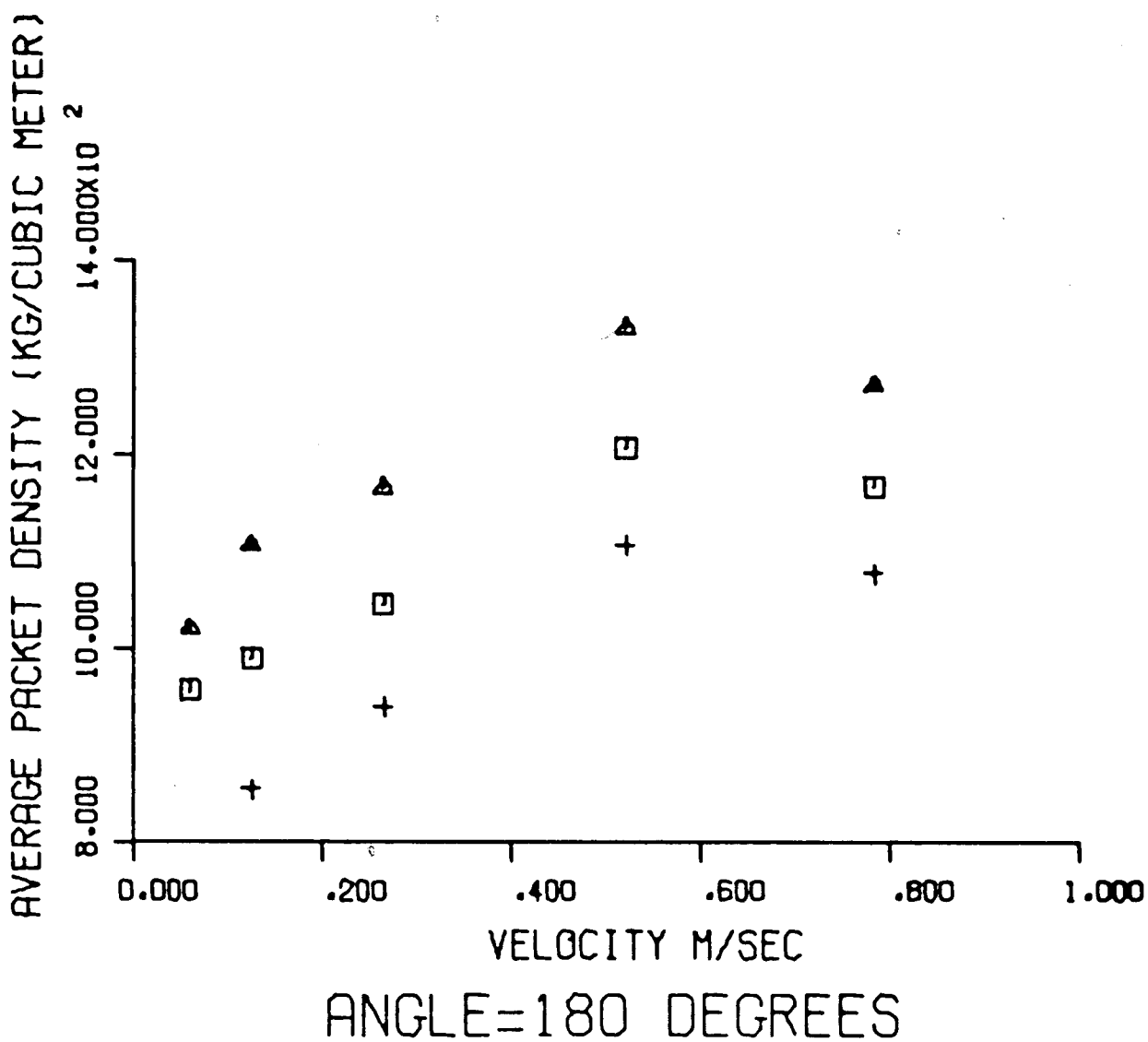

Figure 46 - Effect of Velocity on Average Packet Density

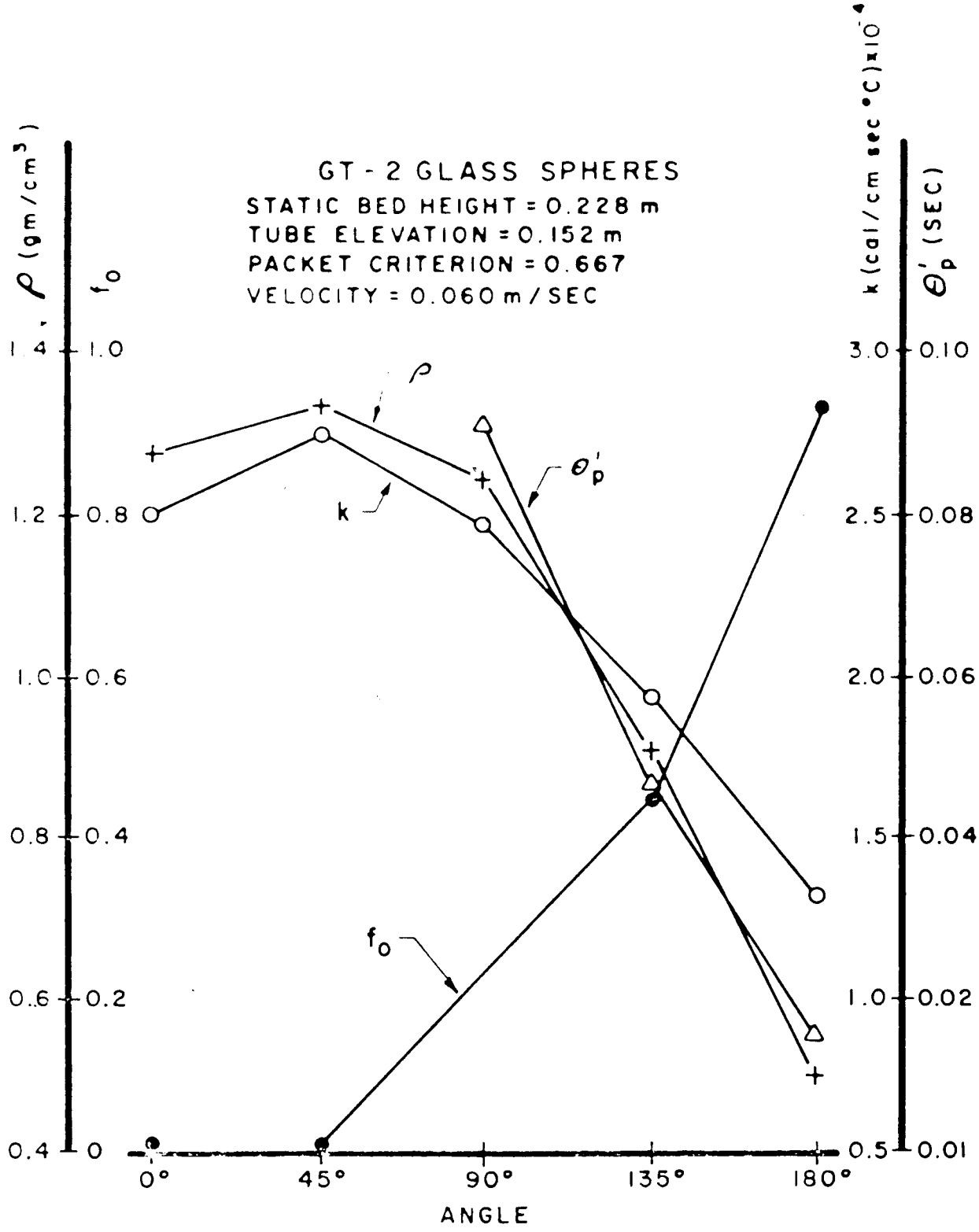

Figure 47 - Effect of angular position on packet thermophysical properties

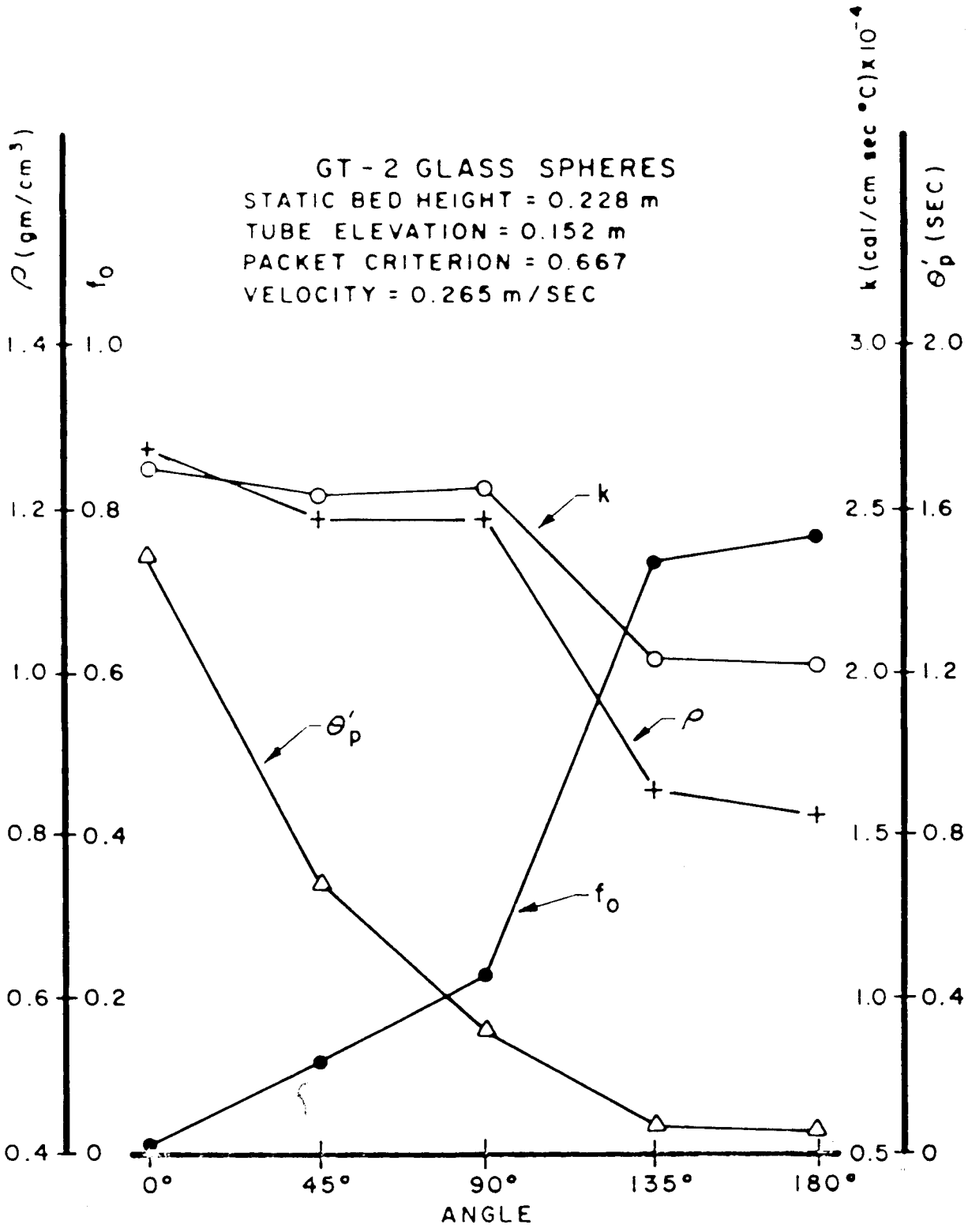

Figure 43 - Effect of angular position on packet thermophysical properties

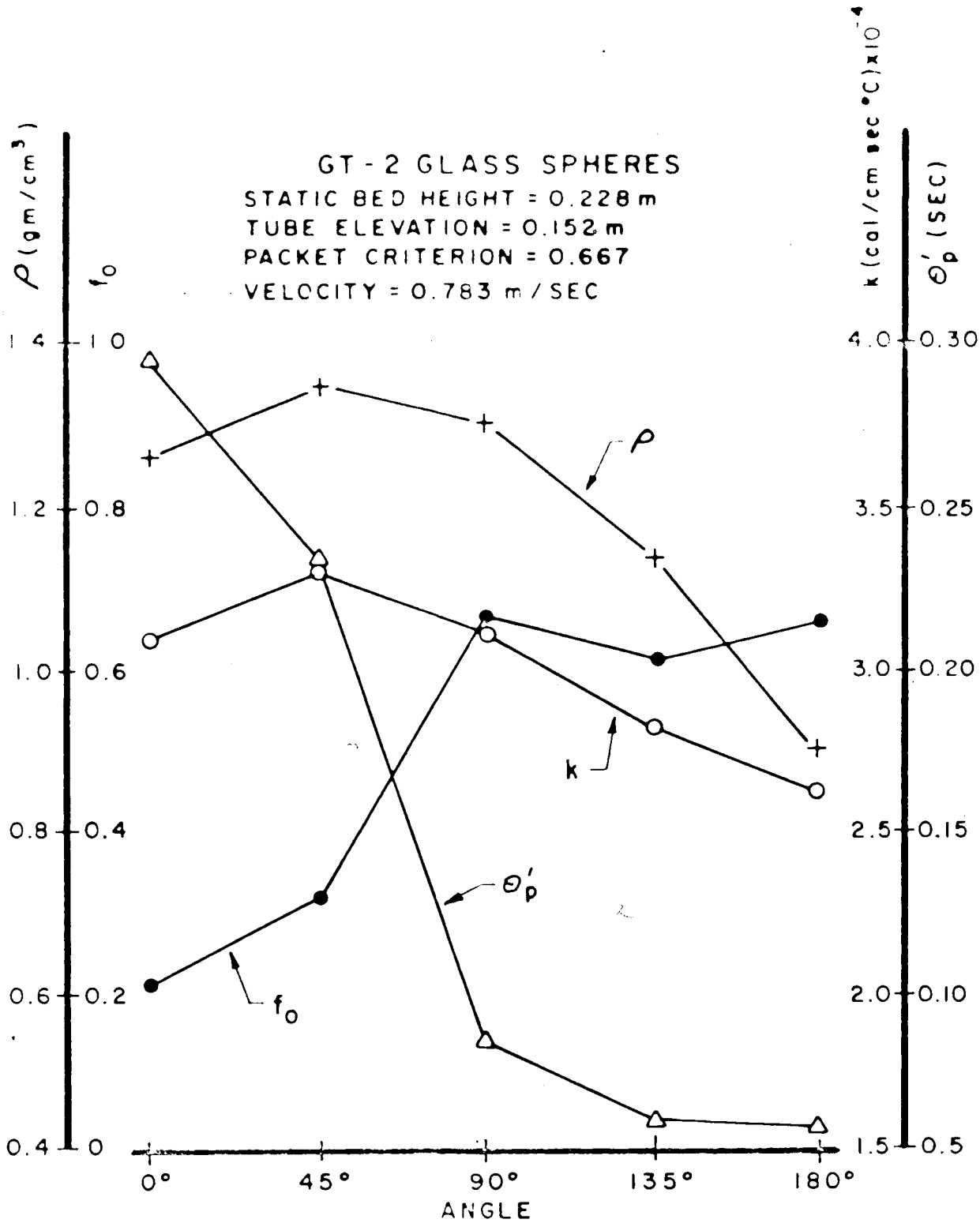

Figure 49 - Effect of angular position on packet thermophysical properties

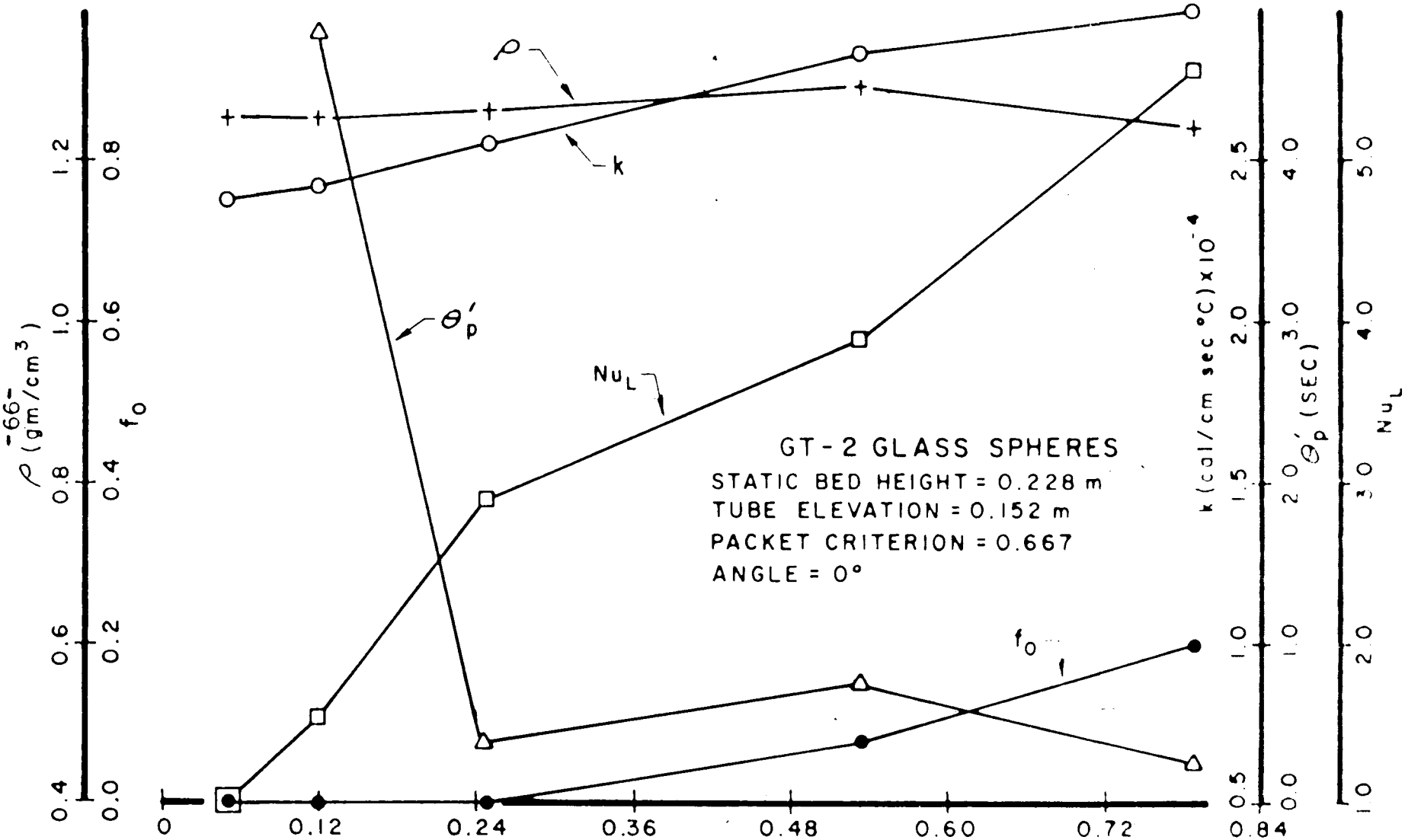

Figure 50 - Effect of velocity on packet thermophysical properties

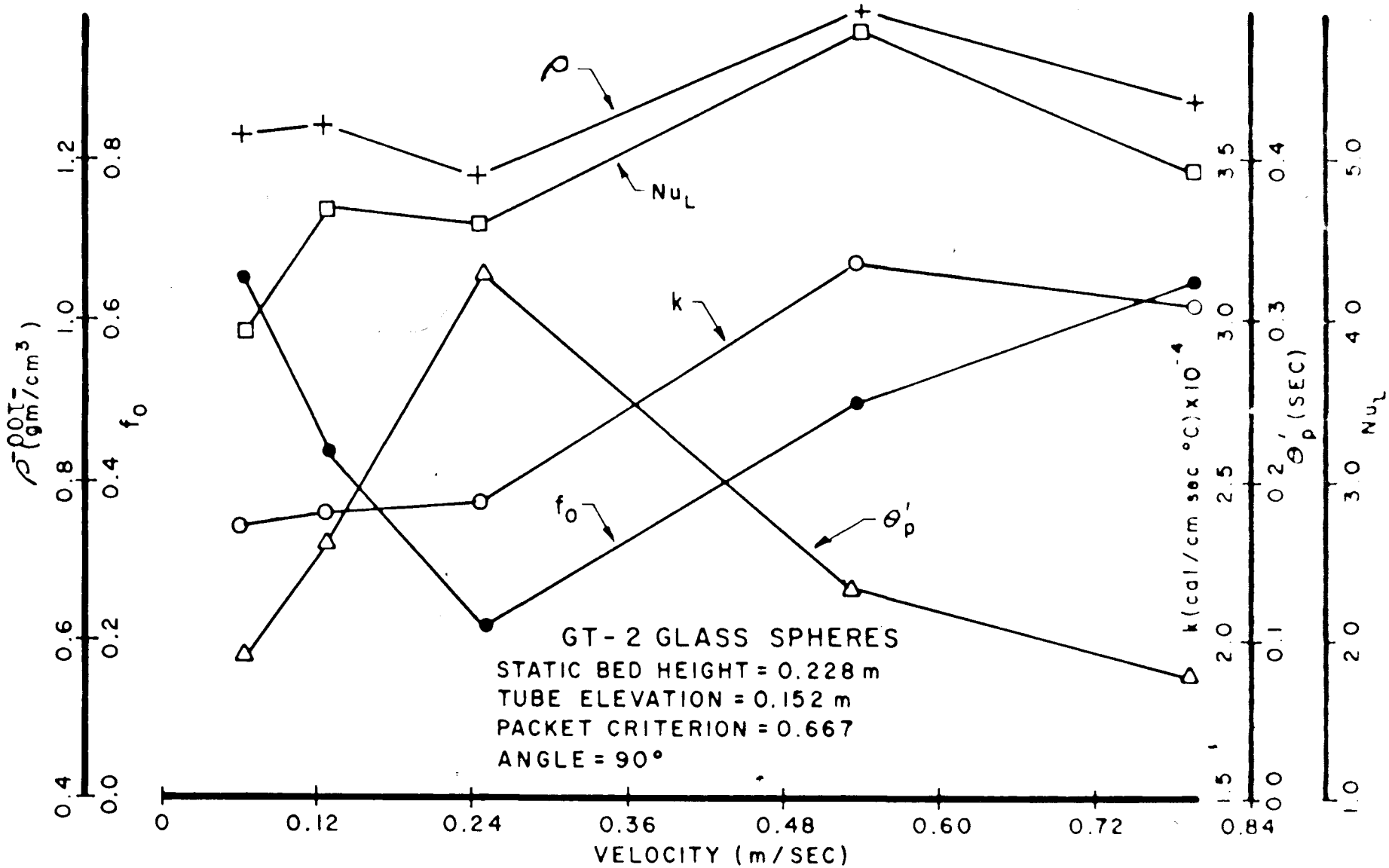

Figure 51 - Effect of velocity on packet thermophysical properties

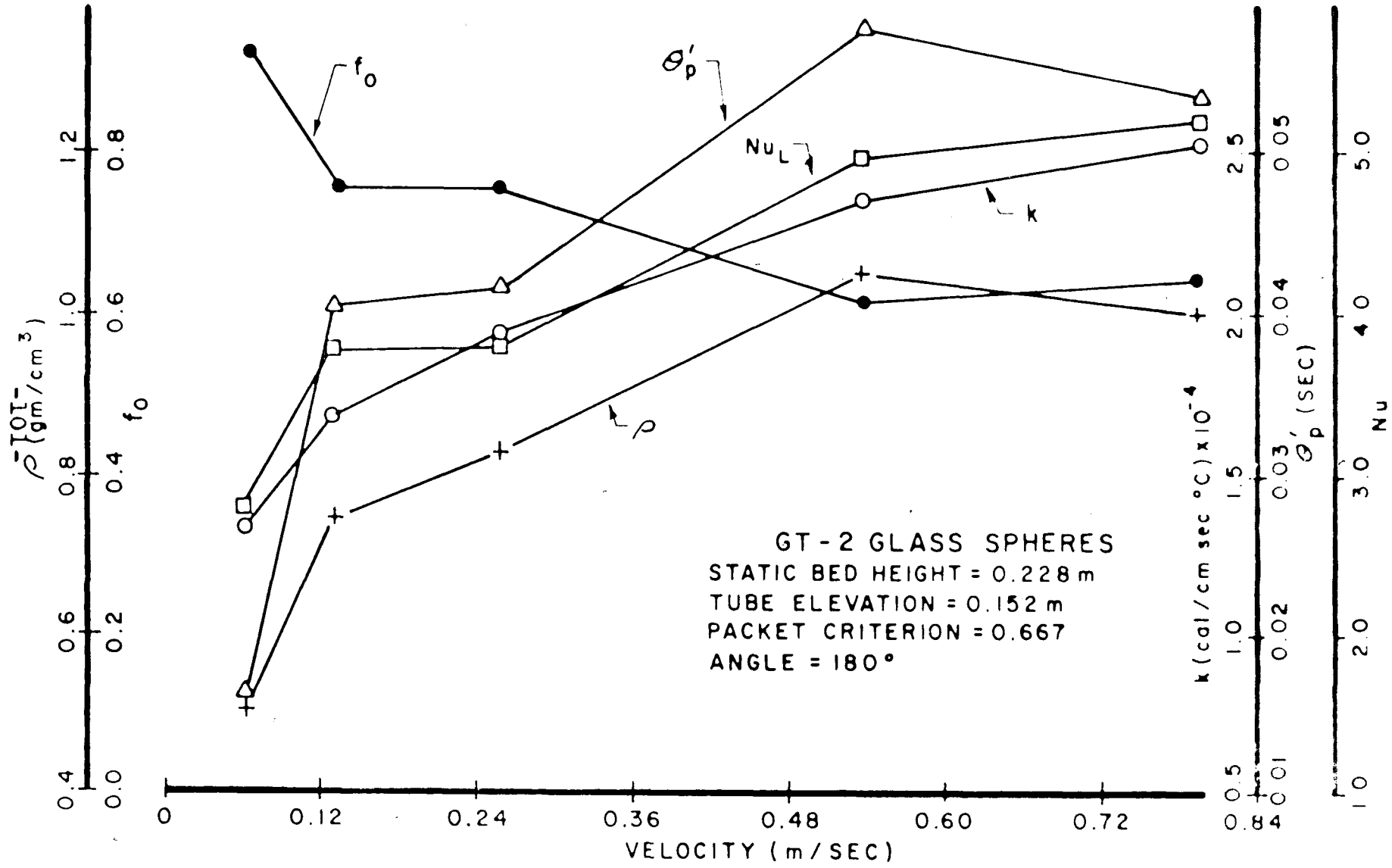

Figure 52 - Effect of velocity on packet thermophysical properties

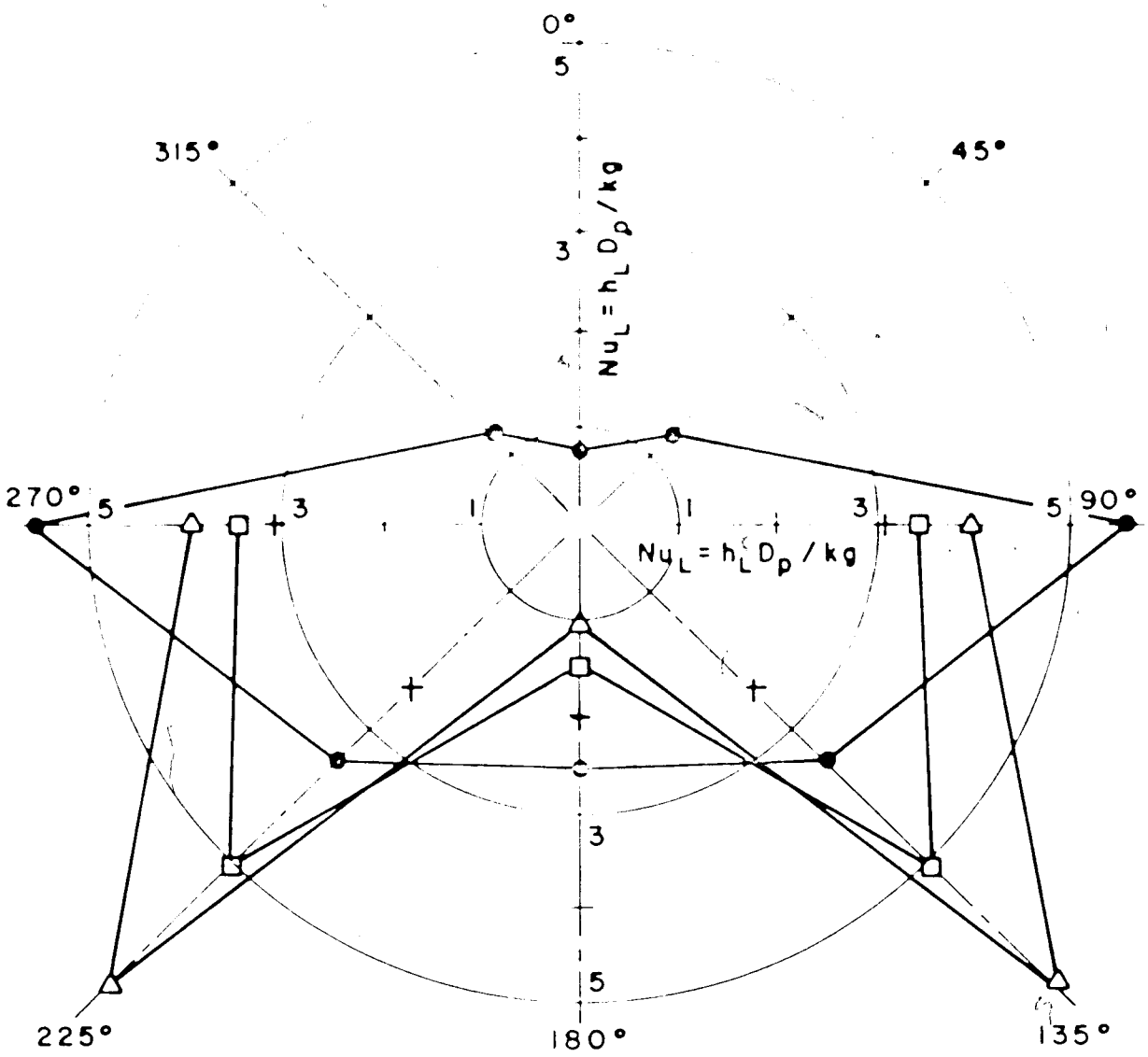

GT-2 GLASS SPHERES
VELOCITY = 0.060 m/SEC

STATIC BED HEIGHT = 0.228 m
TUBE ELEVATION = 0.152 m
0.333 PACKET CRITERION = +
0.500 PACKET CRITERION = □
0.667 PACKET CRITERION = △

STATIC BED HEIGHT = 152 m
TUBE ELEVATION = 0.076
DATA = ●

Figure 53 - Effect of angular position on Nusselt number

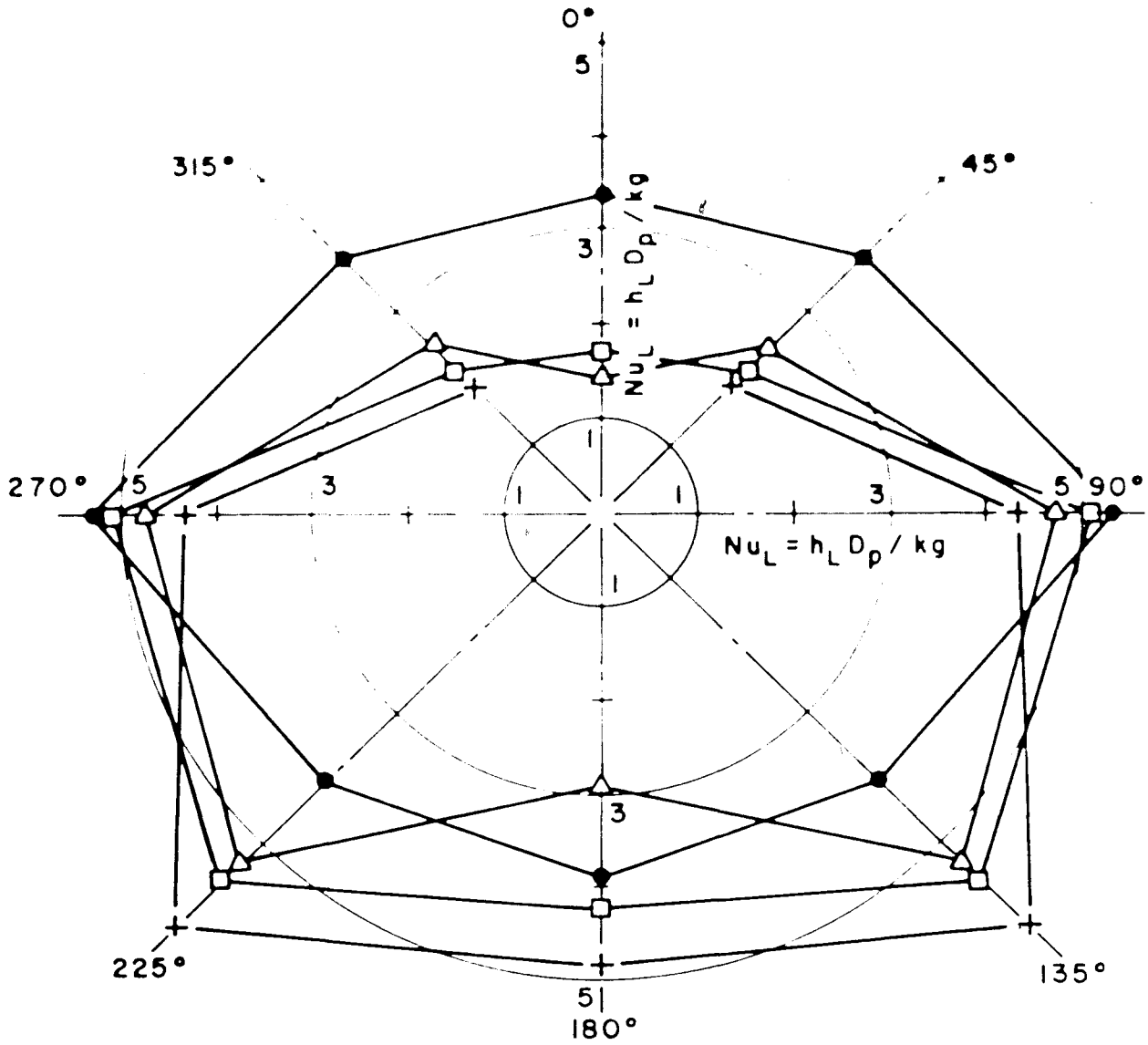

GT-2 GLASS SPHERES
VELOCITY = 0.125 m / SEC

BY PACKET MODELS:
STATIC BED HEIGHT = 0.228
TUBE ELEVATION = 0.152
0.333 PACKET CRITERION = +
0.500 PACKET CRITERION = □
0.667 PACKET CRITERION = △

CHANDRAN'S DATA:
STATIC BED HEIGHT = 0.152 m
TUBE ELEVATION = 0.076
DATA = ●

Figure 54 - Effect of angular position on Nusselt number

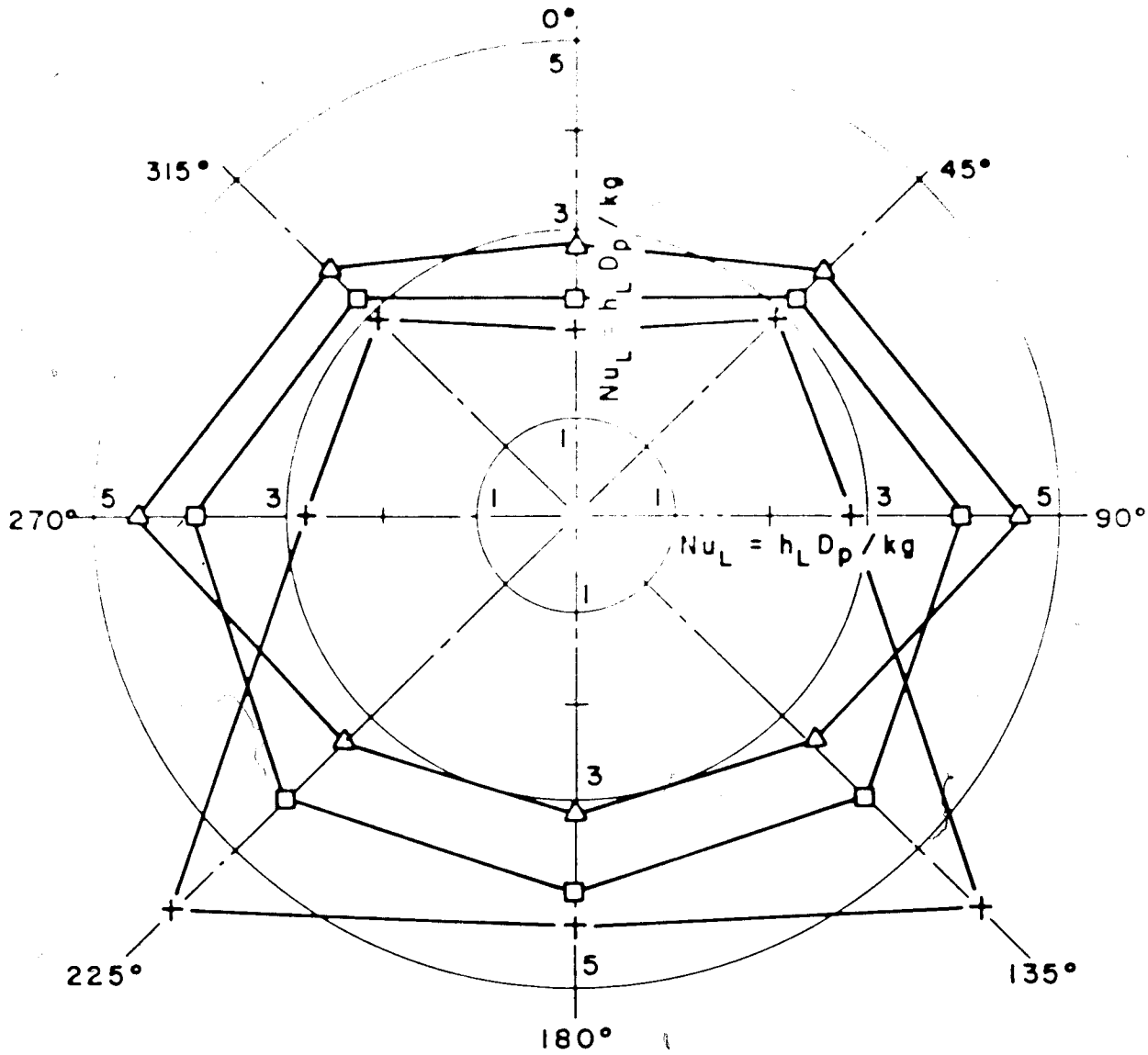

GT-2 GLASS SPHERES

STATIC BED HEIGHT = 0.228 m
TUBE ELEVATION = 0.152 m
VELOCITY = 0.265 m / SEC

0.333 PACKET CRITERION = +
0.500 PACKET CRITERION = □
0.667 PACKET CRITERION = △

Figure 55 - Effect of angular position on Nusselt number

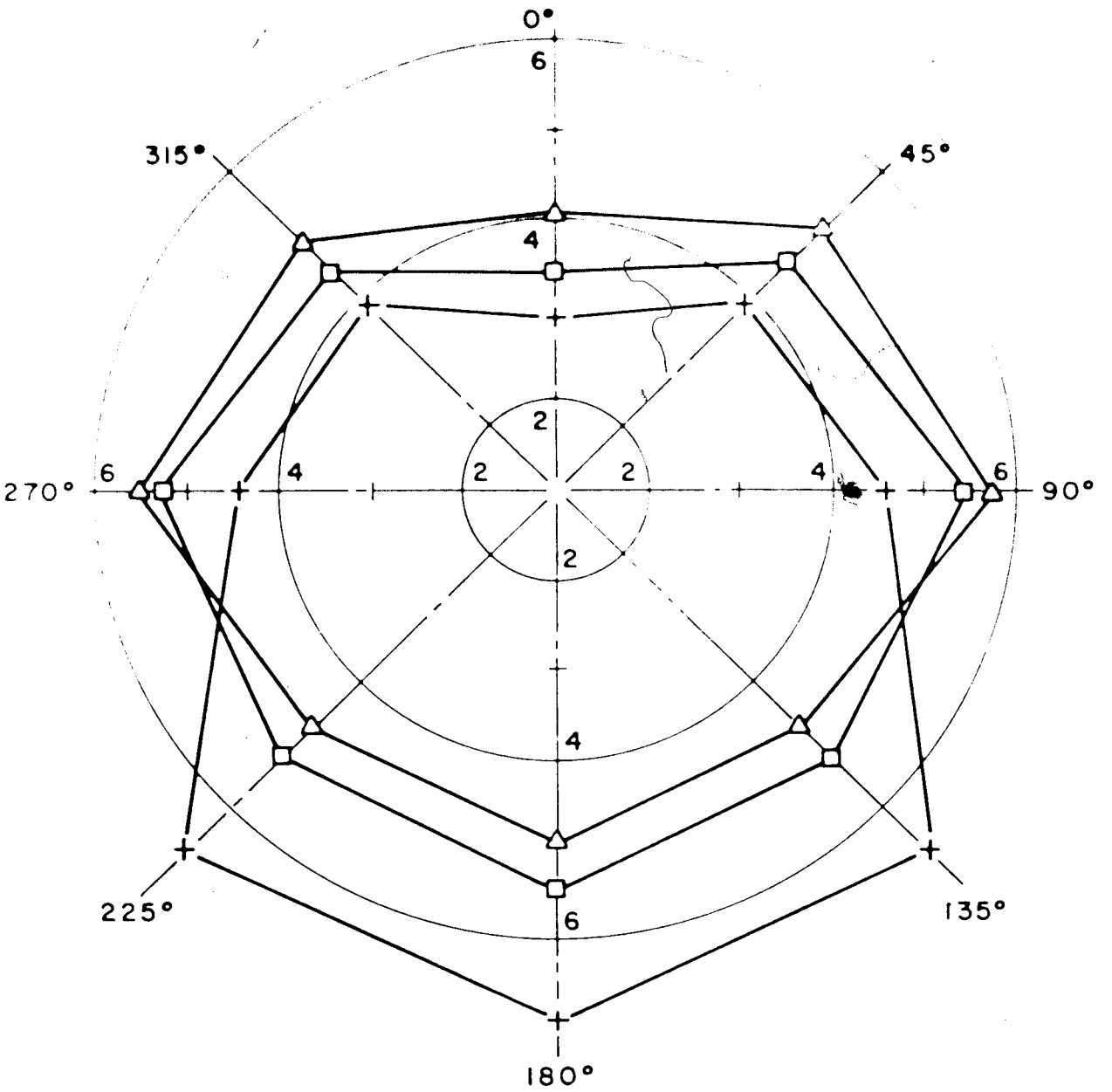

GT-2 GLASS SPHERES

STATIC BED HEIGHT = 0.228 m
TUBE ELEVATION = 0.152 m
VELOCITY = 0.521 m / SEC

0.333 PACKET CRITERION = +
0.500 PACKET CRITERION = □
0.667 PACKET CRITERION = △

Figure 56 - Effect of angular position on Nusselt number

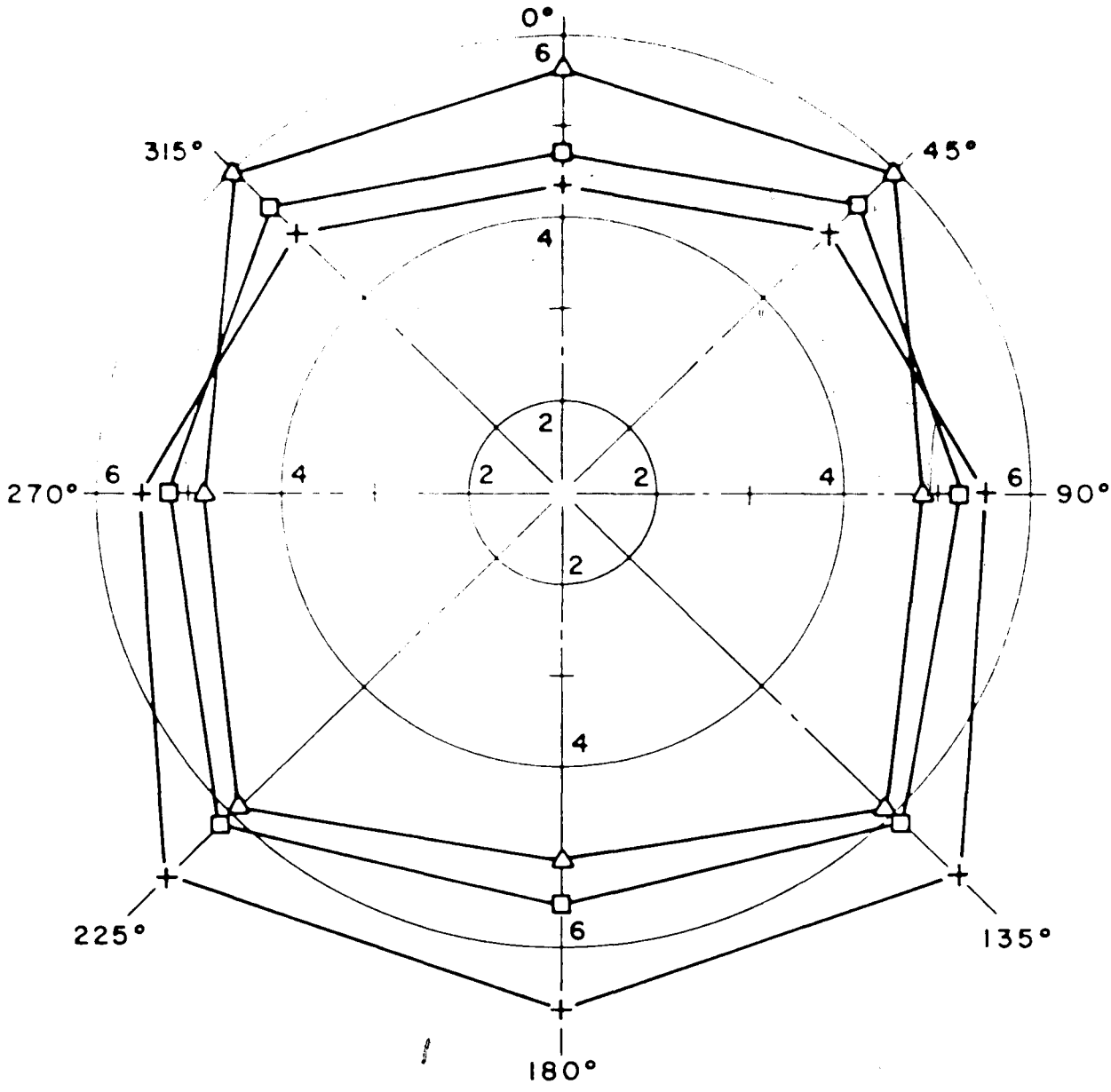

GT-2 GLASS SPHERES

STATIC BED HEIGHT = 0.228 m
TUBE ELEVATION = 0.152 m
VELOCITY = 0.783 m / SEC

0.333 PACKET CRITERION = +
0.500 PACKET CRITERION = □
0.667 PACKET CRITERION = △

Figure 57 - Effect of angular position on Nusselt number

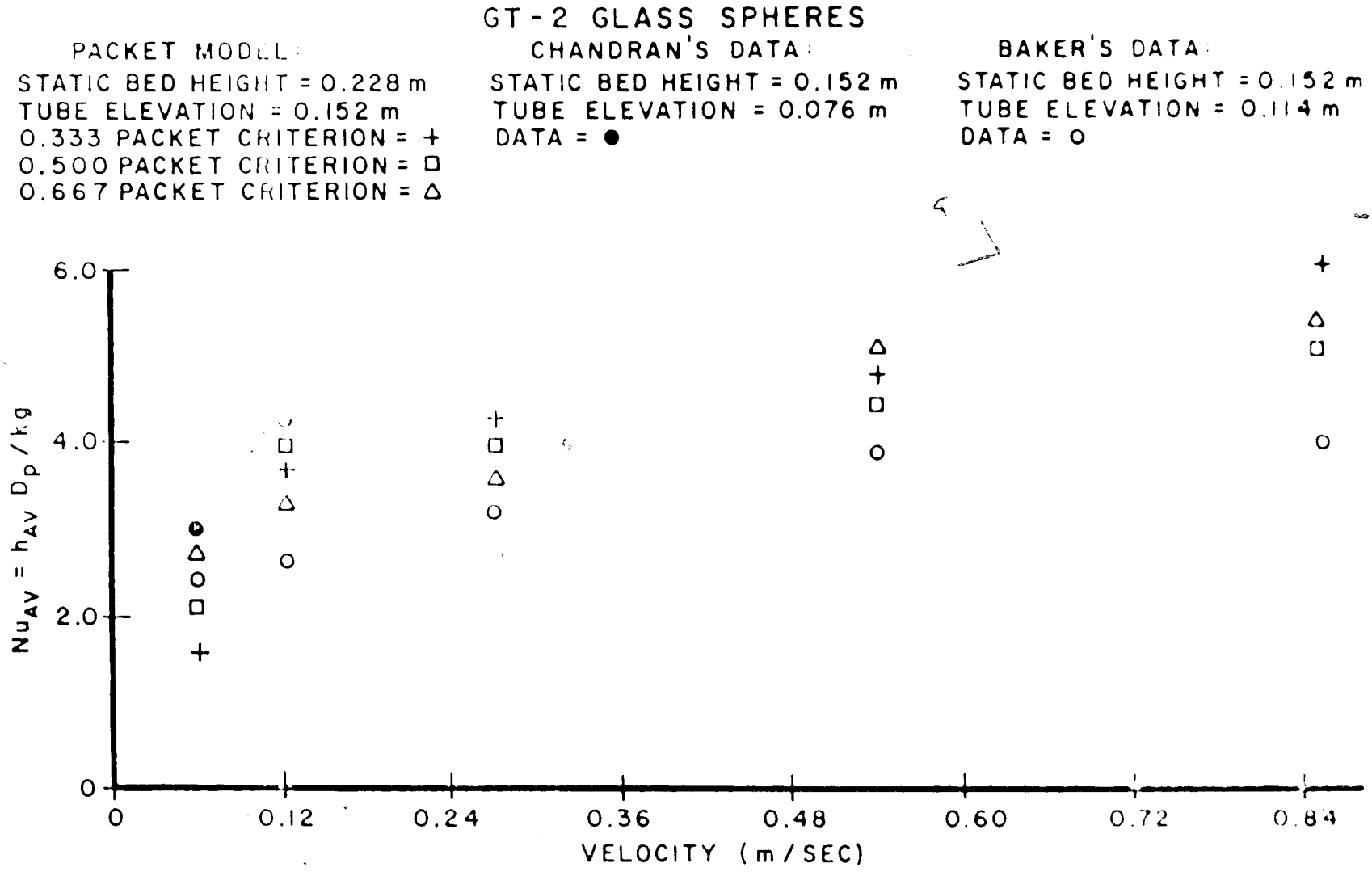

Figure 58 - Effect of velocity on average Nusselt number

BIBLIOGRAPHY

1. B. M. Legler, "Fluidized-Bed Processing in the Nuclear Fuel Cycle," Chemical Engineering Progress Symposium Series 66, No. 105 (1970): 167-174.

2. N. H. Coates and P. L. Rice, "Sulfur Dioxide Reduction by Combustion of Coals in Fluidized Beds of Limestone," A.I.Ch.E. Symposium Series 70, No. 141 (1974): 124-129.

3. B. S. Lea, E. J. Pyrcioch and F. C. Schora, "Hydrogasification of Coal in High-Pressure Fluidized Beds," Chemical Engineering Progress Symposium Series 66, No. 105 (1970): 152-157.

4. V. J. Kavlick and B. S. Lee, "High Pressure Electrothermal Fluid-Bed Gasification of Coal Char," Chemical Engineering Progress Symposium Series 66, No. 105 (1970): 145-151.

5. J. E. Hanway, "The Use of Fluidized Bed Technology in Pollution Control," A.I.Ch.E. Symposium Series 67, No. 116 (1971): 236-244.

6. R. S. Burton, R. C. Bailie and S. Alpert, "Municipal Solid Waste Pyrolysis," A.I.Ch.E. Symposium Series 70, No. 141 (1974): 116-123.

7. W. L. Davis and W. Glazier, "Large-Scale Fluidized Bed Drying of Iron-Ore Concentrate," A.I.Ch.E. Symposium Series 70, No. 141 (1974): 131-138.

8. J. Feinman and G. L. Minner, "A Fluidized Bed System for Simulation of Heat Treating of Steel," Chemical Engineering Progress Symposium Series 66, No. 105 (1970): 215-220.

9. K. I. Burgess, I. I. Inculet and M. A. Bergougnou, "Ore Benefication in a Fluidized Bed by Means of an Electric Field," Chemical Engineering Progress Symposium Series 66, No. 105 (1970): 236-242.

10. E. Douglas and C. P. Sayles, "Dry Sorting Using Pneumatically Fluidized Powders," A.I.Ch.E. Symposium Series 67, No. 116 (1971): 201-209.

11. J. F. Davidson and D. Harrison, Fluidization (London: Academic Press, Inc., 1971) p. 476.

12. J. S. M. Botterill, Fluid-Bed Heat Transfer (London: Academic Press, Inc., 1975) pp. 243-246.

13. M. Leva, M. Weintraub and M. Grummer, "Heat Transmission Through Fluidized Bed of Fine Particles," Chemical Engineering Progress 45, No. 9 (1949): 563-572.

14. W. M. Dow and M. Jakob, "Heat Transfer Between a Vertical Tube and a Fluidized Air-Solid Mixture," Chemical Engineering Progress 47, No. 12 (1951): 637-648.

15. O. Levenspiel and J. S. Walton, "Bed-Wall Heat Transfer in Fluidized Systems," Chemical Engineering Progress Symposium Series 50, No. 9 (1954): 1-13.

16. H. S. Mickley and D. F. Fairbanks, "Mechanism of Heat Transfer to Fluidized Beds," A.I.Ch.E. Journal 1, No. 3 (1955): 374-384.

17. H. S. Mickley, D. F. Fairbanks and R. D. Hawthorn, "The Relation Between the Transfer Coefficient and Thermal Fluctuations in Fluidized-Bed Heat Transfer," Chemical Engineering Progress Symposium Series 57, No. 32 (1961): 51-59.

18. J. D. Gabor, "Wall-to-Bed Heat Transfer in Fluidized and Packed Beds," Chemical Engineering Progress Symposium Series 66, No. 105 (1970): 76-85.

19. A. P. Baskakov, "The Mechanism of Heat Transfer Between a Fluidized Bed and a Surface," International Chemical Engineering 4, No. 2 (1964): 320-323.

20. L. B. Koppel, R. D. Patel and J. I. Holmes, "Part IV: Wall to Fluidized Bed Heat Transfer Coefficients," A.I.Ch.E. Journal 16, No. 3 (1970): 464-471.

21. E. N. Ziegler and W. T. Brazelton, "Mechanism of Heat Transfer to a Fixed Surface in a Fluidized Bed," Industrial and Engineering Chemistry Fundamentals 3, No. 2 (1964): 94-97.

22. L. B. Koppel, R. D. Patel and J. I. Holmes, "Part III: Residence Times and Age Distributions at Wall Surface of a Fluidized Bed, Application of Spectral Density," A.I.Ch.E. Journal 16, No. 3 (1970): 456-464.

23. J. S. M. Botterill and J. R. Williams, "The Mechanism of Heat Transfer to Gas-Fluidized Beds," Trans. Instn. Chem. Engrs. 41, No. 5 (1963): 217-230.

24. N. M. Rooney and D. Harrison, "Flow Patterns Near Horizontal Tubes in a Gas-Fluidized Bed,"

25. W. R. Uzgo, J. C. Chen and N. Eberhardt, "A Capacitance Method for Measurement of Film Thickness in Two-Phase Flow," Rev. Sci. Instrum. 44, No. 12 (1973): 1714-1716.

26. F. T. Ozkaynak, "Investigation of Packet Residence Time and Its Relation with the Heat Transfer Coefficient in Fluidized Beds," Unpublished Ph.D. dissertation, Lehigh University (1974).

27. R. P. Baker and J. C. Chen, "Heat Transfer from a Horizontal Tube in Shallow Fluidized Beds," Report No. TS-752, Department of Mechanical Engineering and Mechanics, Lehigh University (1975).

28. H. A. Vreedenberg, "Heat Transfer Between a Fluidized Bed and a Horizontal Tube," Chemical Engineering Science 9 (1958): 52-60.

29. N. I. Gel'perin, V. Ya. Kruglikov and V. G. Ainshtein, "Heat Exchange Between a Fluidized Bed and the Surface of a Single Tube During Longitudinal and Transverse Flow of Gases Around it," Khim. Prom., No. 6 (1958): 34-39.

30. W. E. Genetti, R. A. Schmall and E. S. Grimmett, "The Effect of Tube Orientation on Heat Transfer with Bare and Finned Tubes in a Fluidized Bed," A.I.Ch.E. Symposium Series 67, No. 116 (1971): 90-96.

31. D. Kunii and J. M. Smith, "Heat Transfer Characteristics of Porous Rocks," A.I.Ch.E. Journal 6, No. 1 (1960): 71-77.

32. S. Yogi and D. Kunii, "Studies on Effective Thermal Conductivities in Packed Beds," A.I.Ch.E. Journal 3, No. 3 (1957): 472-480.

33. M. Kimura, "Effective Thermal Conductivity of Packed Beds," Chem. Eng. (Japan) 21, (1957): 472-480.

34. Davidson and Harrison, pp. 509-511.

35. J. M. S. Botterill, Fluid Bed Heat Transfer, pp. 256-260.

36. B. V. Berg and A. P. Baskakov, "Investigation of Local Heat Transfer Between a Fixed Horizontal Cylinder and a Fluidized Bed," International Chemical Engineering 14, No. 3 (1974): 440-443.

37. R. Chandran, "Local Heat Transfer Data," unpublished results, advisor Professor J. C. Chen, Department of M.E. and Mechanics, Lehigh University, May 1976.

38. D. H. Glass and D. Harrison, "Flow Patterns Near a Solid Obstacle in Fluidized Bed," Chemical Engineering Science 19 (1964): 1001-1002.

39. J. F. Davidson and D. Harrison, Fluidization, p. 148.

VITA

I was born on October 11, 1952 in Pittsburgh, Pennsylvania. I received a Bachelor of Science degree in Mechanical Engineering in June 1974 from Lafayette College.

I was awarded the American Society of Mechanical Engineers Margorie Fox Rothermal Scholarship for graduate study. In September 1974 I entered the graduate mechanical engineering program at Lehigh University where I was granted a departmental fellowship. I am a member of Pi Tau Sigma and Tau Beta Pi.

I am presently a Teaching Assistant for the Department of Mechanical Engineering and Mechanics.